FACULTY OF SCIENCE AND TECHNOLOGY

MASTER THESIS

Study programme / specialization: Environmental Technology / Offshore Environmental Technology & water science and technology

The spring semester, 2022

Open / Confidential

Author: Andreas Bakke

.....
(signature author)

Course coordinator: Roald Kommedal

Supervisor(s): Roald Kommedal

Thesis title: Bioengineered methanotrophic photogranules for tertiary UASB effluent post-treatment.

Credits (ECTS): 30

Keywords: Oxygenic photogranules, cyanobacteria, photobioreactor, post-UASB treatment, methanotroph, syntrophy

Pages: 65

+ appendix: 72

Stavanger, 15.05.2022
date/year

Acknowledgement

This thesis is submitted as the final fulfilment of the required academic process for the master's degree in environmental technology at the University of Stavanger.

I would like to thank my supervisor Roald Kommedal associate professor at the University of Stavanger for presenting me with the objective of the thesis, and academic discussions during my progression.

I would like to give my special gratitude to former PhD student Anissa Sukma Safitri which now can be presented as doctor. I would like to congratulate her on passing her PhD and thank her for the support, enthusiasm, constructive feedback, and guidance during my thesis.

I would also like to show my gratitude to Mona Werthus Minde and Caroline Ruud at the material lab at UiS for helping me with the XRD analysis.

Abstract

The need for aeration when treating wastewater is the most extensive energy requirement wastewater treatment plants (WWTP) has today. This thesis investigated an attached growth process which utilise genetic features in cyanobacteria in syntrophy with other phototrophs and heterotrophs for tertiary up-flow anaerobic sludge blanket (UASB) effluent post-treatment. The oxygen produced from phototrophs was used by heterotrophs to oxidise residual COD including dissolved methane in the UASB effluent, which produce carbon dioxide that phototrophs use to produce more oxygen. Additionally, nutrient removal polishing treatment analysis was also performed. The goal of this thesis was to sustain and grow the biomass in a granular structure when seeding hydrostatically grown oxygenic photogranules in a photobioreactor used for post-UASB treatment. There was also an aim to examine if they could be enriched with methanotrophs for dissolved methane removal. To reach the goal and aim presented, a literature review is done since this is a new technology. The literature review investigates how OPGs are formed and what characteristics are important for granule formation. It also explores other studies that has tried to remove methane using the syntrophy between phototroph and methanotrophs. The OPG biomass grew in the PBR running in sequence batch operation and steadily removed the chemical oxygen demand 52,5 % ± 2.2 (± standard error), with best rate was 78,7 %. Enrichment of methanotrophs in suspension was tested in two experiments. One experiment used glass vials and the other experiment was directly in the PBR. Both proved removal of methane. The best removal efficiency from OPGs inoculated with methanotrophs was for the glass vial experiment, averages were: COD 81.5 % ± 1.1(± standard error), NH_4^+ 52.3 % ± 1.1, PO_4^{3-} 49.6 % ± 2.2. Conclusion from the analysis of the experiments is that bioengineered methanotrophic photogranules can be grown in a PBR and used for tertiary UASB effluent post-treatment. There is however a potential for future research because there was relative few OPGs grown in this reactor system compared to others in the literature. From analysis of the two methanotroph experiments it is shown that a higher biomass to liquid ratio would increase the methane removal. A proposal for future research is to cultivate more OPGs using the UASB effluent in a system closed from the atmosphere. The effluent will then have more methane and CO2 in the influent of the PBR which in theory will have more carbon and nitrogen available for growth.

Table of Contents

List of figures

List of tables

List of abbreviations

ATP	Adenosine triphosphate
ANME	Anaerobic methanotrophic arceae
COD	Chemical oxygen demand
EPS	Extracellular polymeric substances
HRT	Hydraulic retention time
MOB	Methane oxidising bacteria
OPG	Oxygenic photogranule
PBR	Photo bio reactor
PAR	Photosynthetically available radiation
SBR	Sequence batch reactor
TEA	Terminal electron acceptor
TN	Total Nitrogen
TP	Total phosphorous
TSS	Total suspended solids
UASB	Up-flow anaerobic sludge blanket
WWTP	Wastewater treatment plant

1 Introduction

One of the extensive challenges wastewater treatment facilities have today is reducing energy consumption. Most of the energy consumption is directly related to aeration. A case study done for ten different Wastewater Treatment Plants (WWTP) found that in all plants, aeration consumed the most energy ranging from 40-75% of the total energy requirements (Stasinakis, 2015). Aeration's primary purpose is to supply the heterotrophic bacteria degrading organic material with enough oxygen. Oxygen is provided so the bacteria can reduce the Chemical Oxygen Demand (COD) by oxidising the carbonaceous content. A system that does not rely on aeration for oxygen supply would decrease the total energy consumption, which would be both an economic- and environmental benefit. The need for applying innovative technology and solutions to optimise efficiency and reduce the carbon footprint has upgraded wastewater treatment to be an essential and advanced development sector.

The project presented in this thesis aims to develop a system that oxidises dissolved methane in water without the need for aeration. The goal is to successfully engineer a consortium of microorganisms on bio-granules, specifically oxygenic photogranules (OPGs). The formation of the granules will happen hydrostatically before being seeded in a photobioreactor (PBR) working in a Sequence Batch Reactor (SBR) operating system. The photogranules consist of photosynthetic cyanobacteria in which we will try to inoculate a culture of methanotrophic bacteria (MOB). The cyanobacteria and MOB will then live in syntrophy with each other. This syntrophy will make the system's oxygen supply self-sustainable, resulting in a reduced requirement for operation costs. The main cost for a system like this is providing natural light to enhance the photosynthetic activity in the reactor. One of the main challenges with using a granular media is that the organisms within the granule consortium may detach and become suspended in the liquid without forming new granules.

This thesis originally aimed to create a bioprocess model for the mixotrophic growth of cyanobacteria in the PBR using AQUASIM as a modelling tool. The scope of the thesis changed when photogranules were inoculated in the photobioreactor. Bacteria detached from the granular media and became suspended in the liquid. The same thing happened for three different inoculations. Because of this, there was no working reactor system to verify the model against, and therefore, the aim of the thesis was reformulated to: *How can we sustain and grow the biomass in a granular structure when seeding hydrostatically grown oxygenic*

photogranules in a photobioreactor used for tertiary UASB effluent post-treatment, and can they be enriched with methanotrophs to increase methane removal?

Figure 1 compares the process using OPGs with emphasis on cyanobacteria as phototroph and MOB as heterotroph with the traditional way to oxidise the carbonaceous material in wastewater; the activated sludge process (Henze et al., 2000). The activated sludge process requires intensive aeration and often needs chemicals to help gather flocs and aggregates from the biological activity to better settle the residual activated sludge or secondary sludge (Crittenden et al., 2012). As illustrated in Figure 1, using photogranules also produces secondary sludge. However, this waste has a different composition than the activated sludge process. The granules are heavy due to minerals being precipitated in the core of the granule (Milferstedt et al., 2017a), resulting in a lower settling time for granules compared to flocs made in regular treatment systems (Trebuch et al., 2020). The increased retention gives the OPGs a competitive advantage because they have a lower risk of washing out of the system.

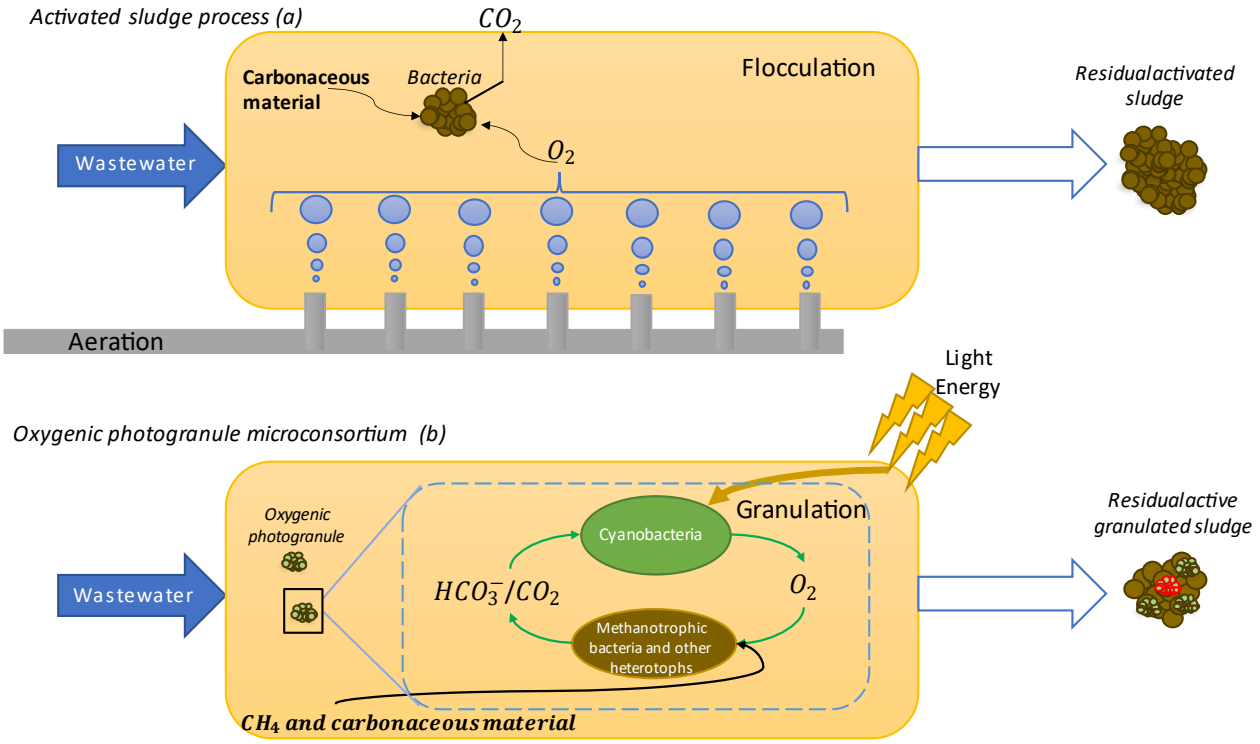

Figure 1: Comparison of the (a) Activated Sludge Process and (b) oxygenic photogranule microconsortium with enrichment of methanotrophs. Figure (a) is a simplified description of the activated sludge process, illustrating the need for aeration. Figure (b) is a simplified description of OPGs with methanotrophs in an SBR. It highlights the conversion process happening in the photogranule with the methanotrophic enrichment. The figure is inspired by(Tiron et al., 2017).

The experiment provided in this report contributes as one unit process in a project experimenting with a more extensive system (see Figure 2). The project is called "the hippy project" and is a collaboration between several experimental studies at UiS. Most relevant to this thesis is the Up-flow Anaerobic Sludge Blanket (UASB). The UASB produce and capture biogas from the effluent of primary treatment. Subsequently, some of the biogas dissolve in the liquid according to henrys law (Lobato et al., 2012). Due to mass-transfer limitations which leads to supersaturation of methane there might be even more methane dissolved in the liquid. A problem with this is that methane is highly volatile, and thus it would escape from the liquid to the atmosphere in an open system leading to higher carbon emissions from the treatment process. The solution proposed to this problem is treating the UASB effluent in an air closed PBR with the OPG engineered methanotrophic syntrophy presented in this thesis.

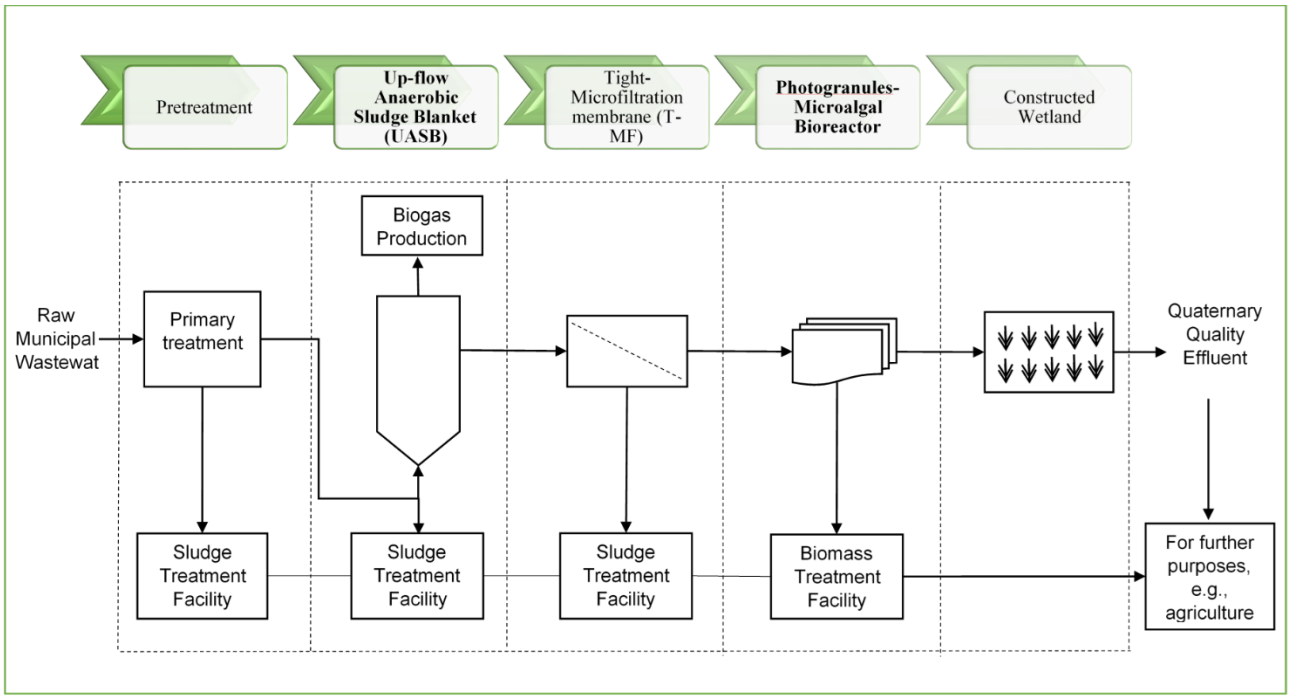

Figure 2: Simple schematic of the overall hippy project showing the treatment progression from pre-treatment to UASB treatment to membrane treatment -> for methane treatment using OPGs -> constructed wetland treatment.

2 Literature review

Treating wastewater using oxygenic photogranules is a new technology and it is still only used in experimental studies. The use of OPGs presented in this thesis will try to introduce a novel function to the photogranules by enriching them with methanotrophs. The goal is to make them specialists in removing methane. This is done to try and clean the effluent from anaerobic processes which have a high methane content. Since this is a new technology a short literature review is conducted to present the formation process and discuss existing problems and positive results. To best understand the process the review will start with discussing the microorganisms that are central in the formation of granules and removal of methane. The review continues with presenting what OPGs are and highlight important biological mechanisms for their development. The review will further investigate OPGs applications in wastewater treatment by looking at how they are formed using activated sludge. Also investigating how hydraulic retention time (HRT), seeding density and agitation impact the microbial community and characteristics of the granules. And lastly what to expect when enriching OPGs with methanotrophs.

2.1 Microorganisms

Microorganisms have been used in wastewater treatment since the first trickling filter was installed at Salford near Manchester, England, in 1893 (Stanbridge, 1976). The use of microorganisms has since developed to be a popular method for oxidizing the carbon content in the wastewater. Biological processes for wastewater treatment are usually divided into two main categories, suspended growth processes and attached growth processes (often referred to as biofilm processes) (Tchobanoglous et al., 2014c). The main challenge with both these methods is the need for oxygen when microorganisms convert the carbonaceous material to carbon dioxide, water, and energy for re-growth. Oxidation of carbon is a combustion process which requires a significant amount of oxygen. Today the most common method for adding oxygen to the system is through aeration.

Aeration is the preferred method for supplying microorganisms with sufficient quantities of oxygen. Supplementing oxygen to the process is necessary because of the low solubility of oxygen in the water and, consequently, the low rate of oxygen transfer, making the natural air-water interface insufficient (Tchobanoglous et al., 2014d). That does not mean it is impossible to utilize the oxygen already in the air in biological treatment systems. The modern trickling

filter with plastic packing material is designed with 90-95% of the volume in the tower to consist of void space. The void space maintains air circulation to provide the organisms with adequate oxygen from the natural draft (Tchobanoglous et al., 2014c). However, this process is often coupled with blowers to increase the amount of oxygen in the void space because of the high oxygen demand. Oxygenic photogranules are an attached growth process but do not require aeration to supply oxygen to the system. The photosynthetic activity of cyanobacteria provides oxygen in the system.

2.2 Cyanobacteria

Cyanobacteria (also known as the blue-green algae and often referred to as microalgae) is comprised of a large, ecologically, and morphologically heterogeneous group of oxygenic, phototrophic bacteria (Madigan et al., 2019a). Cyanobacteria has significant relevance in the evolution and formation of today's atmosphere by converting the once anoxic atmosphere into the oxygenated atmosphere on Earth today (Madigan et al., 2019a). The climate changing was a consequence of cyanobacteria's ability to photosynthesise and produce oxygen, leading to the Great Oxygenation Event (Chisti, 2018; Madigan et al., 2019a). Today many may associate algae with adverse effects such as eutrophication of lakes (Harper, 1992). However, cyanobacteria can be a useful resource when used in biotechnology, either in the production of biofuel & bioenergy (Tibocha-Bonilla et al., 2018), or to be used in water and wastewater treatment like oxygenic photogranules (Abouhend et al., 2018; Ouazaite et al., 2021; Tenore et al., 2021).

Cyanobacteria are phototrophs, and thus they have chlorophylls and pigments. These traits make them different from chemotrophs because phototrophs do not require chemicals as a source of energy. They convert light energy into adenosine triphosphate (ATP). Some photosynthetic reactions can be anoxygenic, but all cyanobacteria and algae do oxygenic photosynthesis, which produces oxygen (Madigan et al., 2019e). Of all the prokaryotes, cyanobacteria are the only one that can use water as an electron donor, photons for energy, and CO2 as a carbon source. Some strains can also fixate nitrogen from air (Heidorn et al., 2011). These attributes make them very suitable for use in wastewater treatment.

2.2.1 Growth, metabolism, and motility

Cyanobacteria is a part of the phytoplankton community. Phytoplankton cells carry essential biomolecules like nucleic acids (DNA and RNA) and (ATP). Common for all these molecules is the need for a fixed set of chemical elements to construct them. Synthesizing proteins,

carbohydrates, and lipids constrain the chemical makeup of the cells. The chemical composition may vary among phytoplankton species. However, for plankton, in surface waters of different oceans, there is a degree of uniformity, and the ingredients used are always similar (Tyrrell, 2001). Therefore, there is possible to find a ratio of the essential chemicals present per average phytoplankton biomass produced. This was done by Redfield (1934); he found that for every 106 atoms of carbon, there are 16 atoms of nitrogen and 1 atom of phosphorous. The 106C:16N:1P ratio is the Redfield ratio named after the scientist who discovered it. From this ratio, we get the idealized chemical reaction in equation 1. This average can be used as a reference when looking at nutrients that may limit growth for phytoplankton species like cyanobacteria (Tyrrell, 2001). Light is the energy source used to drive this biological reaction and produce biomass in cyanobacteria.

$$106CO_2 + 16HNO_3 + H_3PO_4 + 78H_2O \rightleftharpoons C_{106}H_{175}O_{42}N_{16}P) + 150O_2 \qquad \text{Equation (1)}$$

Cyanobacterial photosynthesis resembles the photosynthesis seen in other oxygenic eukaryotes like plants and algae, but they do have some traits that make them unique. Even though systems in photosynthetic organisms have a lot of similarities, one of the areas where they exhibit the greatest dissimilarity is the mechanisms that harvest and distribute energy to their photosystems. Cyanobacteria use both reaction centres photosystem I and photosystem II (Figure 3) for light-driven mechanisms to operate electron transfer from H_2O to NADP+, same as most other eukaryotic organisms (Dmitriy et al., 2013). One characteristic of cyanobacteria different to most algae and plants is that they only produce chlorophyll *a*, not chlorophyll *b/c/d*. This is because cyanobacteria have phycobilisomes that are bound at the surface of the photosynthetic membrane which can account for 60% of the overall protein mass (Mazel & Marlière, 1989). Phycobilisomes are the light-harvesting complex in cyanobacteria composed of various chromophorylated phycobiliproteins, in addition to nonchromophoric and hydrophobic polypeptides termed linkers (Singh et al., 2015). It is the phycobilisomes that give cyanobacteria their unique blue-green colour. The phycobiliprotein complexes absorb much light in the visible spectrum. The extended absorbance capacity is beneficial for the organisms when harvesting energy from light (Shively et al., 2009). This may explain why cyanobacteria are known to grow in a wide range of light intensities, from shallow levels of intensity (1 µmolePAR·m-2·s-1) to what is considered bright light surroundings (700 µmolePAR·m-2·s-1) (Stal, 1995; Tandeau de Marsac & Houmard, 1993; Vézina & Vincent, 1997).

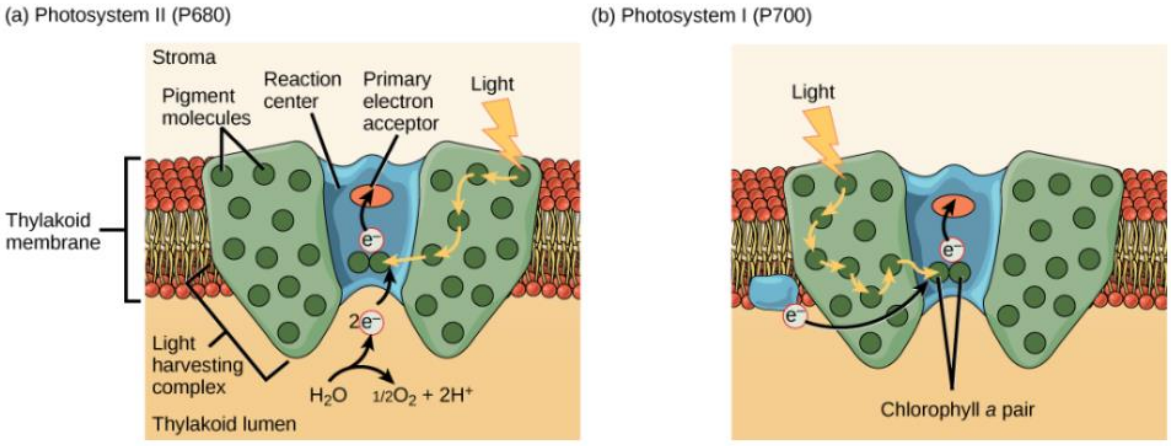

Figure 3: Illustration of the general mechanisms involved in (a) photosystem II and (b) photosystem I. Illustration from (Carter & Lumen-Learning, 2017)

Cyanobacteria also move depending on the light conditions. Using their motility, they advance into more suitable light environments (Nultsch & Häder, 1979; Sgarbossa et al., 2002). This feature seems to be an important one in granule formation. There has been reported evidence that suggest that this activity is involved in structuring the cyanobacterial mats and the ball-like structure we see in cyanobacterial aggregates like granules (Garcia-Pichel & Castenholz, 2001; Walter et al., 1976). A more recent study Ouazaite et al. (2021) used an experimental and modelling approach to quantify phototrophic O2 production and O2 diffusion in filamentous photogranules as well as heterotrophic O2 consumption. Here they found that spatial distribution between the heterotrophic and phototrophic communities did not significantly impact photogranule activities. What did have a significant impact was light penetration into the photogranule, where the photosynthetic response to light was detectable almost immediately. This highlight the fact that the photosynthetic activity in cyanobacteria may be the biggest contributor to the morphology of the granules because activity in the granules is almost non-detectable during light attenuation.

2.3 Methanotrophs

According to the intergovernmental panel on climate change's fifth assessment report Stocker et al. (2013): "concentrations of CO_2, CH_4, and N_2O now substantially exceed the highest concentrations recorded in ice cores during the past 800,000 years". The report also says that methane concentrations in the atmosphere have increased significantly since 1750 due to anthropogenic effects. The concentrations measured in 2011 was 1803ppb which exceeds the pre-industrial era by about 150%, this is calculated to account for 17% of all global warming (Stocker et al., 2013).

A key organism for reducing the methane in the biosphere is methanotrophic bacteria/archaea also called methanotrophs. Methanotrophs are a subset of a diverse group of microorganisms called methylotrophs. Methylotrophs are capable of growth on compounds containing only one carbon bond (C_1). What is unique about methanotrophic microorganisms is that they use methane as a substrate for growth. Not all methylotrophs are capable of oxidizing methane (Hanson & Hanson, 1996).

Methanotrophs ability to oxidize methane give them diverse habitats and they are found in a variety of ecosystems: the open ocean (Tavormina et al., 2017), soils (Li et al., 2021; Yun et al., 2015), in association with plant roots (Rahalkar et al., 2016) and leaf surfaces (Iguchi et al., 2013), and at the oxic interface of many anoxic environments (Madigan et al., 2019b; Milucka et al., 2015; Oswald et al., 2016). Soil containing aerobic methanotrophs does consume atmospheric methane and is, therefore, a vital biological sink for atmospheric methane. At the oxic interface of anoxic environments found in wetlands, lakes, and sediments, the methanotrophs play a crucial role in the global carbon cycle by converting methane to cell material and carbon dioxide before it can reach the atmosphere (Iguchi et al., 2013; Madigan et al., 2019b). The activity seen by methanotrophs in the global carbon cycle can be replicated and used for bioremediation in several ways (Singh & Singh, 2017). The problem for bioremediation purposes is that methane is extremely volatile. Therefore, the challenge is to oxidize the methane before it escapes into the atmosphere. One way of oxidizing trapped methane before volatilization in terrestrial bioremediation is designing a methane oxidizing soil layer above landfills which usually vent directly to the atmosphere (Park et al., 2002). This study will test an aquatic bioremediation method by oxidizing the methane dissolved in water of an anaerobic treatment process before it escapes into the atmosphere using an air shut system.

2.3.1 Growth and metabolism

Methanotrophs are a variety of oligotrophic organisms consisting of both bacteria and archaea. Some species can grow aerobically, and some species grow anaerobically (Hanson & Hanson, 1996). Which population thrive depends on the available terminal electron acceptor (TEA). Aerobic methanotrophs are typically driven by methane oxidizing bacteria from members of the *Methylococcales*. Anaerobic methanotrophy are typically driven by members of the anaerobic methanotrophic archaea (ANME) (Case et al., 2017). When oxygen levels become scarce anaerobic methanotrophs take over, they then exploit alternative TEAs, i.e., sulfate

(equation 2), nitrate, nitrite, and metals for oxidizing methane (Case et al., 2017; Madigan et al., 2019b).

$$CH_4 + SO_4^{2-} \rightleftharpoons HS^- + HCO_3^- + H_2O \quad \text{Equation (2)}$$

At elevated oxygen levels, aerobic methanotrophs thrive. This is a more efficient way to break down CH_4 because of the availability and highly electronegative structure of O_2 (Cai et al., 2016; Case et al., 2017) (equation 3). The elevated oxygen levels may be a result of photosynthetic activity from organisms in anoxic interfaces which leads to more aerobic methanotrophic activity (Milucka et al., 2015; Oswald et al., 2016). This is an attribute that may be useful in the OPGs due to anoxic interfaces that may be present within the granule matrix, especially during light attenuation.

$$CH_4 + 2O_2 \rightleftharpoons CO_2 + H_2O \quad \text{Equation (3)}$$

The necessity for O_2 as a reactant in the first oxygenation of CH_4 can explain MOBs obligatory aerobic behaviour. Aerobic methanotrophs possess a crucial enzyme, methane monooxygenase. The enzyme catalyses the incorporation of oxygen from O_2 into CH_4, forming methanol (CH_3OH) (Miyaji, 2011). The electron flow in the membrane establishes the proton motive force and fuels ATPase (Madigan et al., 2019b). The MOBs assimilate most of their cell carbon from the C_1 compound formaldehyde (CH_2O), how much depends on the pathway used (Madigan et al., 2019c). There are two main pathways for MOB metabolism – the serine pathway, and the ribulose monophosphate pathway.

The serine pathway

In the serine pathway, one molecule of CO_2 and one molecule of CH_2O produced from the oxidation of CH_3OH react to synthesize acetyl-CoA. Synthesizing acetyl-CoA costs energy and reducing power provided by two molecules of ATP and NADH, respectively (equation 4). In the course of the serine pathway, several enzymes from the citric acid cycle are employed, and one enzyme is unique for the pathway *serine transhydroxymethylas* (Madigan et al., 2019c).

$$CH_2O + CO_2 + 2NADH + 2ATP \longrightarrow_{\sim CoA} acetyl{\sim}S{\sim}CoA + H_2O \quad \text{Equation (4)}$$

The ribulose monophosphate pathway (RuMP)

RuMP provides an alternative pathway for the incorporation of C_1 in methanotrophic metabolism. For generating new cell material, all the carbon is derived from CH_2O, which makes this pathway more energy efficient (equation 5). The efficiency comes from CH_2O being at the same oxidation level as the cell material. Consequently, there is no need for reducing power, which means that all the NADH needed for the oxidation of CH_4 can further be oxidized in the electron transport chain (Madigan et al., 2019c).

$$3CH_2O + ATP \longrightarrow glyceraldehyde - 3 - P \qquad \text{Equation (5)}$$

These two pathways classify methanotrophs. Methanotrophs divide into three different categories: type I, type x, and type II. All types are gram-negative bacteria related to the Proteobacteria, but type I and type X affiliate with the gamma subdivision, whereas type II are in the beta subdivision (Hanson & Hanson, 1996). Type I and type X methanotrophs use the ribulose monophosphate pathway when assimilating formaldehyde. They seem to be dominant in niches where there are low concentrations of methane and nitrogen levels are relatively high (Hanson & Hanson, 1996). Type II employs the serine pathway for their formaldehyde assimilation. Contrary to type I and X, type II are most found in environments with relatively high concentrations of methane, low concentrations of dissolved oxygen, and limiting nitrogen supply (Hanson & Hanson, 1996). All types have advantageous traits in wastewater treatment. In the PBR for this thesis's experiment at first, there will be elevated methane levels in the reactor favouring type II. However, running in SBR mode, most methane will probably be digested before new media is introduced. Therefore, it will also be favourable to have type I and X methanotrophs that thrive with low methane levels. Conclusively, all types of methanotrophs should be present in the OPGs to reduce the CH_4 as efficiently as possible.

2.4 Consortium & syntrophy

A *consortium* can be defined as a two- or more membered association of microbes, usually living in an intimate symbiotic fashion (Madigan et al., 2019b). There can be more than one reason why bacteria flocculate together and form aggregates/mats in consortiums. One reason for this behaviour is that different organisms can benefit from each other when trying to break down recalcitrant compounds. A review done on interspecific interactions in mixed microbial cultures by Mikesková et al. (2012) highlighted particularly efficient biodegradation of polycyclic aromatic hydrocarbons, synthetic dyes, polychlorinated biphenyls, and other

organic pollutants. The variety of degradative enzymes innate to each consortium member combines to produce catabolic enzyme activity jointly among the members in the consortium. An example of methanotrophs in nature is the oxidation of CH_4 by ANME living in a consortium with Sulphate-Reducing Bacteria in anoxic marine environments (see equation 2) (Madigan et al., 2019d). Sulphate-Reducing Bacteria reduction of sulphate provides an essential TEA for the ANME when oxidating methane (see equation 1). The syntrophy between these organisms plays a vital role in the global carbon cycle as a methane sink.

Another reason for the formation of microbial consortiums is retaining nutrients in nutrient-poor environments. A study done on Himalayan glaciers by Takeuchi et al. (2001) reported that a dark-coloured material called cryoconite accelerates glacier melting substantially. The article describes cryoconite as a "stromatolite-like algal mat, a product of microbial activity on the glacier". The mat contains filamentous cyanobacteria and other bacteria that grows on the ice by entrapping minerals and organic particles in their matrix. Entrapping organic particles and nutrient-rich minerals allows high algal activity despite living on the poor nutrient meltwater from the glacier. Demonstrating that aggregate consortiums like OPGs occur naturally as a response to living in ecological niches where suspended cultures struggle. These mats seem to be important in the ecological niches and bioprocesses of the glaciers in the Himalayas. Glaciers are an excellent example of a problematic niche to live in due to low supply of nutrients. However, OPG-like layered microbial structures are also found in other environments that might have alternative disadvantages like lakes (Boedeker & Immers, 2009) and seawaters (Brehm et al., 2004; Malin & Pearson, 1988).

The definition of a *consortium* fits well with the symbiotic behaviour we see from MOB and cyanobacteria living in the granular media. The cyanobacteria will use its photosynthetic ability to fixate carbon from CO_2 and harvest energy from light to produce oxygen. The methanotrophic bacteria will utilize the oxygen as an electron acceptor when oxidizing dissolved methane in water. This reaction produces CO_2 as the end-product which the cyanobacteria can use to drive the photosynthetic reaction. This syntrophy should contribute to make the systems oxygen supply independent.

2.5 Oxygenic Photogranules (OPGs)

The use of granular biomass for wastewater treatment has been researched since 1980 (Lettinga et al., 1980) but the first patent for oxygenic photogranules came by Park and Dolan in 2015 (Park & Dolan, 2015). The idea for the patent came from observing the transformation of

activated sludge into a granular structure. The activated sludge came from an urban wastewater treatment plant. Wastewater was incubated at room temperature in 20mL scintillation vials without mechanical agitation and was exposed to natural light. After several weeks, they discovered a light-driven consortium of microorganisms living on the surface of granules embedded in a matrix of extracellular polymeric substances (EPS), now termed oxygenic photogranule (Park & Dolan, 2015).

In Figure 4 we can see the transformations of photogranules from inoculum to mature activated photogranules in a reactor. It shows how the suspended culture gathers in flocs, forming bigger and bigger aggregates, before becoming an ecosystem, relying on activity from multiple interacting microbial populations to sustain the granule emergence shown in (c) and (d). In the maturation process, net density is increased by compaction. Filamentous cells are lost, but inside the OPGs, precipitation of minerals like calcite (especially in environments with hard water) creates a concentrated granule that can reach densities up to 1.5 kgL^{-1} with a 30% volatile solids content per total solids (Milferstedt et al., 2017a). Calcite is reported by Milferstedt et al. (2017a) to be the mineral precipitated in the centre of biogranules during compaction but there is little research on what is actually inside the core of the OPGs. Because of wastewaters nutrient content, phosphorous and nitrogen minerals like struvite and apatite is likely to be found along with calcite inside the OPG core (Bellier et al., 2006; Desmidt et al., 2015; Rahman et al., 2014). Filamentous granules have a density that more resembles water and have a volatile solids content of more than 70% (Milferstedt et al., 2017a).

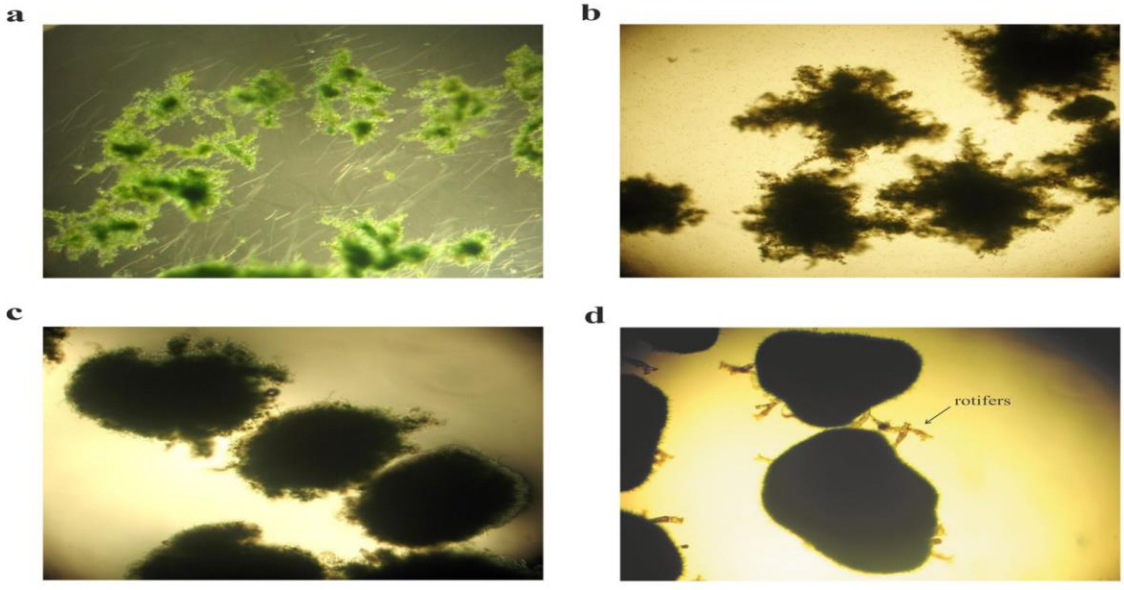

Figure 4: General illustration of how suspended algae flocs together and form granules from (Tiron et al., 2017). Images are taken with 40x magnification light microscopy. (a) show flocking of the suspended culture, (b) aggregates start to form, (c) aggregates are forming to granular structure, (d) mature oxygenic photogranule.

The OPGs vary in size from 0.1-5 mm. They have a settling velocity of 36-360 mh^{-1} (much faster compared to activated sludge flocs 0.6-15 mh^{-1}) and water content between 78-95% (Abouhend et al., 2020; Milferstedt et al., 2017a). They are typically rough spherical structures with a mix of algae and mostly filamentous cyanobacteria. The formation of OPGs is a natural phenomenon that also occurs outside activated sludge systems, like the cryoconite structures on Himalayan glaciers (Takeuchi et al., 2001) mentioned in section 2.3.1. A picture containing granules produced in the reactor from experiments done in this thesis is shown in Figure 5. The picture show how diverse the size distribution is and how some granules appear to be more filamentous than other. The picture is taken halfway into the experiment (day 45 of 89).

Figure 5: Picture of the OPGs produced in the PBR at day 45.

2.5.1 Important characteristics for granule formation

When granules are forming, several biological activities work together in a symbiotic fashion, leading to a finished granule—the morphology and characteristics of the finished granule result from how these different biological activities work together. Therefore, there will be parameters we can engineer to form granules with desired attributes. Consequently, there will also be parameters that will stop granule formation when alternated too much. For example, loading and retention can change the selection of genetic activity in the bacteria and activate undesired biological activity that favours growth in suspended culture rather than staying in the granule aggregates.

In van der Ha et al. (2011) cleaning wastewater using a syntrophic relationship between methanotrophs and phototrophs is studied. The main difference from that experiment to the experiment in this thesis is that they established the relationship in a suspended culture. A noteworthy divergence from the suspended culture in van der Ha et al. (2011) to granulated structure like Abouhend et al. (2018) is that the dominant phototrophs in the suspended culture were algae of the genus *Scenedesmus sp.*, not a cyanobacteria strain. This suggests that there may be a disadvantage in selecting for algae species over cyanobacteria when establishing the reactor environment for OPGs because some algae seem to thrive better in suspended cultures. Later studies of suspended heterotroph/phototroph cultures have also found microalgae (not cyanobacteria microalgae) and algae to be the thriving specie (Li et al., 2022; Wu et al., 2022). This does not mean that having algae and microalgae in the OPGs will cause the granular structure to collapse and detach. The report done by Milferstedt et al. (2017b) shows, using 23S rRNA analysis, that algal sequences are present but played a minor role compared to cyanobacteria in all sequences, with cyanobacteria accounting for 85 ± 18%. An example of this is Abouhend et al. (2018) batch operation experiments which show traces of both algae species *Acutodesmsus* sp. and *Scenedesmus* sp. in the OPGs biomass, but the dominant phototrophic community consist of *Oscillatoriales*, which is an order of cyanobacteria.

2.5.2 Filamentous cyanobacteria in oxygenic photogranules

Filamentous algae are often seen as a problem in aquatic habitats like lakes, rivers and ponds because of the glue-like stringy structure, which forms large clusters (Zhu et al., 2019). However, in the matrix of granular consortiums, this glue-like stringy nature is a desired feature because it helps entrap microbes and nutrients in the granular biomass during early formation of photogranules (Kuo-Dahab et al., 2018; Milferstedt et al., 2017b; Trebuch et al., 2020). The

difference to many filamentous algae seen in nature that form in biological mats is that in OPGs, the mats curve inward and form spherical aggregates in a symbiotic relationship with other microbes. While doing so, they precipitate minerals to the centre of the structure, forming a dense core in which the mats bend around until a spherical structure establishes (Abouhend et al., 2018; Kuo-Dahab et al., 2018; Milferstedt et al., 2017b). Nevertheless, overgrowth of the filamentous cyanobacteria community may impose problems. In an experimental study by Wang and Li (2022) they had different reactor set-ups for tests of low-strength wastewater, one of the reactors did not produce mature photogranules. This was due to an overgrowth of the phototrophic community compared to other bacteria, which leads to a competitive disadvantage for the slow growing autotrophs like ammonia and nitrate oxidisers competing for CO_2 (da Costa et al., 2020; Tchobanoglous et al., 2014c). One problem with this competition was the abundance of the dominant phototroph *Chlamydomonas* (algae) which stop moving in unfavourable environments and shrinks and shreds flagella. This results in less motility of the phototrophic community and makes collision through Brownian motion less likely; this hinders cell aggregation. But another problem was algae blooms caused by cyanobacteria specie *Oscillatoria*, indicating that overgrowth of cyanobacteria needs to be regulated, if not it may lead to bulking sludge as it did in (Wang & Li, 2022). A way to control this behaviour might be to control the light intensity so there is not too much photosynthetically active radiation (PAR) available. There seem to be no study investigating light intensity in correlation with early granule formation as of now.

Milferstedt et al. (2017b) was the first to report the importance of filamentous cyanobacteria in photogranulation. They studied granulation for both hydrostatic- and turbulently mixed conditions. Using white-light and fluorescence microscopy (Figure 6), they found that photogranulation involves the enrichment of motile and filamentous cyanobacteria in both environments. They also saw that filamentous cyanobacteria are most dense in the outer layer of the granules. This observation has later been confirmed in a study by Abouhend et al. (2020) which looked at the growth progression of OPGs (Figure 7). More specifically Abouhend et al. (2020) found that photogranules of <3mm in diameter cyanobacteria was spread over the whole body but granules >3mm cyanobacteria form an outer layer which encloses the non-cyanobacterial core biomass. Using structural equation modelling, they confirmed that in all sizes of photogranules filamentous cyanobacteria was the dominant specie, excluding the core centre where they are basically absent. In Milferstedt et al. (2017b) they also reported similar findings from a 23S rRNA algae/cyanobacterial analysis where algal sequences was a minority

in the 23S rRNA inventories when compared to cyanobacteria which on average represented 85 ± 18% of all the 23S rRNA sequences they did.

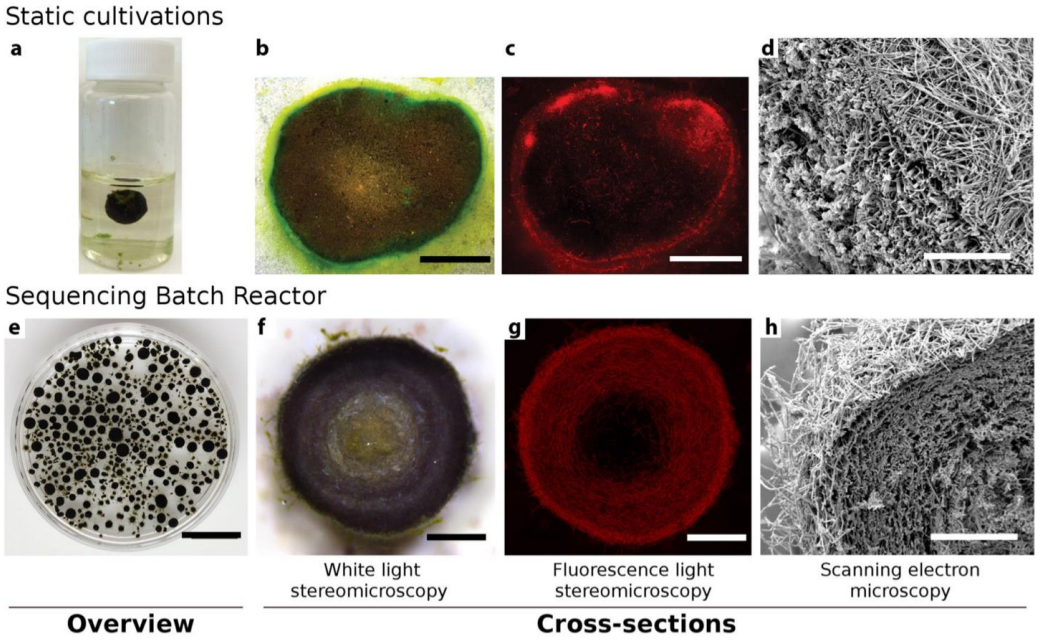

Figure 6: Comparison of granule formation in static cultivation and SBR from (Milferstedt et al., 2017b). (a) & (e) show an overview of the OPG in static cultivation and SBR, respectively. (b) & (f) show results from the white light stereomicroscopy of the OPG in static cultivation and SBR, respectively. (c) & (g) show the results from fluorescence light stereomicriscopy of the OPG in static cultivation and SBR, respectively. (d) & (h) show the results from scanning electron microscopy of the OPG in static cultivation and SBR, respectively.

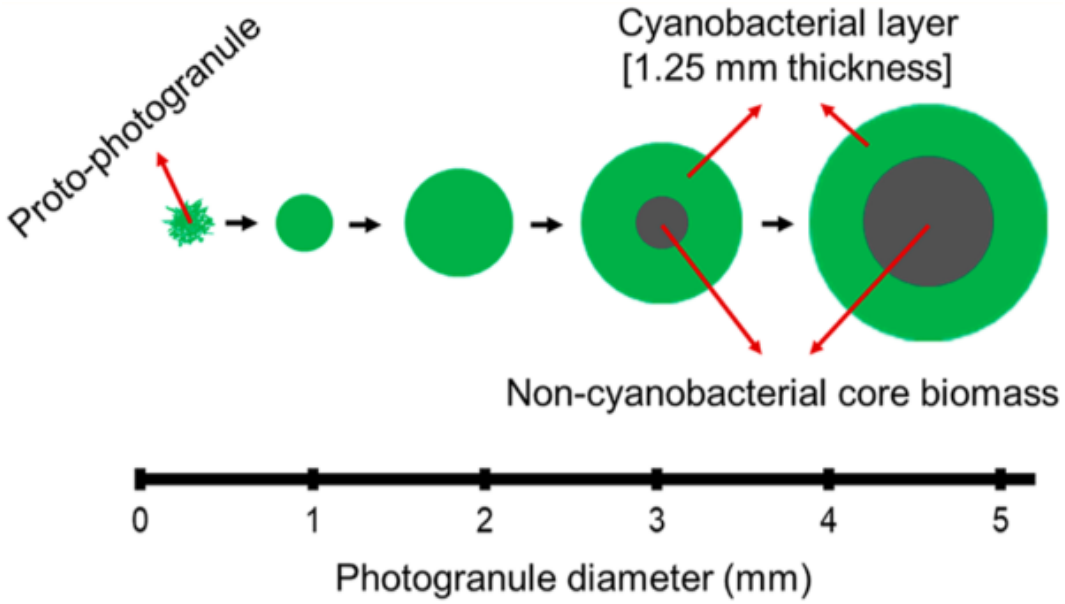

Figure 7: Illustration of the cyanobacterial layer thickness dependant on the size of the OPG from (Abouhend et al., 2020).

Several studies have identified the correlation between cyanobacterial activity and the size of the granules (Abouhend et al., 2018; Abouhend et al., 2020; Milferstedt et al., 2017b; Ouazaite

et al., 2021). The study done by Abouhend et al. (2020) investigated how the photogranules growth occurs with changes to the phototrophic community and granular morphology. The results showed that as the size of the granules increase, filamentous cyanobacteria thrive and become enriched as other phototrophic organisms like diatoms and green algae diminish significantly. The method used for examining the phototrophic community took advantage of characteristics unique to cyanobacteria like production of phycobilin, and cyanobacteria not producing chlorophyll- *b* and *c*. From Figure 8a we see that when the smallest group (<0.2 mm) grew to the size of 0.5-1 mm, the fraction of chlorophyll *a* in the biomass increased from 0.69 ± 0.05% to 1.14 ± 0.08%, while chlorophyll- *b* and *c* fraction shown in Figure 8b and 7c decreased from 0.13 ± 0.01% to 0.12 ± 0.01% and 0.11 ± 0.01% to 0.08 ± 0.01%, respectively. We also see in Figure 8d that phycobilin increased from 2.9 ± 0.19% to 6.1 ± 0.2%, which is a 110% increase in the same size range. Because of these results, they suggest that the enrichment of the phototrophic community up to 0.5-1 mm in diameter was primarily due to cyanobacteria (Abouhend et al., 2020). The study used granules that were formed under hydrostatic shear in a reactor system, but matching results were found for granules of the same size formed hydrostatically (Kuo-Dahab et al., 2018).

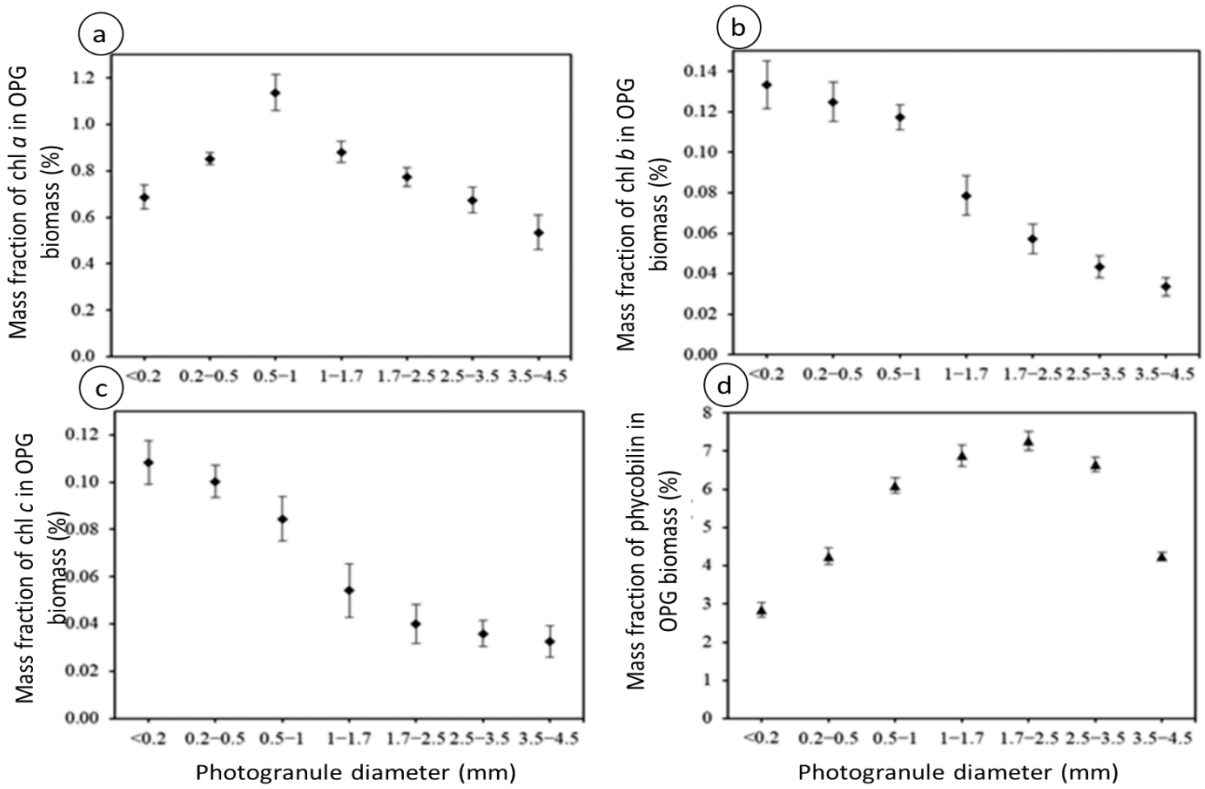

Figure 8: Figure is adapted from the figure presented in (Abouhend et al., 2020) showing the results from their experiments. There are four diagrams, and all y-axes are relative to the same x-axis (photogranule diameter in mm). Diagram (a) show mass fraction of chl a in OPG biomass (%), diagram (b) show mass fraction (%) of chl b in OPG biomass, diagram (c) show mass fraction of chl c in OPG biomass (%), diagram (d) show mass fraction of phycobilin in OPG biomass (%).

2.5.3 Extracellular Polymeric Substances

When microorganisms work together to establish the three-dimensional structural communities known as biofilms there are some essential genetic features that make this possible. One of the arguably most important is the release of a sticky polymeric substance EPS. The composition of EPS consists of extracellular DNA, polysaccharides, and cytoplasmic proteins (Madigan et al., 2019f). The role of EPS in biofilms is to protect and hold attached cells together by bacteria excreting this glue-like component when grazing across the biofilm matrix which entraps other microbes, and nutrients (Kuo-Dahab et al., 2018; Madigan et al., 2019f; Wingender et al., 1999). EPS can be classified into two types known as soluble EPS and bound EPS. Soluble EPS come in the form of soluble macromolecules, slime, and colloids. It is found either in the outside wall of cells or completely dissolved in solution (Laspidou & Rittmann, 2002; Siddharth et al., 2021). Bound EPS are found as capsule, sheaths, and condensed gels, they are closely packed in a two-layer structure with a tightly bound inner layer, and a more loosely bound outer layer (Laspidou & Rittmann, 2002; Siddharth et al., 2021). The combination of the characteristics in soluble and bound EPS create desired features in traditional activated sludge systems because they gather flocs and create aggregates of microorganisms. It results in better settling and decrease the chance of activated sludge being washed out of the system (Nouha et al., 2018)

In oxygenic photogranules EPS have two distinct functions according to (Kuo-Dahab et al., 2018). One of the features provides the same function as in activated sludge systems with entrapment of microbes forming flocs and aggregates. Another feature is in combination with filamentous cyanobacteria. Kuo-Dahab et al. (2018) found that EPS in hydrostatically grown granules is recycled by cyanobacteria in early formation of OPGs. The base-extractable proteins of EPS in the decaying sludge inoculum are recycled for growing the phototrophic biomass. They postulate that in a closed vial sludge anoxic decay must first happen before an oxic environment can prevail. Showing that in hydrostatically grown granules degradation of EPS is as important as generation of EPS (Kuo-Dahab et al., 2018).

2.6 Application and formation in wastewater treatment technology

Bio granules naturally form in specific environments, but they also form in activated sludge aggregates from wastewater treatment. When preparing new granules, activated sludge from a local WWTP is the only substrate needed. How they form is explained following chapter.

The formation of OPGs engineered with methanotrophic activity can classify into three different segments, (1) hydrostatic granule formation (2) seeding hydrostatically formed granules while forming new granules in the PBR (3) methanotrophic bacteria culture enrichment.

2.6.1 Hydrostatic granule formation

Most studies follow Milferstedt et al. (2017b) report for cultivating OPGs. The report presents a low maintenance procedure where granules grow in closed vials exposed to natural light. The vials are not stirred, agitated, or moved in any way. Vials are filled with a small amount of activated sludge, leaving some headspace in the top before being air shut with a rubber stopper. During several weeks' granules form within the vials. One study by Kuo-Dahab et al. (2018) has used the method for static batches described by Milferstedt et al. (2017b) but took activated sludge from two different treatment plants (Amherst and Hadley) and compared them, intending to investigate chlorophyll formation and EPS. How they described the different phases of hydrostatic cultivation concerning chlorophyll gives a structured and detailed insight into what happens in the granule formation of static batches. Amherst WWTP will be referred to as plant A and Hadley WWTP will be referred to as plant B. Domestic wastewater is the primary source for both facilities. Plant A operates with pre-denitrification and intermittent aeration to support biological nitrogen removal, while plant B operates with conventional activated sludge with nitrification. Plant B also receive storm runoff with high nutrient concentration from agriculture.

The formation splits into four phases, (1) The sludge compaction period, (2) the phototrophic bloom period, (3) the main granulation period, (4) the maturation period (Kuo-Dahab et al., 2018). This representation of granule formation concurs with the development of granules done in our lab.

Phase 1: The sludge compaction period

This stage occurs during the first three days of cultivation. Here sludge settles, and then most of the vials start to show sludge rising. The rising in the vials is an indication of flotation of solids by nitrogen gas from denitrification (Henze et al., 1993). While floating sludge height starts to decrease due to further compaction of the granules. The concentration of chlorophyll remains low during this process.

Phase 2: The phototrophic bloom period

Phase 2 typically occurs between 3 and 14 days of the cultivation. The main indicator for this phase is the visual colour change. The biomass changes colour from a brownish sludge look to a green/blue-green algae/cyanobacteria look. Here a more inward construction of the biomass is seen. Chlorophyll increases substantially during this phase, especially chlorophyll *a* (Kuo-Dahab et al., 2018). The relatively high increase in chlorophyll *a* versus chlorophyll *b* suggest that cyanobacteria are the thriving phototrophic organism. This is because there is both chlorophyll *a* and *b* in algae, contrary to most cyanobacteria which do not produce chlorophyll *b*. An average chlorophyll *a/b* ratio for planktonic algae is 2.2 ± 1.2 mgL^{-1} (Wood, 1979), while the cultivation sets in this experiment reached around 7 mgL^{-1} (Kuo-Dahab et al., 2018). These measurements are also consistent with microscopic observations which found that green algae bloom takes place first when filamentous cyanobacteria take over and becomes the dominant phototrophic group. Cyanobacterial dominance happens in phase 2 and stays this way for the remainder of the formation. Light microscopy also found that filamentous cyanobacteria exhibit motility through gliding which spreads EPS by grazing. This concurs with the literature (Kuo-Dahab et al., 2018; Milferstedt et al., 2017b; Sgarbossa et al., 2002; Wingender et al., 1999).

Phase 3: The main granulation period

After 14 to 21 days of cultivation, the main granulation period typically starts. The development of a more spherical/granular structure appears during phase 3. The sides of the consortium contract together, forming a rounded shape. During the experiment done in (Kuo-Dahab et al., 2018) they saw that the two different sludge contracted at a different pace. Sludge from plant A running pre-denitrification contracted faster than sludge from plant B using conventional activated sludge with nitrification. Chlorophyll levels from both plants showed a similar trend so far. However, differences in chlorophyll *a/b* ratio (Figure 9) seem to contribute to the difference in contraction rates among the two cultivations.

Phase 4: The maturation period

The final phase occurs 21-28 days from the beginning of hydrostatic cultivation. From observations, filamentous cyanobacteria decrease their motility significantly during this phase (Kuo-Dahab et al., 2018). In this phase, granules are fully formed and have developed a complex matrix.

Figure 9 shows all the phases in the hydrostatic cultivation of OPGs. The picture of each phase correlates with the phases described in this chapter. Diagrams of chlorophyll levels in the

different phases are also representative for each phase. The figure in total describes the strong correlation between chlorophyll and granulation and the chlorophyll *a/b* ratio show that the phototrophic organism thriving is cyanobacteria. Another study done by Abouhend et al. (2020) also found similar trends in chlorophyll *a/b* ratio for their cultivation which substantiate the importance of cyanobacteria in oxygenic granule formation. The same study also found that as the size of the granules increases from 0.5-1 mm to 3.5-4.5 mm (largest size class of the study), the chlorophyll levels decrease from 1.14 ± 0.08% to 0.54 ± 0.07% respectively. This is an indication of significant phototrophic population reduction as the granule are fully matured. This phototrophic detachment, however, do lead to new granule formation (Ansari et al., 2019; Milferstedt et al., 2017b; Trebuch et al., 2020) as described in the following chapter.

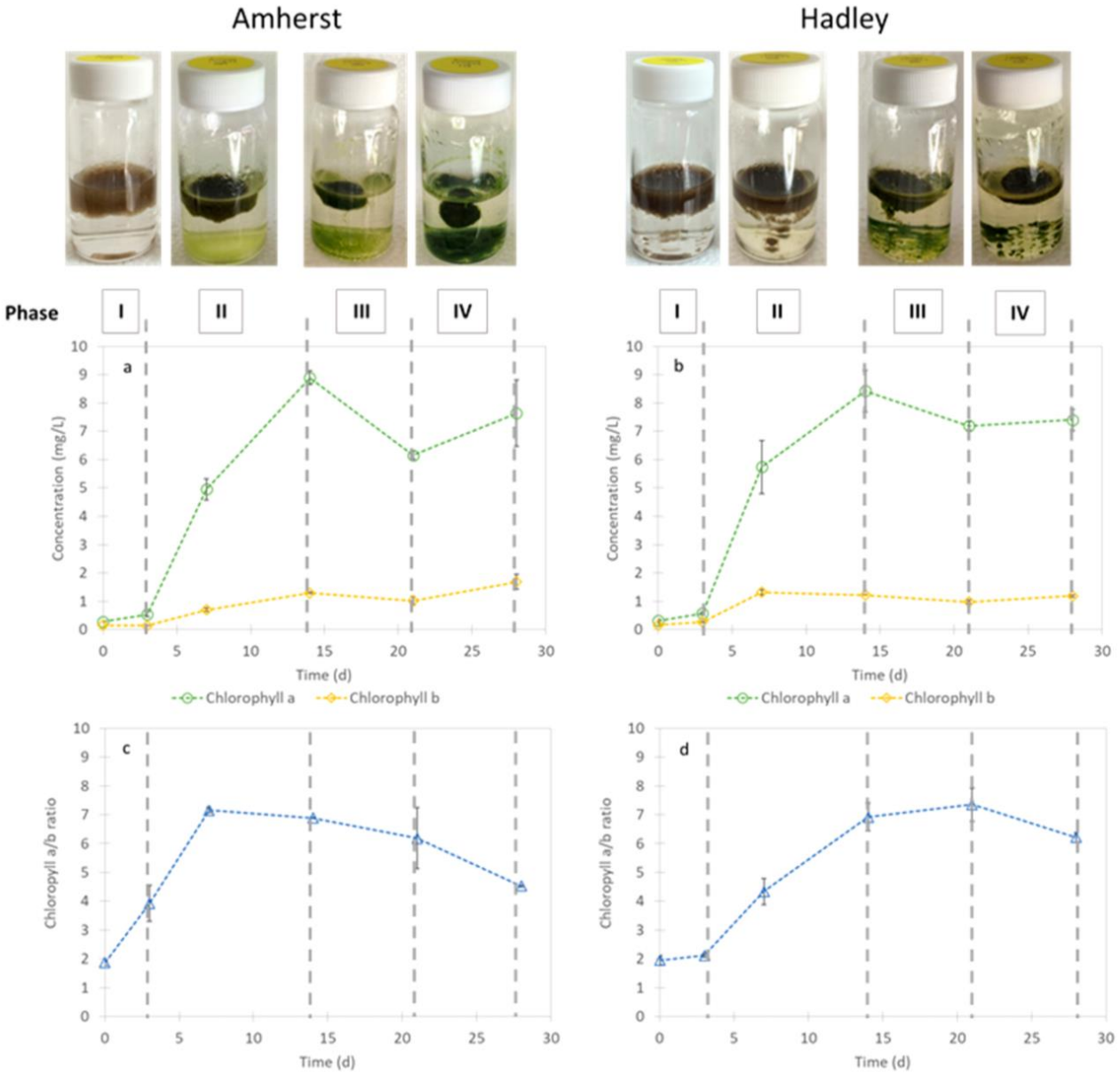

Figure 9: Hydrostatic cultivation of two different activated sludges with picture for each phase relative to the diagrams that show chlorophyll a and chlorophyll b levels as well as the ratio between them. Error bars represent the standard deviation from three replicates for chlorophyll. Figure is from (Kuo-Dahab et al., 2018).

2.6.2 Seeding hydrostatically formed granules in PBR

Matured OPGs explained in "Phase 4" of the previous chapter are ready to be transferred to the reactor system. The granules should not be seeded directly in the reactor. This is because the new system includes many environmental changes that will make the biomass grown in the granular matrix vulnerable. To avoid lysis where the cell disintegrates or other contributors that harm the bacteria culture, we first acclimatise the OPGs in Erlenmeyer flasks filled with the same media as in the reactor (UASB effluent). Granules are seeded into the reactor when acclimatised and ready for the new reactor system. Seeding the reactor with too many granules

a negative impact on the characteristics of the granules (Ansari et al., 2019). Ansari et al. (2019) tested three different seeding densities in three different reactors and found that low/medium-seed systems showed better photogranulation compared to high-seed systems. Low/medium-seed had enhanced production of EPS in their cellular matrix as well as a higher yield in offspring production from mature photogranules (Ansari et al., 2019).

Milferstedt et al. (2017b) explain the progression of photogranules in the SBR system from seeding hydrostatically formed photogranules. They started with less than 70 granules. The granules partially disintegrated in the start-up phase, leaving a lot of new particles in the bulk phase. The particles in the bulk phase started to morphologically reassemble in bacterial flocs. However, unlike regular flocs found in activated sludge systems, they contained microscopically detectable motile, filamentous cyanobacteria. The experimental study in Ansari et al. (2019) also found that for the three first days in batch operation, photogranules gradually disintegrated, which led to the advancement of several new aggregates. Milferstedt et al. (2017b) further go on to explain that the motility could be qualitatively assessed by microscopy. Ansari et al. (2019) reported the same and describe the observed motion of the cyanobacteria as “motile, with flexing and gliding motion” (Ansari et al., 2019). Hydrostatically grown photogranules have such high concentrations of filamentous cyanobacteria in their outer layer (Abouhend et al., 2020) this is likely the reason for why they are in such abundance in the SBR bulk. Milferstedt et al. (2017b) goes on to call these flocs with high concentrations of cyanobacteria “protogranules: the first discernable state of photogranulation” (Milferstedt et al., 2017b). During the first 19 days, biomass in the reactor increased from 1 g of total suspended solids to 3.35 g of total suspended solids (Milferstedt et al., 2017b). The number of photogranules in the reactor grew from 70 to approximately 600,000 (assessed by image analysis). Therefore, it can be concluded that the growth of individual granules is not the only contributor to the increased biomass, but the production of offspring is also a significant contributor (Milferstedt et al., 2017b). After the 19 days Milferstedt et al. (2017b) started wasting biomass which gave the reactor a more balanced biomass concentration. The granules continued to increase in both size and number. After 100 days, the granules maintained a stable distribution of size.

The same results were also found here as in the hydrostatically formed granules (Kuo-Dahab et al., 2018) as in turbulently mixed granules (Milferstedt et al., 2017b) where increase in phototrophic community and chlorophyll *a* increased. Nevertheless, in the granules formed with agitation, they could see a relative difference in the number of phototrophs in the OPGs

depending on size, contrary to statically grown granules where size and phototrophic communities have low variability. The larger granules had fewer phototrophs compared to the smaller ones. Limited light supply may be the explanation for the difference in thickness and phototrophic communities as biomass density inhibits light penetration from the environment (Milferstedt et al., 2017b).

A proposal for how the formation of new OPGs happens in the reactor is shown in Figure 10, which is an illustrative model made by (Ouazaite, 2021). The model describes how cells disintegrate and detach from the OPGs to make new bacterial aggregates and photogranulation possible. The model explains the overall concept presented in (Ansari et al., 2019; Milferstedt et al., 2017b; Trebuch et al., 2020) for granule formation in turbulently mixed reactors with sources from other reviews and studies to subsuduze the theories presented. It also suggests a novel theory (see stripped line in Figure 10) that the broken bits of mature OPGs flocculate with other aggregates made from free-living cells in bulk to create new OPGs.

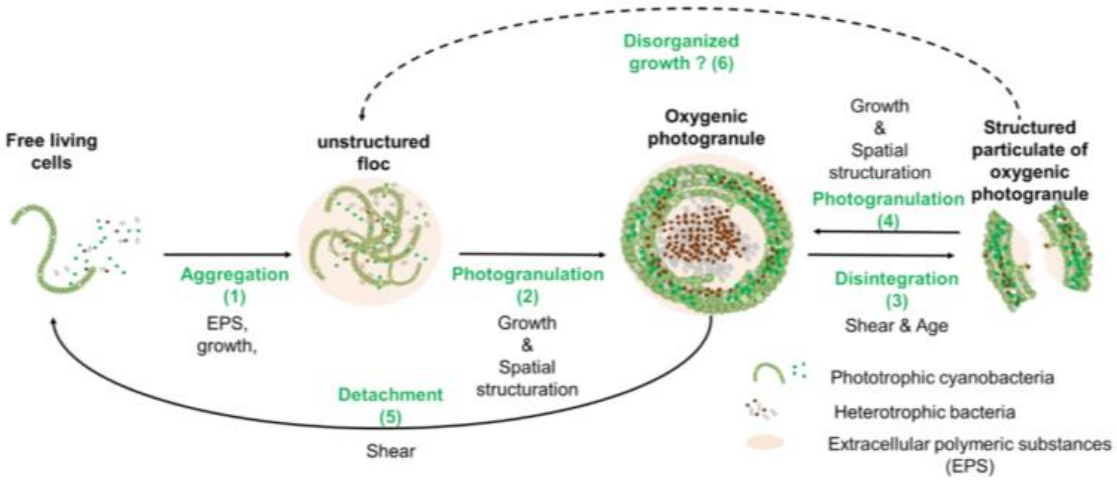

Figure 10: A simplified model presenting the formation of OPGs in agitated reactor systems. The figure consists of six parts with suggested sequence lines between them. The model is adapted from (Ouazaite, 2021, p. 9). In (1) aggregation, we see the transition from free-living cells to unstructured bacterial flocs (Aqeel et al., 2019; Sengar et al., 2018). (2) shows photogranulation with growth and spatial structuration (Joosten et al., 2020; Milferstedt et al., 2017b). In (3) disintegration as a result of shear stress and age (Yuan et al., 2017). (4) Is the formation of fresh granules from the severed parts of the mature granules (Abouhend et al., 2020; Ansari et al., 2019; Trego, 2019). In (5) detachment of mature OPGs which leads to new free-living cells in the bulk (D'Acunto et al., 2019; Solano et al., 2014). And lastly (6) here Ouazaite (2021) propose the idea that there is a potential for the broken bits of the OPGs to gather in unstructured flocs which again may lead to photogranulation.

2.6.3 Maintaining photogranulation in turbulently mixed reactor systems

Since the media used in the PBR comes from the effluent of a UASB, the change to the nutrient loading is limited. The key engineering aspect we can use to select for the genetic activity in the organisms and overall bacterial community after cultivation and enrichment will thus be

the reactor operation mode. One parameter that has a documented impact when cultivating and forming photogranule characteristics is the HRT (Trebuch et al., 2020). The experimental study done by Trebuch et al. (2020) inoculated three lab-scale bioreactors with field samples from different places in the Netherlands and operated them in SBR mode to investigate the effects of HRT. They used field samples instead of seeding already formed granules in the reactor. Consequently, they had to cultivate new OPGs from a suspended culture in the reactor system instead of seeding hydrostatically grown granules. They found that HRT heavily influenced the development of OPGs. When decreasing HRT floccular aggregates formed more rapidly. An HRT of 0.67 d had an assembly time of 11 days, while an HRT of 2 d had an assembly time of 32 days in comparison (Trebuch et al., 2020). They explain these results by looking at separation efficiency and explain that a lower HRT boosted flocculation and granulation by swiftly selecting for biomass with good settling properties. Conclusively, they explain that decreasing HRT improves settling because of selection for well-settling biomass, the critical HRT threshold being 1 day. HRT <1day had settling efficiency >95%, HRT >1day efficiency stayed below 90%. The one thing that remained consistent for all reactors despite changes in HRT and inoculation sample was that the microbial community structure was similar after one month. All had a floccular structure with good separation. Motile filamentous cyanobacteria, together with eukaryotic green algae and EPS producing bacteria, was identified to be the main contributor to the formation of OPGs with good settling properties in all reactors (Trebuch et al., 2020).

2.6.4 Methanotrophs in granules

There seems to be only one documentation of methanotrophs engineered in bio granules. This is an experimental study by Safitri et al. (2021) this also appears to be the only published study that has managed to introduce a novel function to an existing granulated microbial ecosystem. However, there have been previous studies examining the syntrophic relationship between methanotrophs and microalgae in suspended cultures for removing methane in effluents from anaerobic processes, the first supposedly being by van der Ha et al. (2011). Followed by a new study by van der Ha et al. (2012) successfully investigating the possibility of harvesting the energy from the bio flocs after biogas conversion. In all studies the partnership between cyanobacteria and methanotrophic bacteria proved to be an efficient way for removing the dissolved methane without intense aeration for oxygen supply. But van der Ha et al. (2012) concluded that the low availability of dissolved oxygen limited the methanotrophic activity. They further suggested that increasing photosynthetic activity was needed by increasing the

algae to MOB ratio through better design. This problem is be solved in Safitri et al. (2021) study by inoculating MOB in an oxygenic granular structure because dissolved oxygen was always available for the MOB. It also makes harvesting the biomass easier because of the density in OPGs which leads to better settling (Abouhend et al., 2018; Milferstedt et al., 2017a).

Safitri et al. (2021) analysed the microbial community in the photogranules using MiSeq amplicon sequencing. This was done in three phases (1) for the original activated sludge (before methanotrophic enrichment), (2) the inoculum after the enrichment process, (3) continuous reactor operation on three different days. The result from the analysis done by (Safitri et al., 2021) is shown in Figure 11, which shows the relative abundance of different species belonging to the methylotrophic genera in the photogranules. All methanotroph types are represented, the *Beijerinckiaceae* family which are of the Alphaproteobacteria are frequently described as type II methanotrophs. All sequences containing *Beijerinckiaceae* were of the genus *methylocystis* which are considered versatile in both oxygen and methane requirements (Knief, 2015). Type II methanotrophs typically perform well with low levels of dissolved oxygen, but *methylocystis* also perform well with varying methane levels (Hanson & Hanson, 1996; Knief, 2015). Representants for the type I methanotrophs were members of the *methylococcaceae* and *methylomonaceae* (Safitri et al., 2021).

An interesting conclusion by Safitri et al. (2021) from investigating the microbial community was that there was a non-methanotrophic methylotroph community established. This community was likely established due to incomplete oxidation of methane by methanotrophs which led to methanol degradation by methylotrophs, which was also fuelled by O_2 produced by the phototrophic community (Safitri et al., 2021). The established community in Safitri et al. (2021) proved to be efficient for methane removal. When they increased mixing to 125-128 rpm, methane removal exceeded 90%. Increasing the mixing also led to detachment of filaments which results in a morphological change in the photogranules. Granules became smaller and less filamentous; this is desired because increasing the diameter decrease removal rate per photogranule surface area. Consequently, a smaller granule has a more efficient removal rate per surface area.

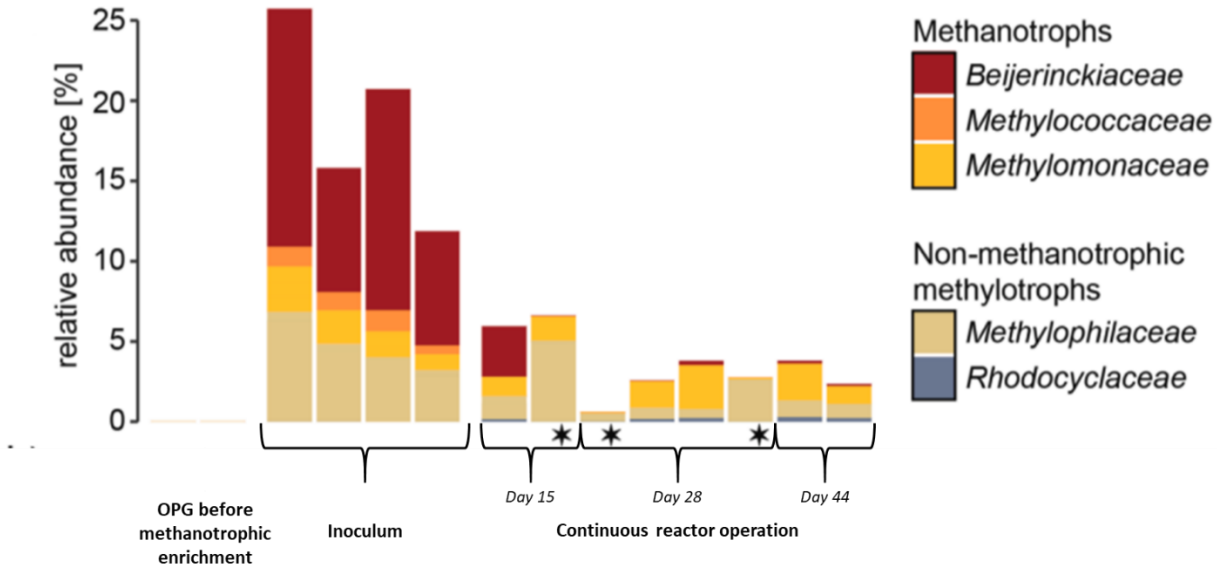

Figure 11: Relative abundance of methanotrophic bacteria in OPGs for three different phases. Before enrichment, after enrichment, and continuous reactor operation on three different days, day 15, day 28, and day 44, respectively.

3 Materials and methods

The overall experimental design for seeding the reactor with OPGs in conjugation with methanotrophic enrichment was done in a three-step process as shown in Figure 12. Firstly (1), the granules were developed and formed in small vials during hydrostatic cultivation. Secondly (2), the granules were transferred to Erlenmeyer flasks for acclimatisation to the UASB effluent before being transferred to the reactor system. When granules had matured in the reactor system, step (3) was adding methanotrophs to the PBR. The seal needed for closing the reactor system from the atmosphere was delayed and did not arrive before there was less than two weeks due to the thesis submission deadline. Therefore, an additional experiment was performed where the enriched methanotrophs was added in six small air shut vials filled with five OPGs and UASB effluent to test the engineered syntrophy between cyanobacteria and MOB. The parameters investigated in the analysis are shown in Figure 12.

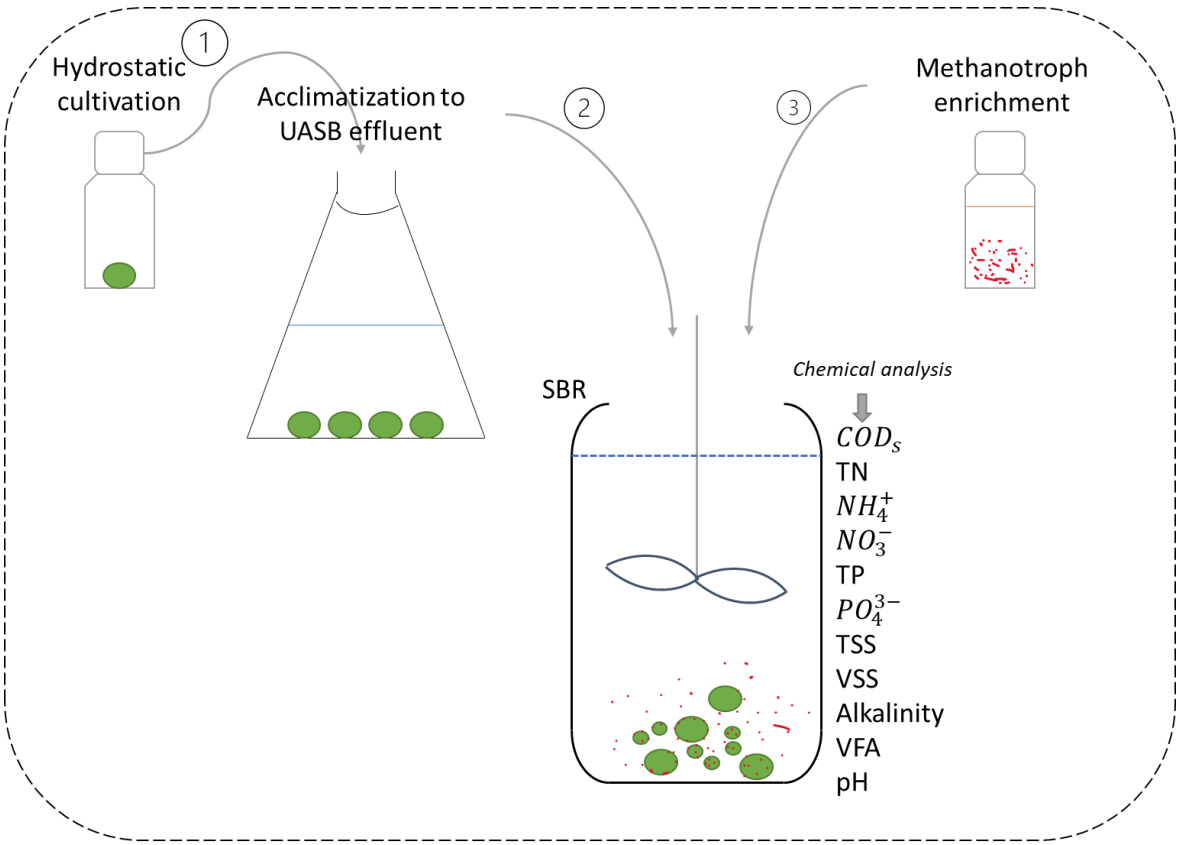

Figure 12: Schematic of the process for forming granules and embedding methanotrophic culture in the OPG consortium. The process is divided in to three steps: (1) hydrostatic cultivation, (2) OPG acclimation, (3) methanotrophic encrichment.

3.1 Oxygenic photogranule development

Hydrostatic cultivation

Cultivation of photogranules were done according to (Milferstedt et al., 2017b) as described in section 2.6.1. Oxygenic photogranules were developed from activated sludge, taken from the aeration basin of IVAR Mekjarvik under static condition without agitation. Light intensity was 106 $\mu mol \cdot m^{-2}s^{-2}$ PAR, fluorescence was measured using a light meter LI-250A (LI-COR, USA) Matured granules were transferred from cultivation vials to Erlenmeyer flasks to acclimate to the UASB effluent.

SBR operating system (without methanotrophs)

The initial seed in the reactor system was about 107 granules. Figure 13 show the reactor setup and illustrate growth of filamentous particles in the bulk before and after decanting. The feed in the SBR came from the UASB and membrane effluent mentioned in the "hippy project". The feed in the UASB was synthetic wastewater; the composition is listed in Table 1. Working volumes of the SBR were 2.4 L, HRT was 12 hours. The cycle for the SBR washout was 2 per day. One cycle involved batch operation with mixing – settling for 1 minute – decanting of settled water – feeding 2 L of new media from the UASB and membrane effluent. The permeate from the membrane did not always produce enough media to refill the SBR reactor volume, and therefore, some effluent from the UASB had to be mixed in directly. The illuminated light intensity was approximately 137 $\mu mol \cdot m^{-2}s^{-1}$ photosynthetically active radiation (PAR), light setup is shown in the picture to the left in Figure 13. Light intensity was measured using a light meter LI-250A (LI-COR, USA)

It should be noted that for the first three inoculations of the OPGs in the PBR, the reactor was operated in a continuous system, not as an SBR system. The working system is the fourth attempt to inoculate the granules in the reactor. Media, light intensities, and granule inoculum quantities remained the same when switching from continuous to SBR for the fourth inoculation.

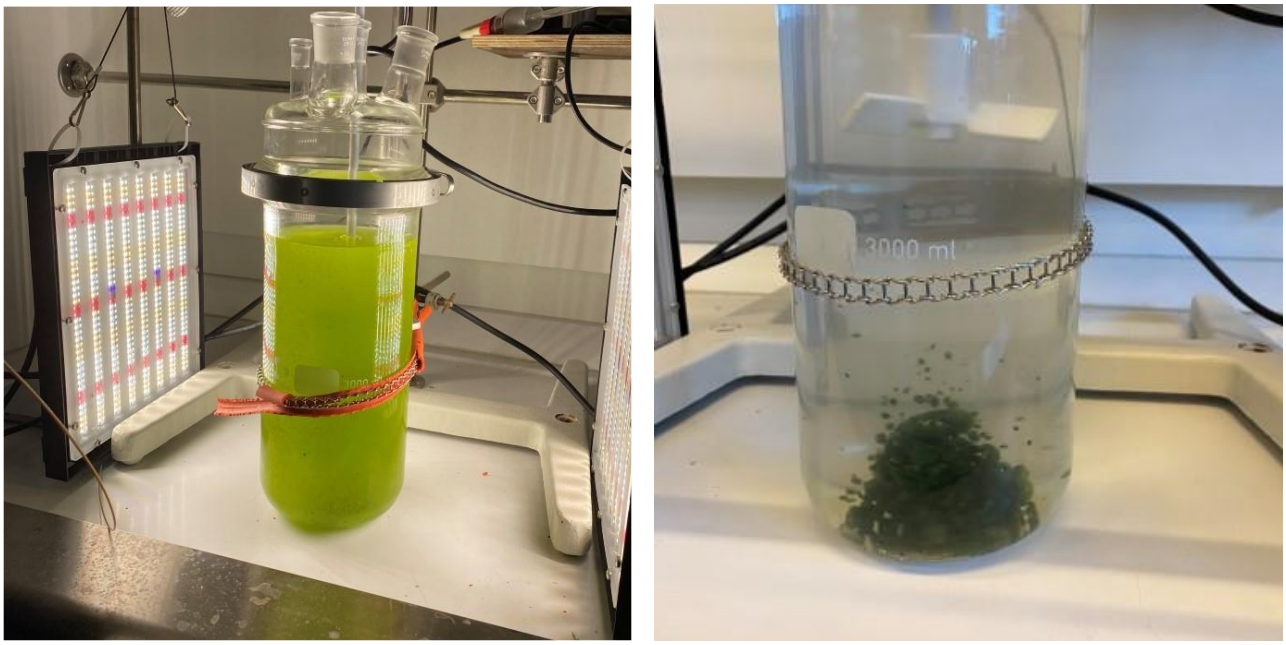

Figure 13: PBR setup in the lab. To the left is a picture of the reactor configuration showing how illumination was integrated on both sides of the reactor, and that we have an overhead stirrer. The left picture shows the content in the reactor before decanting, and to the right is a picture showing the PBR after decanting and refilling of UASB effluent.

Table 1: Ingredients and concentrations of UASB media

Ingredients	**Concentration (mgL^{-1})**
Peptone	17.4
Yeast Extract	52.2
K_2HPO_4	250
KH_2PO_4	100
KCl	40
$MgCl_2$	50
$CoCl_2$	0.4
FeCl2	3.56
$(NH_4)4Mo_7O_{24}$	0.65
$NiCl_2$	0.81
$ZnCl_2$	0.6
$CuCl_2$	0.3
EDTA	0.1
Starch	122
NH_4CH_3COO	50
$NaHCO_3$	400
Glucose	800

3.2 Methanotroph enrichment

Media preparation

A modified nitrate mineral salt solution (Whittenbury et al., 1970) was used as the media for methanotroph enrichment. Modifications to the media were done to resemble the effluent characteristics of an anaerobic process. To achieve this, an increased concentration of phosphate was needed as well as replacing nitrate with ammonium as the nitrogen source. The media was therefore modified according to (Safitri et al., 2021). Media was prepared using tap water. Final composition of the feed was as follows: 150 mgL^{-1} of NH_4Cl, 20 mgL^{-1} of $MgSO_4 \cdot 7H_2O$, 4 mgL^{-1} of $CaCl_2 \cdot 6H_2O$, 5.44 mgL^{-1} of KH_2PO_4, 12.2 mgL^{-1} of K_2HPO_4, 5 mgL-1 of $FeCl_3$, 20 mgL-1 of disodium EDTA, 0.03 ml·L-1 of HCl. From a stock solution, we added 1 mlL^{-1} of trace elements resulting in concentrations of 0.1 mgL^{-1} of disodium EDTA, 0.2 mgL^{-1} of $ZnSO_4 \cdot 7H_2O$, 0.06 mgL^{-1} of $MnCl_2 \cdot 4H_2O$, 0.6 mgL^{-1} of H_3BO_3, 0.06 mgL^{-1} of $Na_2MoO_4 \cdot 2H_2O$, 4 mgL^{-1} of $FeSO_4 \cdot 7H_2O$, 0.04 mgL^{-1} of $NiCl_2 \cdot 6H_2O$, 0.4 mgL^{-1} of $CoCl_2 \cdot 6H_2O$, and 0.02 mgL^{-1} of $CuSO_4 \cdot 5H_2O$.

Procedure

Methanotrophs were enriched under batch conditions from municipal activated sludge from the IVAR wastewater treatment plant at Mekjarvik. For the procedure, 50 mL liquid volume of the media was transferred to 160 mL serum bottles. Next, 10 mL inoculum was added to the media, resulting in a 100 mL gaseous headspace. Enrichments were replicated (4-10 replicates) and incubated with magnetic stirrers for mixing. The serum bottles for all enrichments were sealed with rubber stoppers and capped with aluminium crimp caps. Before the gas injection, headspace gas was mixed by combining about 50 vol% CH_4, 20 vol% CO_2, and 30 vol% O_2. Bottles were then incubated at room temperature.

20 mL of the methanotrophic enrichment culture was transferred from the serum bottles using a serological pipette to a new serum bottle containing 40mL fresh media. This was done every five to seven days. Following each transfer, fresh CH_4 and CO_2 (80%/20% mixture, respectively) were renewed in the headspace. To confirm the composition in the headspace, Agilent 7890B gas chromatography (Agilent, USA) was used. Gas was collected and combined with helium gas in a syringe up to approximately 20 mL (SGE syringe-Europe) before being injected onto the GC with a thermal conductivity detector (Agilent column, 0.32 mm diameter, 30 m length and 0.25 µm film). Helium was used as a carrier gas with a 54 $mL \cdot min^{-1}$ flow rate and oven temperature of 50 °C.

3.3 Engineered OPG and methanotroph syntrophy

Media preparation for glass vials

First, UASB effluent was filled in a 2L reactor; nitrogen was then used to strip down the O_2 levels to below 2 mgL^{-1}. After this, the reactor was filled with CH_4 overnight. The reactor was injected with methane overnight to ensure as much methane dissolved in the liquid media as possible. Figure 14 shows a schematic of the experimental setup for media preparation. There is a headspace in between the liquid and the cap. The cap was tightened and air sealed. As shown in Figure 14, two tubes are attached to the cap. One tube is attached to a Tedlar® gas sampling bag (Sigma Aldrich, Germany). The bag's purpose is to store the methane trying to escape the system when taking samples. Without ventilation, the pressure would not have allowed the liquid to escape the bottle when sampling, and without the bag, methane would have escaped the system while oxygen would have entered the system. The tubes were air sealed using plastic clamps when not in use. COD was tested using test kit described in section 3.4.

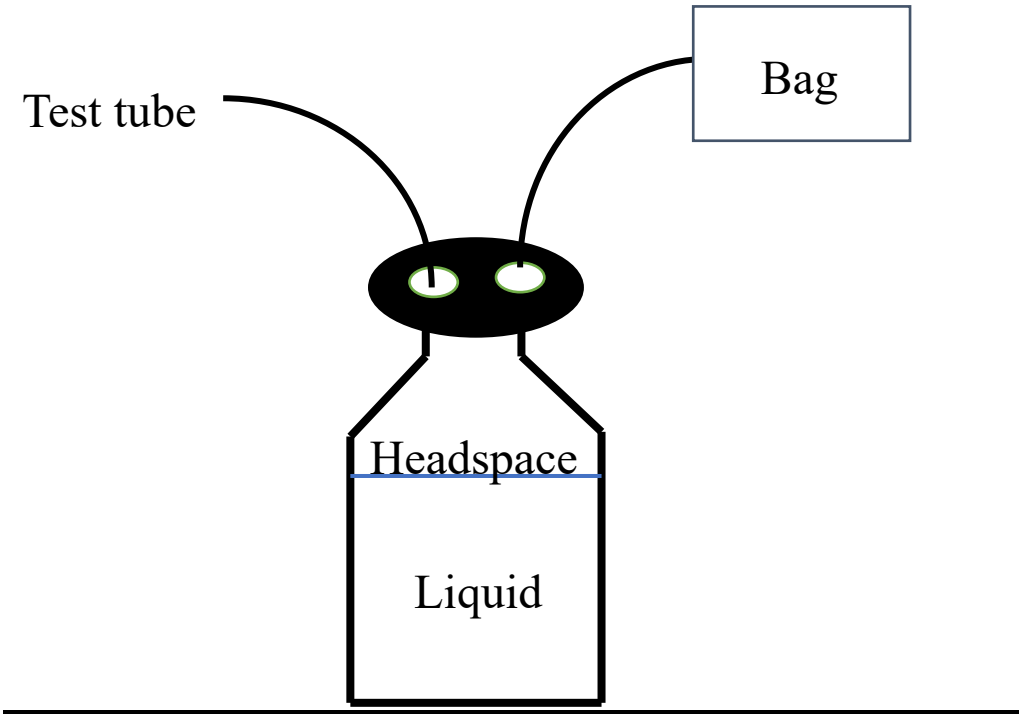

Figure 14: Experimental set up for creating UASB effluent with elevated CH_4 levels

Experimental setup for glass vials

Six glass vials (see Figure 15) air shut with aluminium crimp caps were used as reactors to experiment. Firstly, granules were taken out of the PBR before being washed with tap water.

The vials were then filled with five granules each. Secondly, the prepared media was transferred to the vials using a 0.2 µm filter attached to the syringe to ensure that only dissolved COD was transferred. Lastly, 1 mL^{-1} of enriched methanotrophs in suspension was added. The six small "reactors" was placed on an incubator shaker with 90-100 rpm for agitation with lighting. Light intensity was 106 $\mu mol \cdot m^{-2}s^{-2}$ PAR, fluorescence was measured using a light meter LI-250A (LI-COR, USA); this is roughly the same intensity as light in the PBR. The experiment was conducted over two days. COD, NH_4^+-N, and PO_4^{3-}-P were measured at the end of the experiment using the same test kits described in section 3.5 for further analysis.

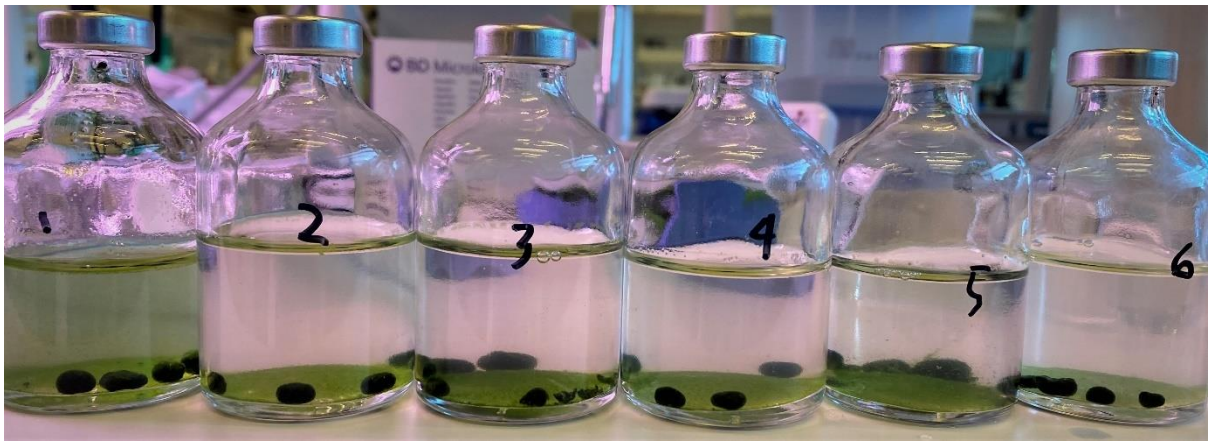

Figure 15: Glass vials used for methanotroph experiment. Each vial contains 5 washed granules, 25 mL^{-1} UASB effluent saturated with CH_4, and 1 mL^{-1} suspended methanotrophs. Picture is taken after the experiment was done.

Methanotroph experiment in PBR

Experiment with methanotrophs were also performed in the PBR once the seal to air shut the reactor arrived, reactor setup with seals and clamps is shown in Figure 16. Methane was dissolved into the media and COD concentration was measured before and after the injection. COD before adding methane was 492 mgL^{-1}, and after adding the methane it was 569 mgL^{-1}. Methanotrophs were then inoculated in the PBR (25 ml of methanotrophs in suspension) and the PBR was sealed from the atmosphere. The next day samples were taken using a 0.2 µm filter attached to the syringe to ensure that only dissolved COD was transferred, and COD was measured once more, now it was 260 mgL^{-1}. To confirm that the methane was consumed by methanotrophs a water sample was taken and put open on the bench for two hours and mixed several times to make sure CH_4 was completely degassed from the liquid. The COD of the degassed sample was measured to be 253 mgL^{-1}. Nutrient removal analysis was also done for this experiment.

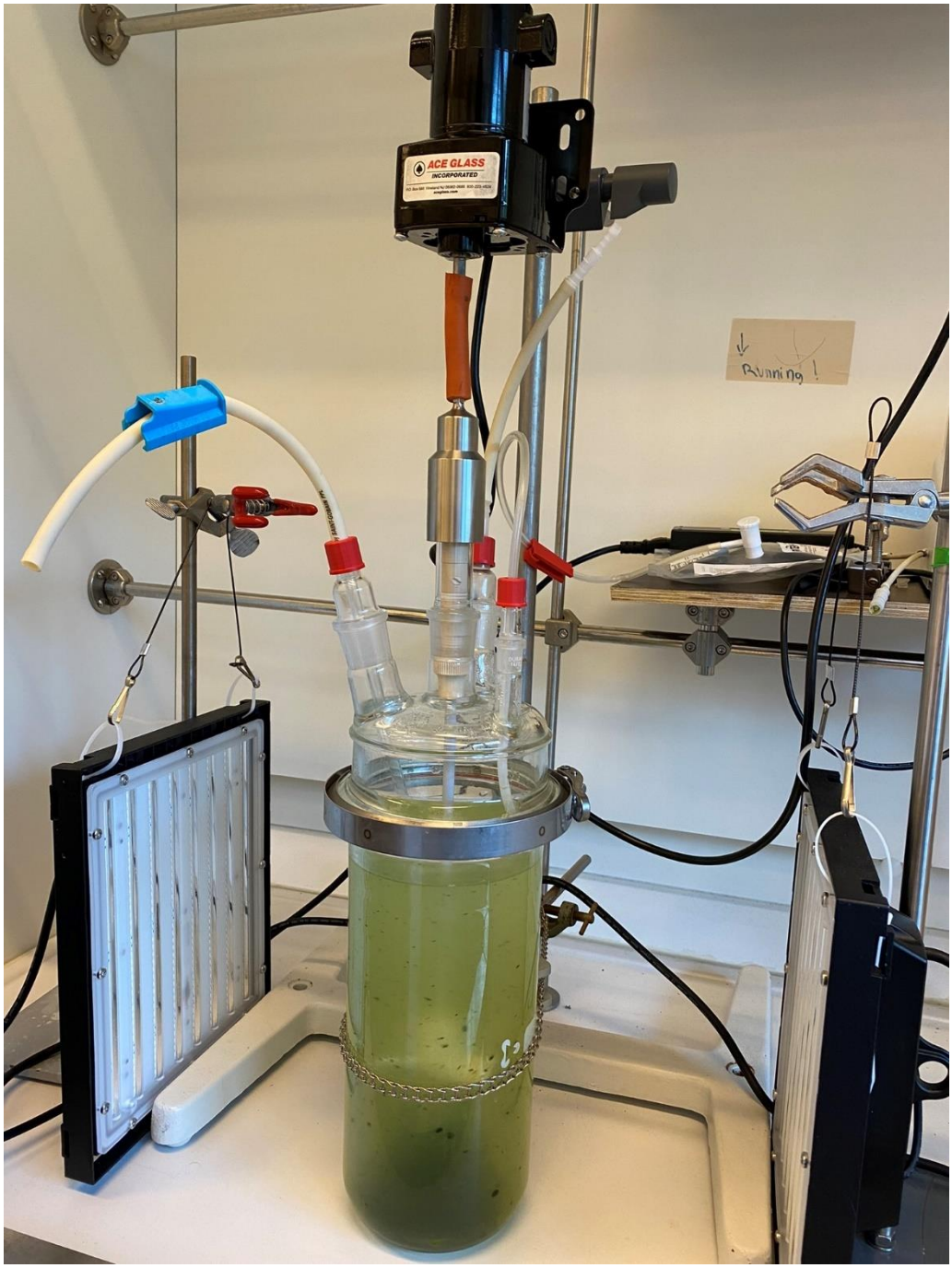

Figure 16: PBR setup with seals and clamps to remove the atmosphere-liquid interface.

3.4 OPG morphology, settling time, and core composition

Settling and diameter of the OPGs were tested for three different OPGs. The granules were classified as small, large, and medium (see Figure 17) based on weight and diameter. Weight was tested using a 5 decimal scale. Diameter of the granules were tested using a petri dish with a ruler underneath. Settling time for each granule was tested in three iterations, using a 500 mL^{-1} graduated cylinder. Each granule was released in the water with a spoon ensuring no extra

velocity from the initial drop. Time was measured from 400 mL to 100 mL (Figure 18). A qualitative X-ray powder diffraction (XRD) analysis was done with help from the material lab at UiS to examine the content of the granule core with a lower detection limit up to 5 % by weight. XRD was done using a D8 Advance Eco diffractometer equipped with a Lynxeye detector (Cu-Kα radiation, 40 kV voltage, 25 mA current). Measuring conditions were set to analyse from 5-90 degrees using a 0,6 mm divergence slit, with a measuring time of 1 degree per minute while rotating the sample continuously during measurement. Phase identification and data visualisation were performed with the software Diffrac.Eva, combined with the PDF-4+ database from the International Centre for Diffraction Data (ICDD).

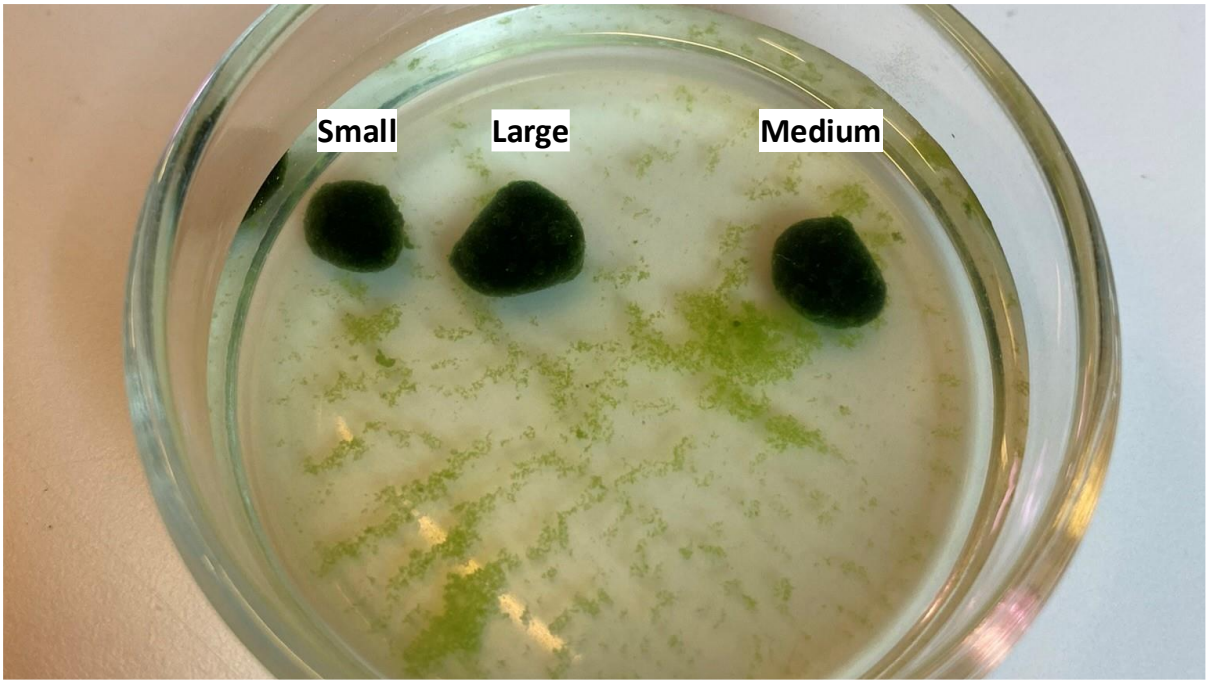

Figure 17: Three granules used for testing sedimentation rate classified as small, large, and medium, respectively from left to right.

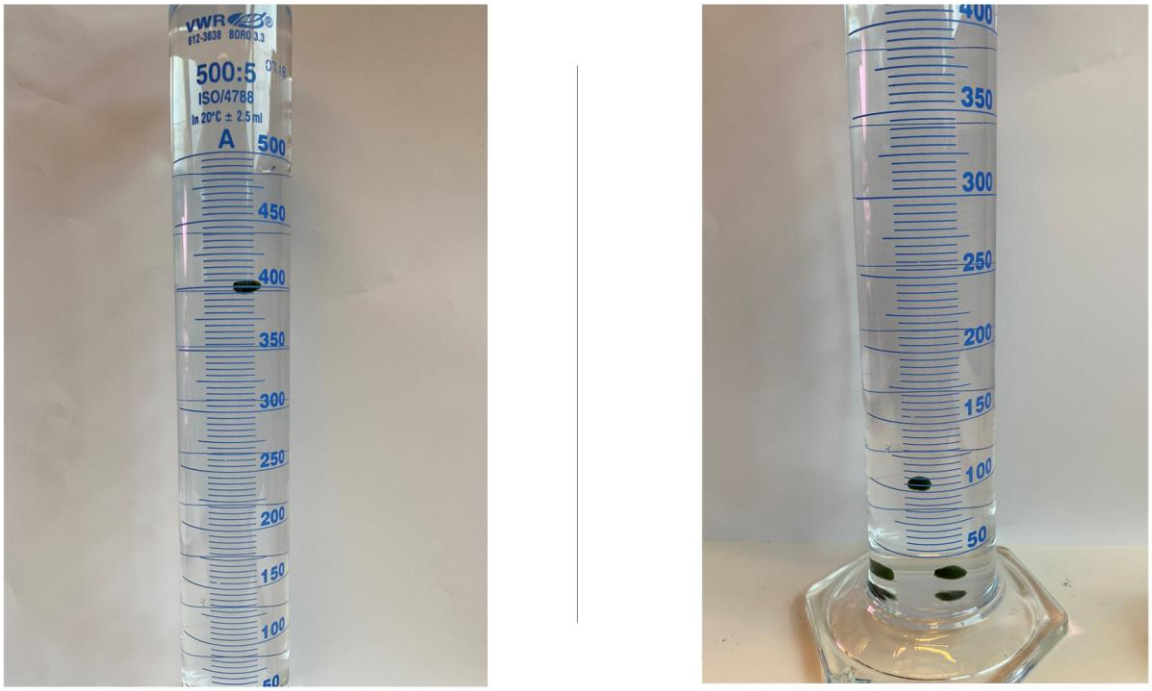

Figure 18: Illustration of the setup for testing sedimentation rate, showing the range of the experiment (400 – 100 mL)

3.5 Analytical methods

Total suspended solids (TSS) was tested using gravimetric analysis standard procedure 2540D (Rice et al., 2012), the pore size of the glass fibre filter was 0.45 µm, diameter was 47 mm (934-AH RTU, Whatman, UK) filter was dried at 105°C for 1 hour after filtering. Filtering was done in duplicates with a blank sample for control. Alkalinity was measured in 50 mL samples containing 20 mL effluent and 30 mL distilled water. Titration was done with a (TitroLine®5000) which also measured pH and temp; acid used when titrating was 40 mM HCL. Total volatile fatty acids and alkalinity were calculated concomitantly using the TITRA 5 software (brouckae@ukzn.ac.za). Titrations were done in duplicates. Test kits were used for determining nutrients and CODs in the influent and effluent. All test kits were from the same producer (Spectroquant® Supelco, Merck KGaA, 64271 Darmstadt, Germany); compounds, kit code and range are presented in Table 2. Test kit for TP and PO_4^{3-} were the same but follow two different procedures. Test kit for CODs was Hg-free. Tests from the kits were done in duplicates.

Table 2: Compounds and range of tests for Spectroquant® test kits

Compound *kit code*	**Test range (mg/l)**
CODs *(09773)*	100-1500
TN *(14763)*	10-150
NH_4^+ *(14544)*	0.5-16.0 NH_4-N
NO_3^- *(14563)*	0.5-25.0 NO_3-N
TP *(14729)*	0.5-25 PO_4-P
PO_4^{3-} *(14729)*	0.5-25 PO_4-P

4 Results

The formation of hydrostatic granules was observed visually as growth happens autonomously. The formation of OPG in the PBR was measured as quantity of granules at different periods. Granules were characterised based on their, weight, diameter, settling time, and content of the granule core. The performance of the granules was analysed based on their removal efficiencies treating the UASB+membrane effluent primarily on COD, methane, and nutrient removal. The correlation between the total nitrogen and nitrate was examined to analyse the nitrogen content. Sampling was only done on weekdays and not done on holidays; thus, the X-axis experimental time was reduced to 60 samples even though the period for experimental analysis in the PBR lasted 85 days. Effluent from the UASB was accumulated in bulk and stored in the fridge (2-4 °C) after 18.03.2022 (sample 28). Stored media from one bulk was empty after four cycles in PBR. Consequently, inlet have sequences (usually 4-days) with unchanged characteristics after this point. The Redfield ratio was calculated for the PBR system to see if the ratio of nutrients available for phytoplankton growth had limitations or not. Calculations for removal efficiencies, organic loading rates, settling time and red field ratio can be found in the appendix.

Performance when enriched methanotrophs culture was inoculated is given for both the glass vial experiment and for the enrichment directly in the PBR. Here also performance was analysed based on their removal efficiencies treating the UASB+membrane primarily on COD, methane, and nutrient removal. The granules for the “glass vial experiment” were taken same day as the experiment (10.05.22). The “methanotrophs in PBR experiment” was not done until 07.06.22 because the delivery of the seal to air-shut the reactor was delayed.

Figure 19 shows temporal progression of photogranulation under static conditions. Activated sludge from the aeration basin of IVAR Mekjarvik transforms into a static oxygenic photogranule when exposed to light in an unagitated environment. For the figure, the same vial was photographed at five different time points.

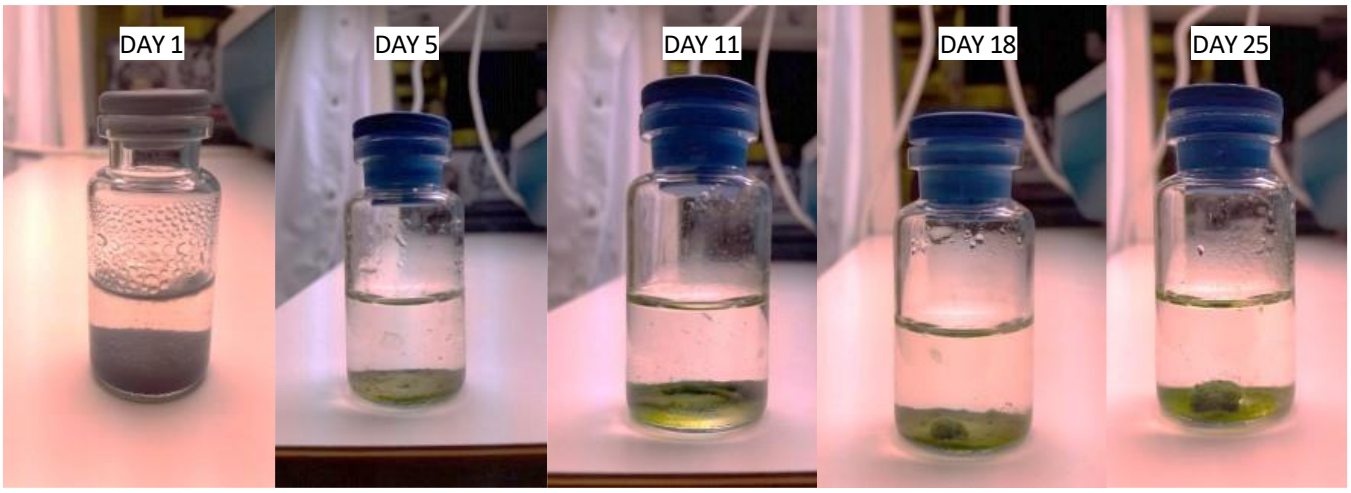

Figure 19: Observed progression of OPGs during hydrostatic cultivation

In Figure 20 quantity of the granules for six different periods is presented. The number of granules decreased by almost 50% for the first weeks (17.02.2022 to 25.02.2022). The following week (25.02.2022 to 08.03.2022) we saw an increase from 55 granules to 76 granules, and every week after that, new granules formed, increasing the amount of OPGs in the reactor to 152 granules in the final week of the PBR experiment (23.05.2022).

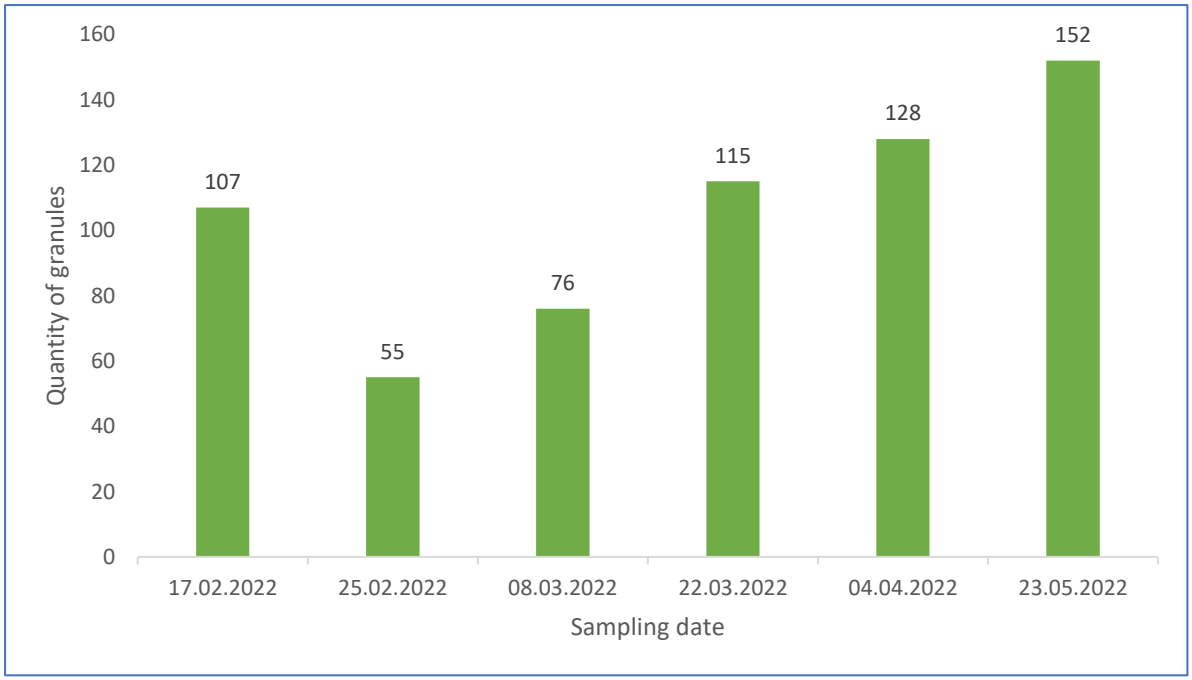

Figure 20: Diagram showing quantity of granules from 17.feb.22 to 25.may.22

Alkalinity in the wastewater fluctuated as seen in Figure 21. For the first 24 days alkalinity was consumed, but then the system started producing alkalinity. Between day 50 and 60 there was an even distribution between consumption and production in the samples.

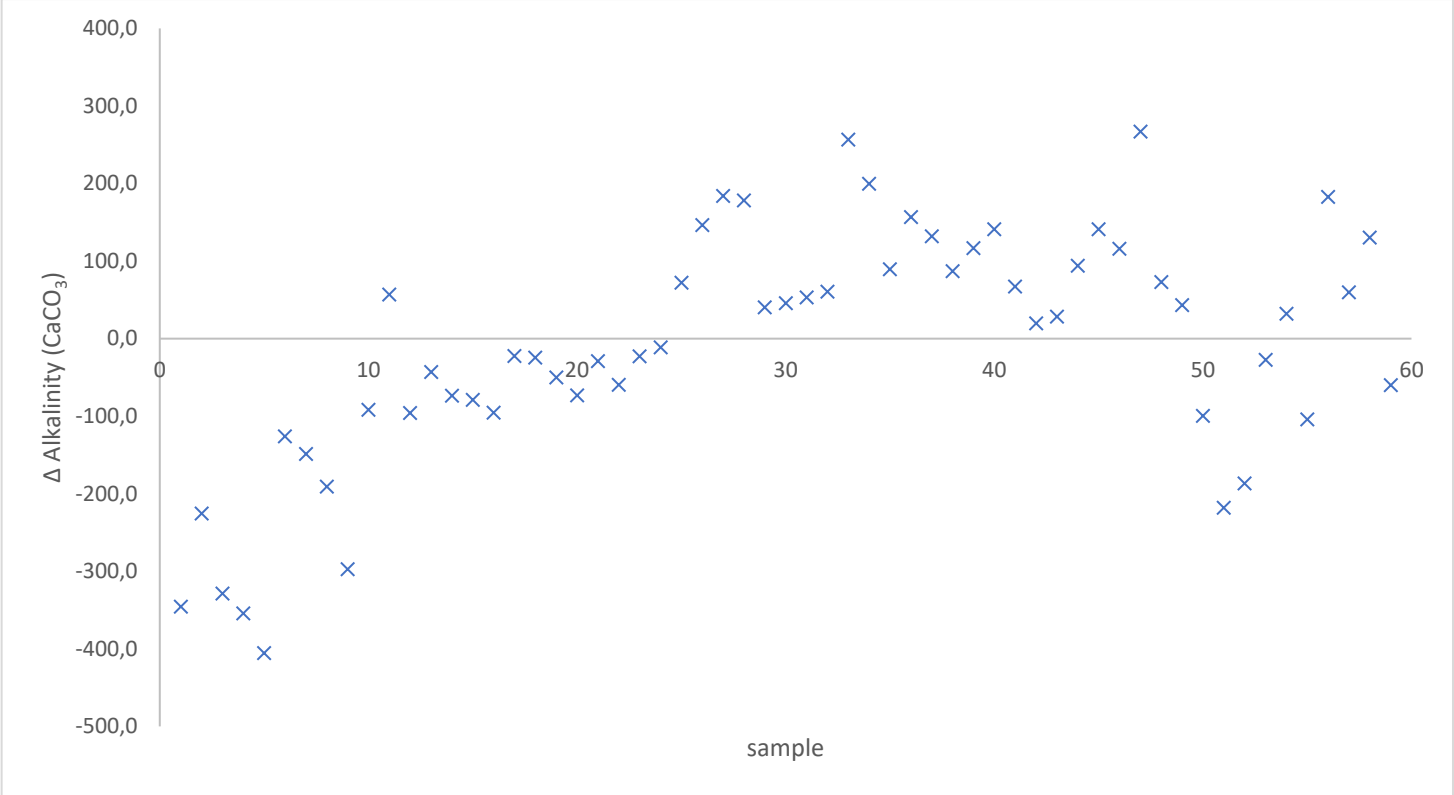

Figure 21: Diagram that shows Δ alkalinty for 59 samples

4.1 Characterisation of OPGs

Table 3 shows weight, diameter and settling time for three different OPGs classified as small, medium, and large, relative to each other (± standard deviation) for three iterations.

Table 3: Weight (mg), diameter (cm), and settling time $m \cdot h^{-1}$ for three different granules (± standard deviation) for three iterations.

Granules	**1 (small)**	**2 (medium)**	**3 (large)**
Weight (mg)	161.4	197.5	233.9
Diameter (cm)	0.8	0.9	1.1
Settling time ($m \cdot h^{-1}$)	396 ± 0.07	432 ± 0.13	396 ± 0.12

There is no TSS in the effluent from the UASB, therefore all TSS accumulated in the effluent is from the PBR system. Since there is no TSS from the UASB the TSS in the effluent should be mostly biomass and therefore have a high content of volatile suspended solids (VSS). TSS and VSS are shown in Figure 22. As shown VSS are almost identical to TSS with an average VSS/TSS ratio of 95,9 %. This symmetry was found during analysis and therefore, VSS was sampled only two times a week.

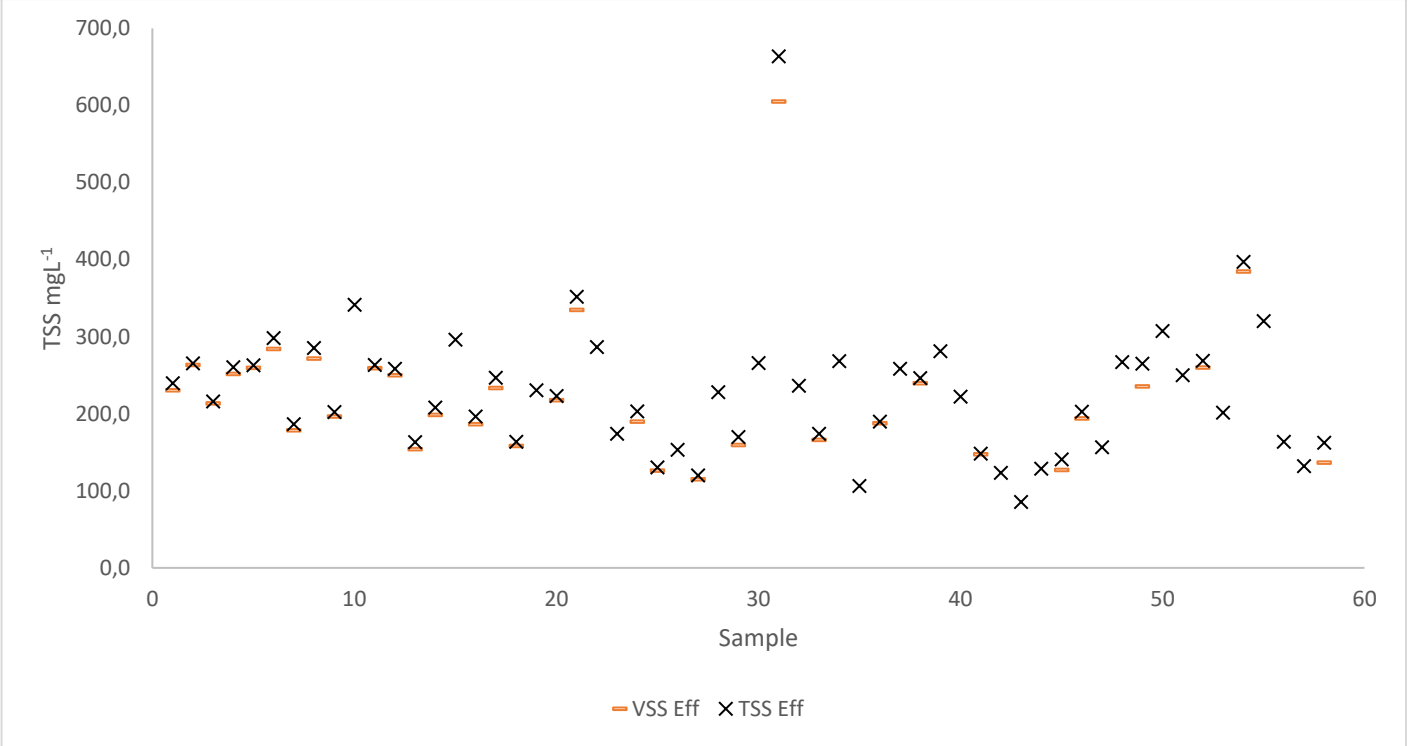

Figure 22: Show the TSS and VSS content for 59 samples

Results from the XRD test matched with the entry from ICCD PDF-4+ database is shown in Figure 23. Similarity in the XRD patterns showed evidence of calcite and apatite, which compared well with fluorapatite from the database. Analysis of the results done by the material lab at UiS gave a 59 %, and 41 %, calcite and apatite content, respectively. Sample of OPGs taken from the reactor is shown in Figure 24 along with the granules picked from the sample which has been cleaned for all filaments and reduced to only the granule core (bald granules).

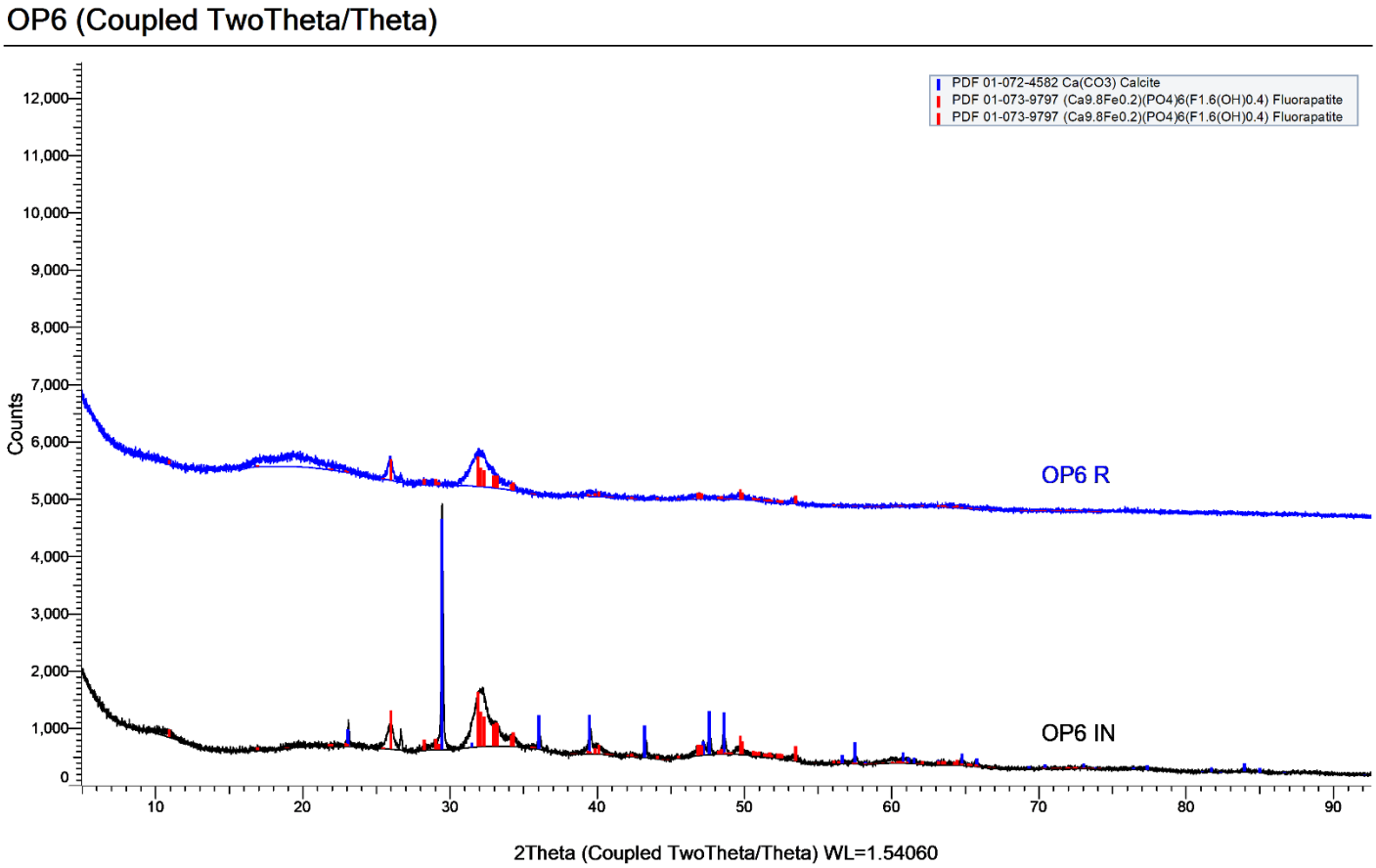

Figure 23: Results from XRD matched with the entry from ICCD PDF-4+ database, showing calcite and fluorapatite present in core of the granules.

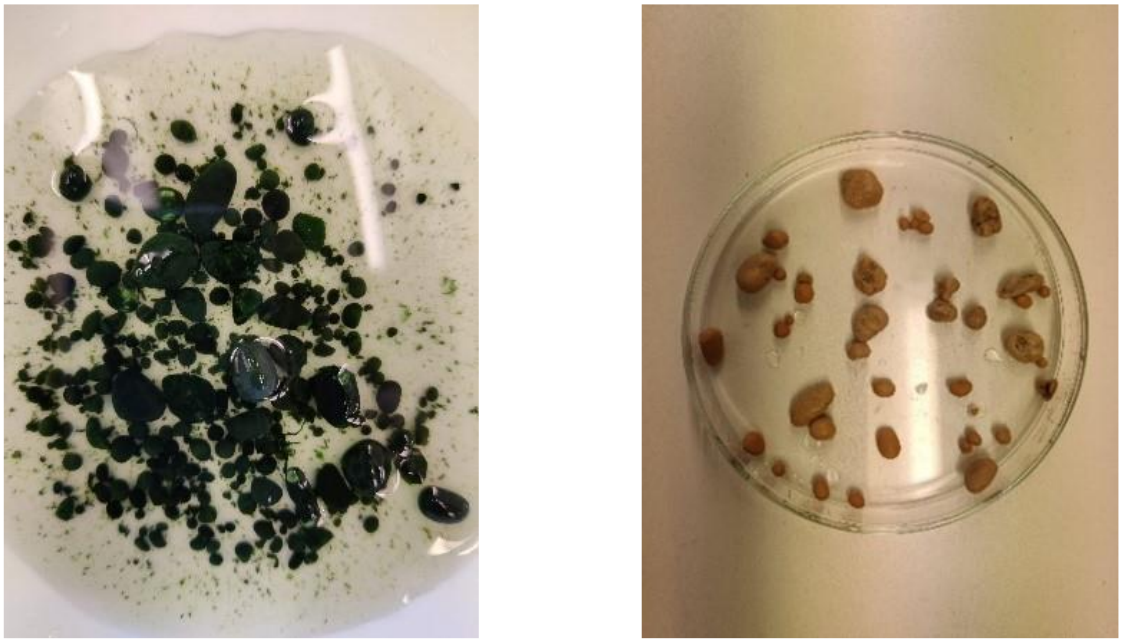

Figure 24: Left picture show sample of untreated OPGs, right picture shows bald granules picked from the sample.

Figure 25 shows the inlet compared to the effluent pH for 59 samples. The lowest effluent and influent pH were 7 for both, and the highest was 9.1 for the effluent and 8,4 for the influent. This graph shows that there is little variation in the pH for the entire experiment and that the water is alkaline at all times except when pH reaches 7, which only happened once.

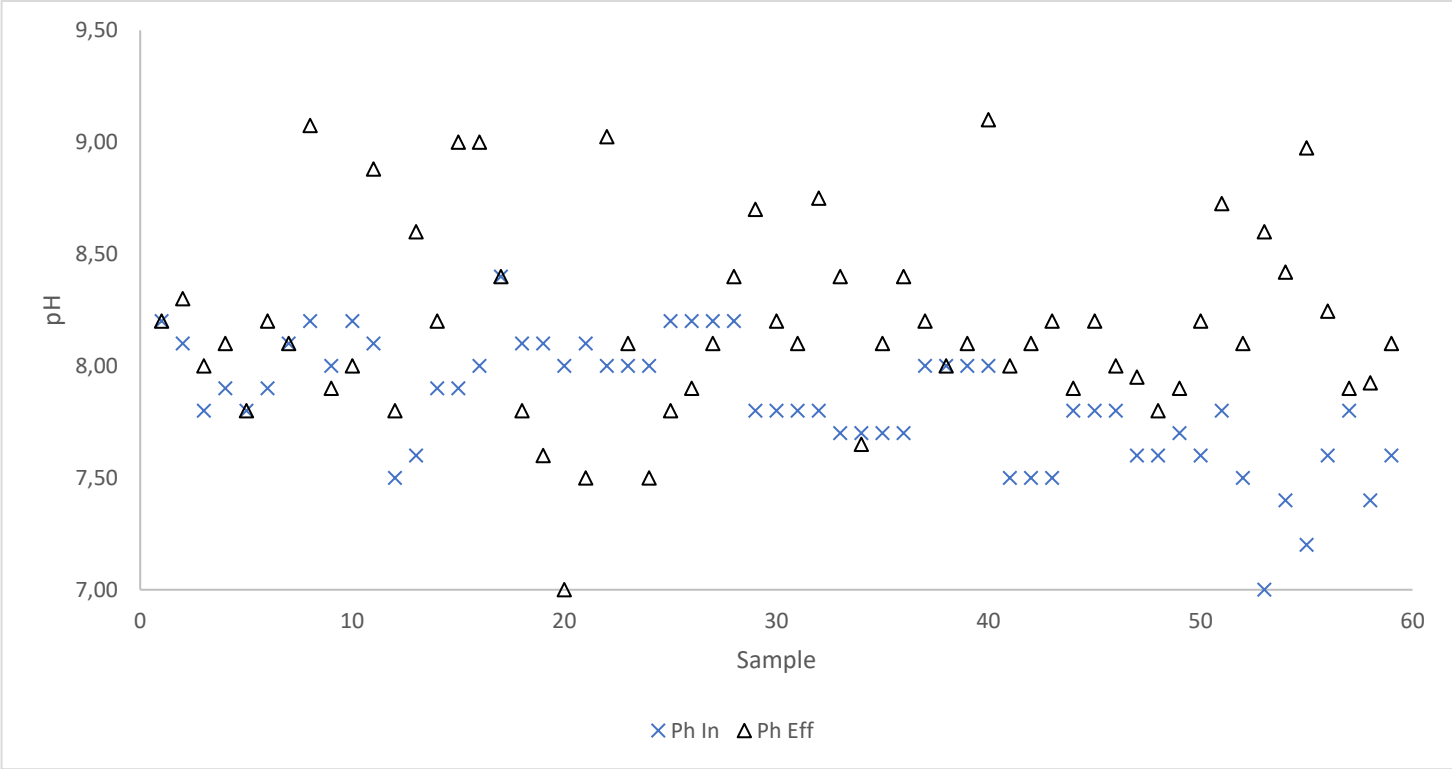

Figure 25: Diagram showing the inlet compared with the outlet pH for 59 sanples

4.2 COD and nutrient removal in the PBR

Loading rates for organics (as COD) and nutrients (as NH_4^+-N and PO_4^{3-}-P) are shown in Figure 26. Organic loading follows the left Y-axis, and nutrient correlates to the right Y-axis.

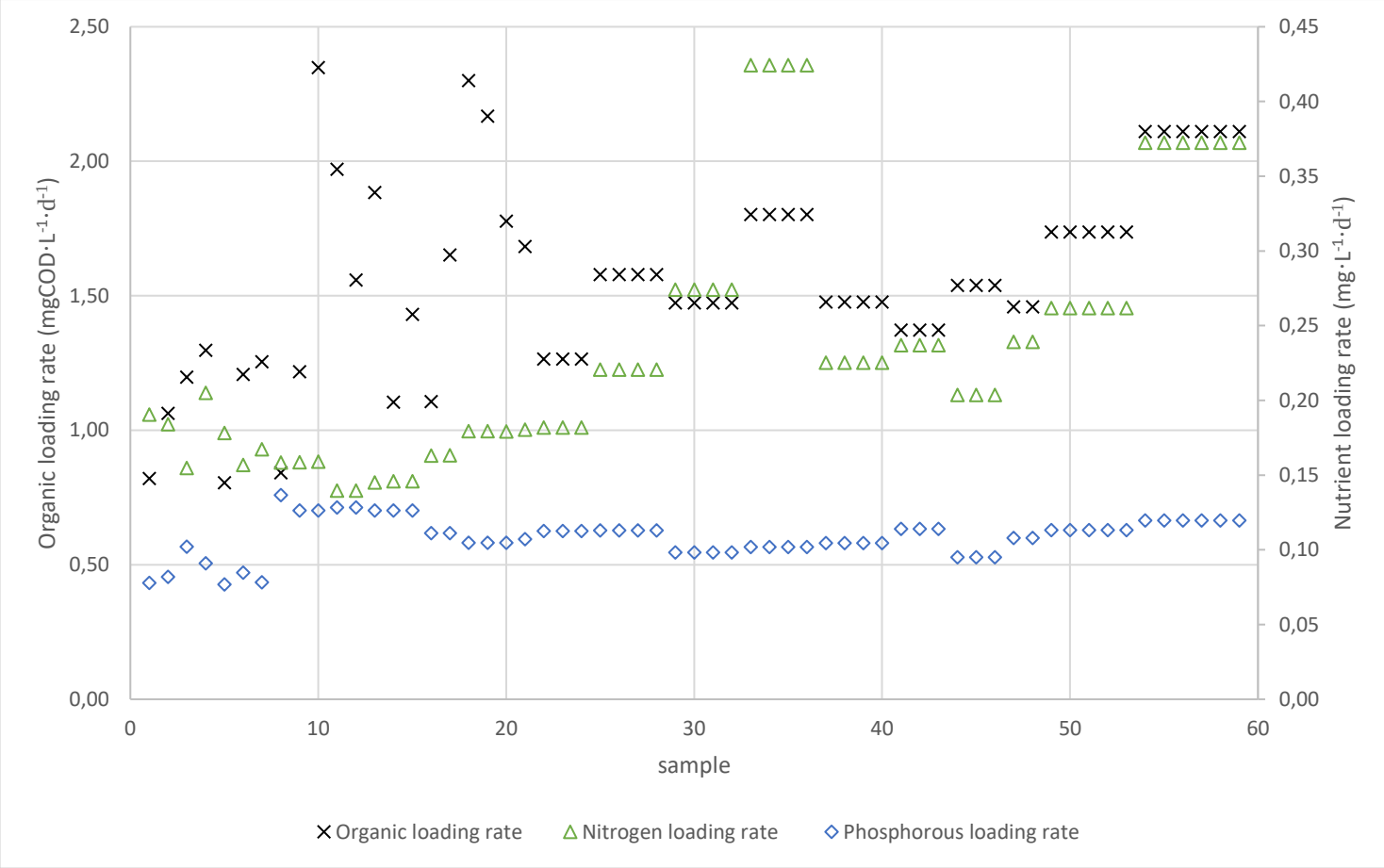

Figure 26: Diagram for loading rates. Y-axis to the left show organic loading rate, Y-axis to the right show nutrient loading rates.

The overall COD removal is presented in Figure 27. The diagram shows the removal efficiency and inlet/outlet concentrations of COD for the experimental period. For the first 21 days, removal efficiency remained unchanged despite variability in organic loading seen in fFigure 26. After 21 days, removal efficiencies were inconsistent. Although characteristics of the media stayed the same in 4-day periods, the COD removal for those periods experiences considerable variability. Past day 39, the system seems to be consistent with mostly good removal performances except for days 48 and 58. The average removal efficiency for the system was 52,5 % ± 2.2 (± standard error), and the best removal rate was 78,7 %.

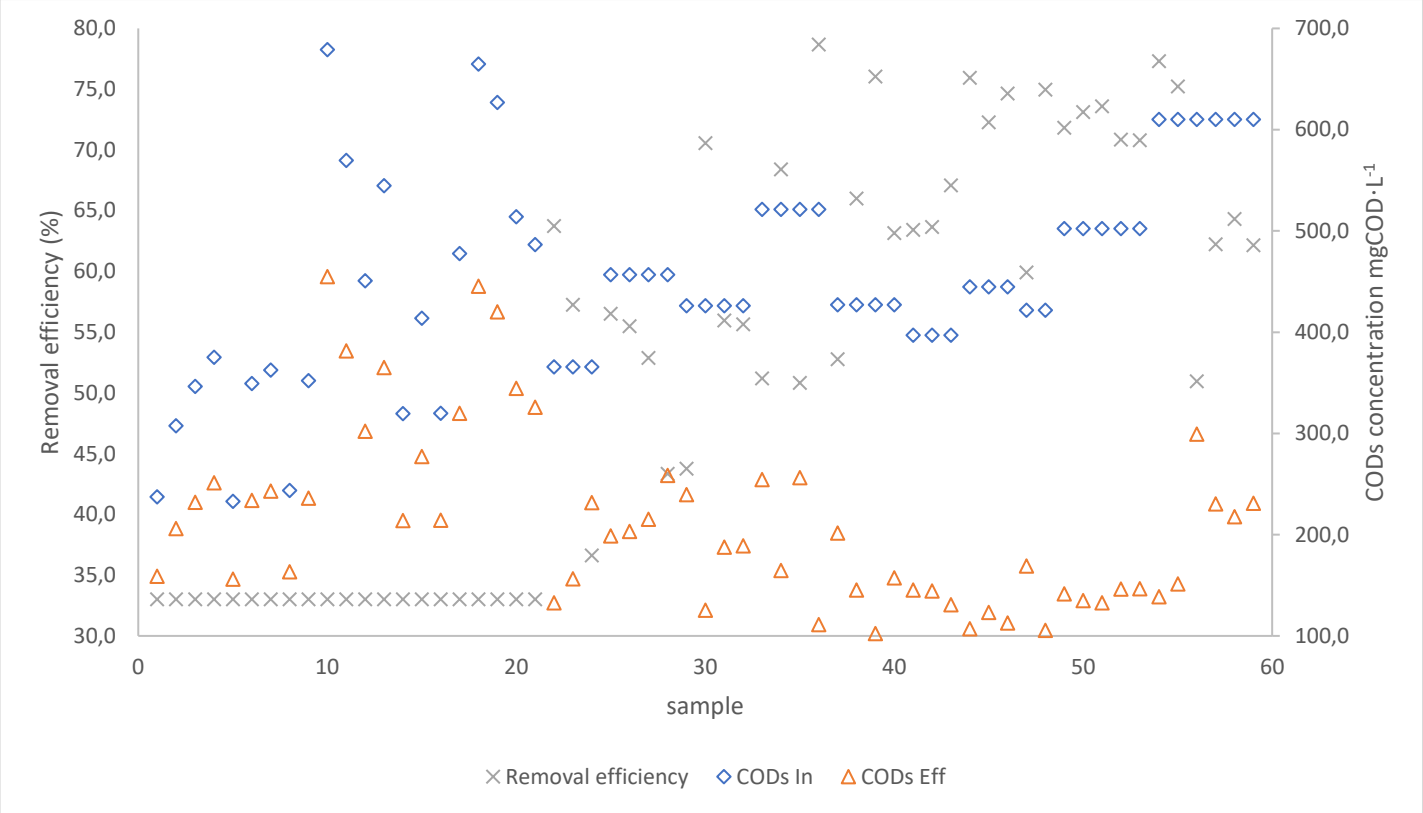

Figure 27: Performance of COD removal, Y-axis to the left show removal efficiency in (%), Y-axis to the right show COD concentration of COD in influent and effluent in mgL^{-1}.

The overall ammonium removal is presented in Figure 29 the sample day is reduced to 55 days because of analytical errors during sampling. The diagram shows the removal efficiency and inlet/outlet concentrations of NH_4^+ for the experimental period. Like COD, the removal efficiency for NH_4^+ has much variability, one difference being that for NH_4^+, it does not seem to be any point where the removal stabilizes. However, the system does remove ammonium each day except from day 25, where the data show a small production of ammonium. The average removal efficiency of NH_4^+ for the system was 43.3 % ± 2.5 (± standard error), and the best removal rate was 83.0 %.

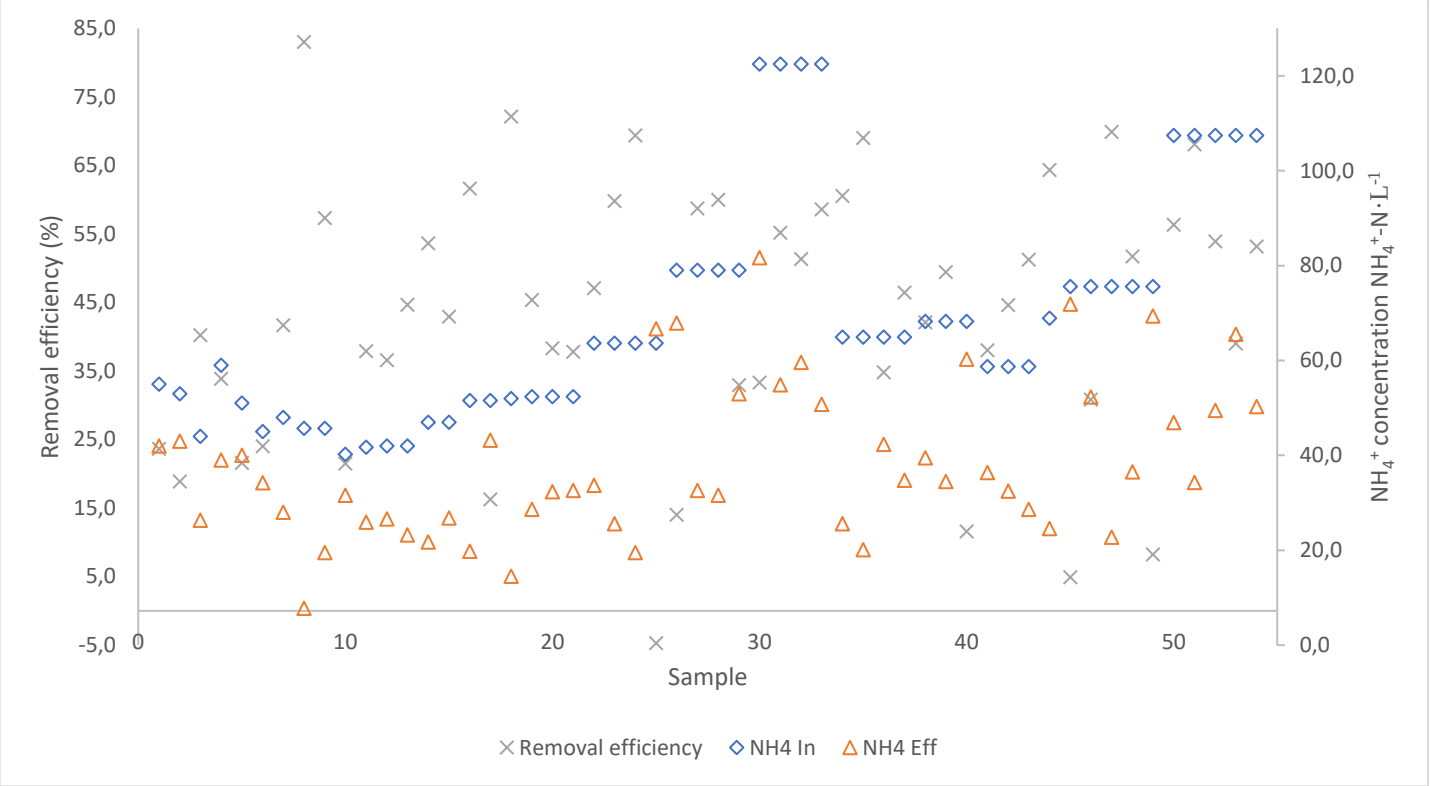

Figure 28: Performance of ammonium removal, Y-axis to the left show removal efficiency in (%), Y-axis to the right show NH_4^+ concentration in influent and effluent in mgL^{-1}.

Figure 29 presents the overall phosphate removal. The diagram shows the removal efficiency and inlet/outlet concentrations of PO_4^{3-} for 59 samples. There is never a production of phosphate as there was for ammonium. Here removal efficiency also varies greatly, with the highest removal being 85,3 % and the lowest being 5 %. The average removal efficiency for PO_4^{-3} was 44.7 % ± 2.0 (± standard error). The influent and effluent phosphate occupied 95.4 % and 90.7 % of the total phosphorous, respectively, and thus phosphorous followed a nearly identical removal trend as phosphate.

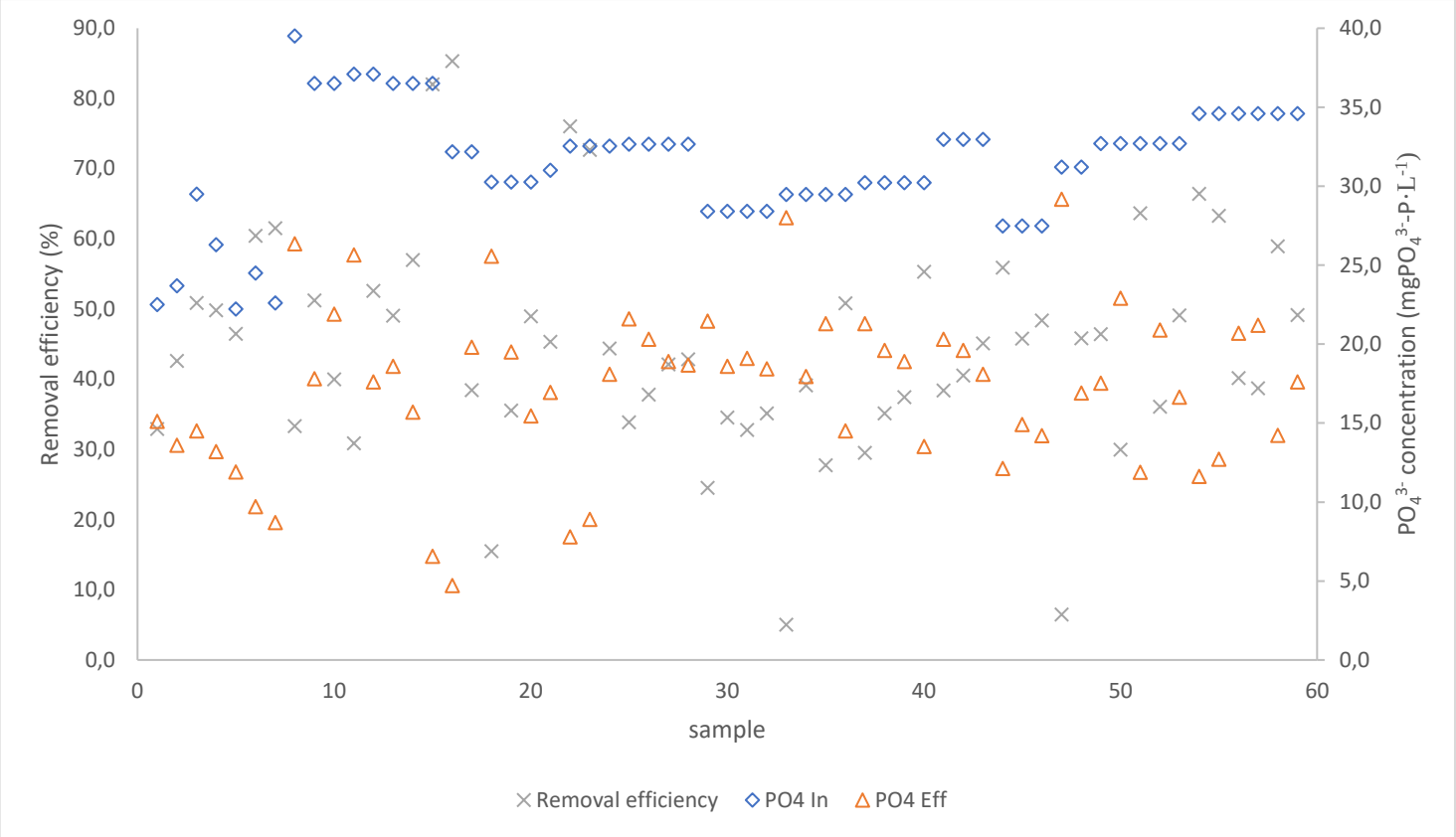

Figure 29: Performance of phosphate removal, Y-axis to the left show removal efficiency in (%), Y-axis to the right show PO_4^+ concentration in influent and effluent in mgL^{-1}. Sampling was not done on holidays and only on weekdays, there was also some days with analytical errors. Thus, the X-axis experimental time is reduced to 55 days even though the experiment itself lasted 85 days.

Figure 30 compares the removal efficiency of total nitrogen to the amount of nitrate in and out of the system. There is an overall production of nitrogen with an average production of 9.2 % ± 6.6 (± standard error). The graph shows a link between the efficiency of nitrogen removal and the amount of nitrate produced in the system.

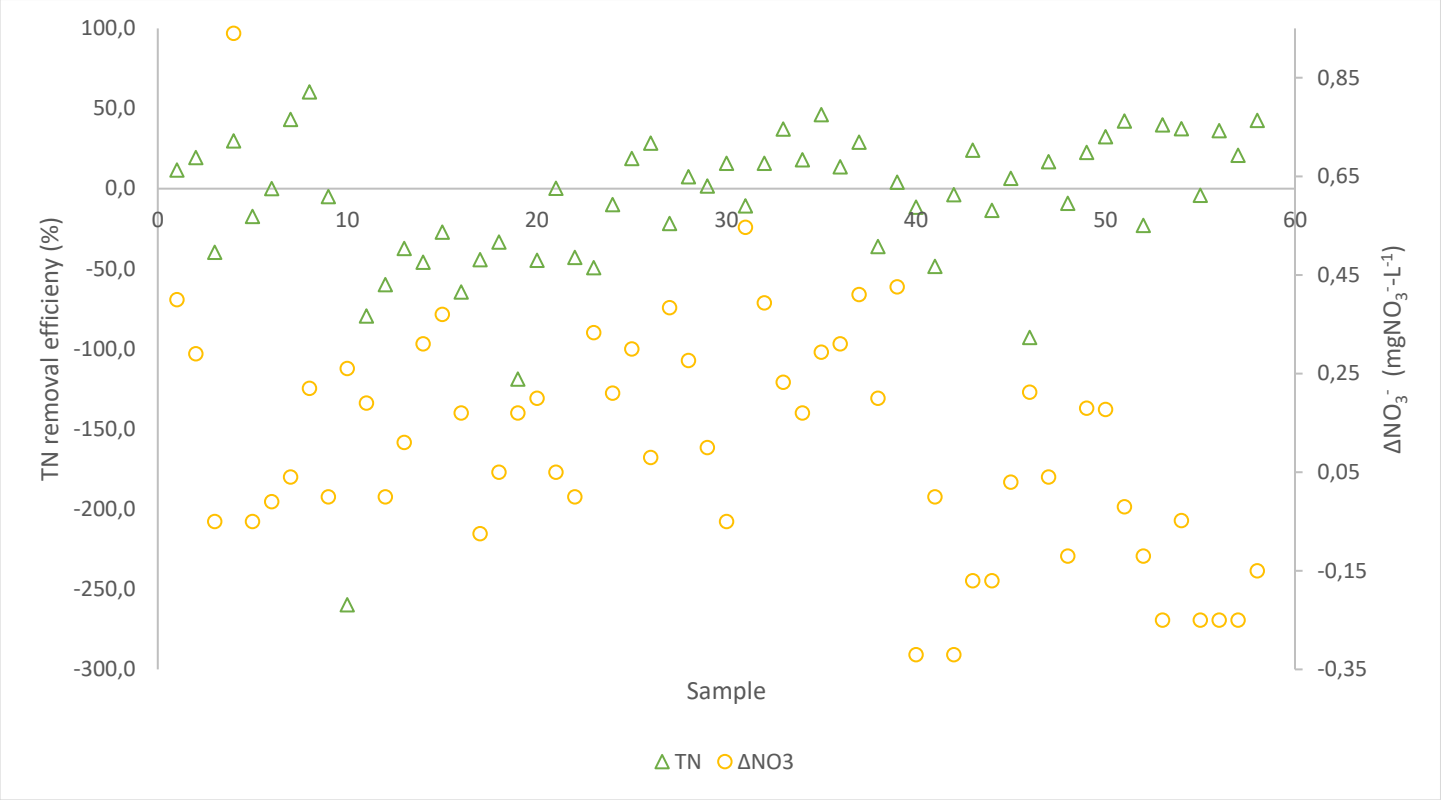

Figure 30: Performance of total nitrogen, Y-axis to the left show removal efficiency in (%), Y-axis to the right show ΔNO_3^- in mgL^{-1} Sampling was not done on holidays and only on weekdays, Thus, the X-axis experimental time is reduced to 59 days even though the experiment itself lasted 85 days.

Redfield ratio

The Redfield ratio was calculated by converting the available COD to the organic compounds found in the wastewater used in the UASB and alkalinity and CO_2. CO_2 was calculated as 4 % of the total COD because the liquid concentration reach equilibrium with atmosphere in an open system. Nitrogen and Phosphorous was calculated using the total phosphorous (TP) and total nitrogen (TN) measured in the analysis see appendix for calculations. Details on the Redfield ratio is presented in the appendix. Redfield ratio was calculated to be 3C:5N:1P.

4.3 Methanotrophic photogranule experiment

Glass vial experiment

Results from the methanotroph experiment are shown in Table 3. Examining results for the vials where the experiment worked; average removal for COD, NH_4^+, and PO_4^{3-} was 81.5 % ± 1.1, 52.3 % ± 1.8, and 49.6 % ± 2.2, respectively (± standard error).

Table 4: Removal efficiency (%) of the methanotrophs experiment for COD, NH_4^+-N, and PO_4^{3-}-N

Sample	Removal efficiency COD (%)	Removal efficiency NH_4^+-N (%)	Removal efficiency PO_4^{3-} (%)
Vial 1	85.7	48.3	42.1
Vial 2	25.5	48.6	59.7
Vial 3	N/A	49.6	48.1
Vial 4	77.4	60.9	48.1
Vial 5	82.7	52.5	51.3
Vial 6	82.2	53.5	48.5

Methanotrophs in PBR

Methanotrophic enrichment in PBR could only be tested once, the test gave a methane removal efficiency of 54.3 %, a TN removal efficiency of 32.0 %, TP removal efficiency of 14.6 %, a NH_4^+ removal efficiency of 60.9 %, a NO_3^- removal efficiency of -1200 %, and a PO_4^{3-} removal efficiency of 55.9 %.

5 Discussion

The main problem with the experiment was the slow progression of new OPGs forming in the PBR. From Figure 20 we can see that granule quantity increased by 45 in 97 days. From the same figure we can see that new OPGs started forming after an initial decline in quantity, but the progression was very slow relative to the literature. An example from the literature is Milferstedt et al. (2017b), which reported 600,000 new photogranules in the course of 19days; others also experienced an abundance of new granules in the inoculation period (Abouhend et al., 2020; Ansari et al., 2019; Ouazaite, 2021). The consequence of the slow progression from our experiment was that there was no time where biomass could be wasted. Looking at the size distribution in our experiment (Figure 5) the OPGs did not have a stable distribution halfway into the experiment (day 45) like Milferstedt et al. (2017b). And since there was always few granules in the PBR there was never a point where biomass could be wasted. Wasting would have created a more balanced biomass concentration which supposedly would have given a more even distribution of size (Milferstedt et al., 2017b). The balanced biomass concentration and even distribution of size would give a more predictable removal rate of COD and nutrients towards the end of the experiment. With enough OPGs to waste, mixing could also have been intensified which leads to detachment of filament on the photogranule surfaces, which leads to less filamentous OPGs (Safitri et al., 2021). Because there never was an extensive accumulation period of fresh OPGs there were limitations to the number of tests that could be done on the granules. There was no room for wasting any granules, and thus no granules were examined for biomass production and nutrient uptake directly. Fluorescence light microscopy was meant to be done to examine the microbial community, but a lack of working equipment made this unfeasible.

Continuous operation mode did not work for any of the three inoculations. A reason for this may be the pressure and shear stress on the hydrostatically grown granules when transferred to a turbulently mixed reactor system. SBR operation of the PBR experienced a 50 % loss of granules as seen in Figure 20 this was probably a result off acclimatisation from batch mode (Erlenmeyer flask) to the SBR system (pressure selection). This kind of behaviour is expected when transferring biomass to a new reactor system where there are many changes at the same time. For both continuous and SBR operation shear, pressure, and acclimatisation, stress the biomass, why this worked for the SBR and not continuous is unknown, but one reason might be the flow regime. The flow regime in continuous operation introduces new media

continuously and this might not give the microorganism enough time to break down the anaerobic effluent before reaching steady state. The continuous flow regime ended up selecting for biomass in a suspended culture rather than the granular structure. Formation of new OPGs using hydrostatically grown granules are usually developed in batch systems when transferred to a system with mixing (Abouhend et al., 2018; Milferstedt et al., 2017b). Seeding granules already formed under hydrodynamic shear to a continuous reactor may have resulted in a working system. Because granules formed under hydraulic shear produce more active phototrophic communities trapped in a more solid EPS matrix according to (Trebuch et al., 2020). The same positive effects are also seen for seeding the proper density of granules to the system. Ansari et al. (2019) showed that when seeding 2L reactors with low, medium, and high (20, 40, and 80 granules respectively), hydrostatically grown photogranules the low/medium seeded reactors performed better. Biomass yield was better for low (0.62 $mgVSS \cdot mg^{-1}COD$) and medium (0.57 $mgVSS \cdot mg^{-1}COD$) compared to high (0.55 $mgVSS \cdot mg^{-1}COD$) (Ansari et al., 2019). After four weeks biomass settling was also better for low and medium systems, low had about 140 mL·g, medium had about 130 mL·g, and high had about 200 mL·g, using sludge volume index 30 (Ansari et al., 2019). Settling time in our system was a simple measure of time from point A to point B measured in $m \cdot h^{-1}$. It was used to characterise the granules. What was found was that the medium sized granule settles the fastest. An explanation for this was that it was rounder than the other two granules tested giving it a better aspect ratio, proving that settling time is mostly determined by the granule core and shape of the granule not the size.

Studies in the literature (Abouhend et al., 2020; Ansari et al., 2019; Milferstedt et al., 2017b; Ouazaite, 2021) used domestic wastewater as the influent, some used synthetic wastewater, and some used municipal wastewater. Synthetic wastewater was used in this study but was different from the other studies because it was treated by a UASB. The anaerobic wastewater treatment can theoretically produce 0.38 litres of methane for every gram COD removed (Tchobanoglous et al., 2014a). The in-house laboratory scale UASB at UiS has proved a reactor performance using high strength municipal wastewater (1200 $mgCOD \cdot L^{-1}$) and reduced it to 300-400 mgL^{-1} while converting organic matter giving a 1.3 $L \cdot CH_4 \cdot d^{-1}$ specific volume methane production (Safitri, 2016). Safitri et al. (2021) calculated by assuming 80% removal efficiency for a typical high strength wastewater that approximately 22 % of all produced methane would be in its dissolved form and most likely leave the digester. A review evaluating greenhouse gas emissions from municipal UASB sewage treatment plants by Heffernan et al. (2012) reported that a total CH_4 production of 11 400 $kgCH_4 \cdot d^{-1}$ from UASB units lead to 23

% of that methane remaining dissolved in the effluent, which concurs with calculations done by Safitri et al. (2021). Methane is very volatile, and the reactor was not air shut for the cultivation of OPGs which mean that some of this carbon will leave the system through volatilisation. The influent nutrient supply seems to be insufficient for rapid growth of the heterotrophic and the phototrophic community in the OPGs. Looking at the Redfield ratio (106C:16N:1P) and comparing it to the ratio found for this experiment (3C:5N:1P), calculations show that this system was both carbon- and nitrogen-limited. This may be one reason for the slow growth of new OPGs.

From calculations of the Redfield ratio nitrogen supply along with carbon limits growth. And by looking at nitrogen removal performance in Figure 30 it shows an average 9.2 % production of nitrogen relative to the removal. This net increase in nitrogen might be because cyanobacteria fixate nitrogen from the air (Heidorn et al., 2011). A reason for elevated nitrogen levels in some samples detected may be due to sampling. Ammonium is removed consistently from the system but accumulates as biomass and NO_3^-. When samples for TN were done, they came straight from the mixed reactor, consequently if a sample for TN has a high concentration of biomass in it, nitrogen levels will be high. By comparing total nitrogen in Figure 30 and TSS content in Figure 22 it shows that on day 10 where TSS were high 341 mgL^{-1} (average TSS concentration was 229 mgL^{-1}) TN was significantly high as well 151,5 mgL^{-1} (average TN concentration was 71 mgL^{-1}). However, NO_3^- production showing the same trend as total nitrogen seen in Figure 30 also indicates that the nitrogen cycle is not completed in the system and nitrogen is therefore not removed due to nitrification. A reason for the uncompleted nitrogen cycle may be the CO_2 concentration. Ammonia-oxidising and nitrate-oxidising bacteria are both aerobic chemoautotrophs that use CO_2 as their carbon source (Tchobanoglous et al., 2014c). If there is not enough CO_2 left after photosynthetic reactions and ammonia oxidisation, the nitrate-oxidising bacteria lack a substrate to complete their reaction which is the last step in the nitrogen cycle. This seem to be the case in this system because ammonia is oxidised (Figure 28), nitrate is produced (Figure 30) but nitrogen is not removed (Figure 30). Another reason to why there does not seem to be denitrification may be because the nitrate produced accumulates as biomass in the phototrophic community through assimilation by microalgae and cyanobacteria (Sanz-Luque et al., 2015). The nitrate produced in the system could also be used as an electron acceptor by ANME for removing methane inside the anoxic regions of the granular matrix where oxygen levels are too low for aerobic methanotrophs, and they cannot reach the oxic interface of the anoxic region (Case et al., 2017). Not removing

nitrogen from the system may be a benefit. When the nitrogen cycle is completed, nitrogen is removed from the system by denitrifiers and nitrogen escapes the system as nitrogen gas. Investigating the possibilities for nutrient recovery (harvest and reuse the nutrients) instead of removal (remove the nutrients from the system through complete oxidation) is often more advantageous, especially for a high value nutrient like nitrogen which is used in fertilizers. Fertilizers is often produced by the Haber-Bosch process fixating nitrogen from air, which is a high-energy process. Therefore, harvesting nitrogen rich biomass and extracting it may be preferred over just removing the nitrogen from the system.

The effluent from the UASB have a relatively higher CO_2 concentration to regular wastewater due to respiration from the microorganisms during treatment in a closed system. Since the phototrophic community in the OPGs use CO_2 as their substrate for growth the UASB effluent have an advantage. However, for the cultivation of OPGs, there was no seal in the PBR blocking the media from the atmosphere. Consequently, the CO_2 gradient reaches equilibrium with air, and we are left with a 4 % CO_2 concentration in the liquid. However, cyanobacteria can use other carbon sources such as HCO_3^- and possibly CO_3^{2-} (Schneider & Campion-Alsumard, 1999). There will be some HCO_3^- from the tap water used in media preparation. The HCO_3^- from the hardness of the tap water could be used to further enhance methane removal because of the increased oxygen availability for bicarbonate photosynthesis. This contribution was calculated by Safitri et al. (2021) to supply an additional 2.58 mM O_2 using tap water with 4 mM HCO_3. Looking at the alkalinity in the reactor in Figure 21 there seem to be alkalinity consumed in the initial inoculation period, but after day 24 alkalinity is mostly produced. This indicate that the extra carbonate from the bicarbonate system was important for the initial inoculation but see a decline in necessity as a resource for the phototrophic community after inoculation. From Figure 25 pH was always above 7 except from one sample in the effluent. This indicate CO_2 is steadily removed from the system. Phosphate was also steadily removed as shown in Figure 29 with an average removal rate of 44,7 % ± 2.0 % (± standard error), but removal efficiencies did not show remarkable results compared to other wastewater treatment systems which range from 70-98 % (Bunce et al., 2018). One of the best removal efficiencies in the literature (98 %) was by Sukačová et al. (2015) which used a microalgal biofilm system in a PBR, which has similarities with this system and indicate a potential for future research. A reason for not achieving a higher phosphorous removal in this system is a result of the carbon/nitrogen-limited system which ultimately also limits phosphorous uptake due to growth limitations.

From investigation of the granule core a 59 %, and 41 %, calcite and apatite composition was found, respectively. Author of this thesis found that content of the OPG core is only communicated one time as of now in the literature, it is reported as calcite by Milferstedt et al. (2017a), but there is no experimental evidence for this in the report, it is only mentioned. Therefore, finding calcite and apatite as the core content may be a novel finding. It was hypothesised apatite might be present in the core as it is a phosphate mineral. Due to the amount of ammonium being oxidised, there was also hypothesised that struvite might be a part of the OPG core, but this was not found in our XRD analysis. Both struvite and apatite are used as nutrients in fertilizer. By recycling the nutrients it contributes to the circular economy principle that minimum waste should be generated for disposal and maximum use is extracted from the resources (Deutz, 2020). By recycling both the nutrients from the biomass and the biosolids from the core a maximum use is extracted from the OPGs resources post treatment. According to Tchobanoglous et al. (2014b) when recycling biosolids to agricultural land it will improve the economics of crop production by not using expensive fertilisers which leads to reduced greenhouse gas emission that would be generated when producing chemical fertiliser and carbon sequestration. Specifically phosphorous and nitrogen recycling of biosolids in wastewater treatment leads to less need for phosphate rock depletion, and less nitrogen production (Desmidt et al., 2015; Rahman et al., 2014). Scanning electron microscopy (SEM) analysis is a proposal for future research to further investigate the chemical elements in the core.

For the experiments with methanotrophs the glass vial experiment performed better than the experiment directly in the PBR 81.5 % and 54.3 %, respectively. It should be noted that since the inoculation of methanotrophs in the PBR was delayed due to delivery of equipment there is only one test done in the PBR while the glass vials could be tested in six different vials. Still the worst performing vial (with all granules intact) had better removal efficiency (77,4 %) than the PBR (54,3 %). However, the experiment done in the PBR did manage to air shut the reactor from the atmosphere. Since the reactor was air shut it was possible to test degassing to confirm the removal of methane. After an initial CODs content of 569 mgL^{-1} reduced to 260 mgL^{-1} in the air shut system a water sample was taken and put on the bench and mixed several times for two hours, the COD of the sample was 253 mgL^{-1}. This proves that the methanotrophs removed almost all the methane in the sample, so even though the CODs removal was just over 50 %, the methane removal may be higher. The increased removal rates in the glass vial experiment compared to the experiment in the PBR may be a result of reactor size relative to quantity of

OPGs. Visually it could be observed that the granules in the glass vial Figure 15 occupied more of the liquid volume than the granules in the PBR Figure 13. Therefore, the increased biomass relative to liquid media in an air closed system seem to have an effect on the CODs removal but methane removal proves to be efficient anyway.

Looking at Table 4 syntrophy between methanotrophs and cyanobacteria in OPGs using air shut glass vials (to make sure no oxygen entered the system other than the photosynthetic activity of phototrophs) showed promising results for the removal of CODs, with methane being the main carbon source (methane was diffused in the liquid overnight). The average removal efficiency was 81,5 %, ± 1.1 % and the best removal was 83,7% for CODs. Comparing the CODs removal results after methanotrophic enrichment with the PBR system without enrichment in Figure 27 which had an average removal efficiency of (52.5 % ± 2.2 %) there is a 29 % increase in removal efficiency, which is significant. The best removal efficiency (78,7 %) for OPGs without methanotroph was still worse than the average removal after adding methanotrophs (81,5 %, ± 1.1 %). The increased performance of CODs removal with the methanotrophs verify that treating UASB effluent with bioengineered OPGs inoculated with an enriched methanotrophic culture is possible. This was already proven by Safitri et al. (2021) which managed to achieve removal exceeding 90 %, this was managed as a result of increased mixing. Increasing mixing intensity minimize the laminar boundary layer around the photogranules. According to Heffernan et al. (2012) that reported a 23 % dissolved CH_4 fraction in the liquid after UASB treatment calculated the loss of CH_4 from the effluent to account for 78 % (20 000 ton CO_2 eq·y^{-1}) of the emissions associated with the configuration. This shows the importance of a UASB post treatment system like the one presented in this experiment from a greenhouse gas emissions perspective. Nutrient removal did not show excellent results compared to the standard OPG system in the PBR without methanotrophs. Comparing average ammonium removal in fFigure 28 (43.3 % ± 2.5 %) to the methanotroph experiment Table 4 (52.3 % ± 1.8 %), there is only a 9 % difference. The 9 % difference would have been more impressive if the initial ammonium removal was higher but is still an improvement. Average phosphorous removal for the experiment shown in Table 4 (49.6 ± 2.2 %) was also better than the standard OPG system without methanotrophs in Figure 29 (44.7 ± 2.0 %). The difference is a 4.9 % increase in removal efficiency, which would be more significant if the initial removal was higher, but it is an improvement. For the experiment, there were observed three disintegrated OPGs in vial 2. Here, the removal efficiency was the lowest 25.5 % ± 1.1%. The reduced removal efficiency for vial 2 with disintegrated OPGs indicate

that the methanotrophs could not oxidise the carbon without the help of the O_2 production from the phototrophic community in the OPGs. Samples could not be taken for vial 3 due to analytical error, which resulted in a leak into the atmosphere. A measurement from a leaked sample would not have given valid answers as some methane would have escaped the system through volatilisation.

6 Conclusion

The conclusions were as following:

- Growing and sustaining biomass in a granular structure when seeding hydrostatically grown oxygenic photogranules in a PBR used for post-UASB treatment was made possible by changing the reactor system from continuous to sequence batch reactor. However, growing the quantity of granules proved to be difficult with this reactor setup. Calculations done compared to the Redfield ratio indicated that availability of nutrients seem to be the limiting factor for growth.
- For the entire experimental period COD was removed from the system, the longer the experiment lasted the better COD removal efficiencies became. This proves the ability for an engineered granulated microbial consortium with syntrophic relationship between heterotrophs and phototrophs to oxidise carbon content without need for aeration to supply oxygen. Average removal efficiency was COD 52.5 % ± 2.2 % (± standard error), NH_4^+ 52.3 % ± 1.1 %, PO_4^{3-} 49.6 % ± 2.2 %. The best COD removal efficiency was 78.7 %, and for the last 20 days average removal rate was 69.3 %.
- Doing two experiments inoculating an enriched methanotrophic culture in suspension to OPGs it was proven that a system for removing dissolved methane without the need for aeration to supply oxygen is feasible. It also increased methane removal from the original OPGs system. Inoculation directly in the PBR had a 54.3 % removal efficiency. But tests done by degassing the liquid showed that methane content was removed from the liquid in the PBR. The system with highest observed biomass to liquid ratio (testing in air shut glass vials) had the best COD and nutrient removal efficiency with averages: COD 81.5 % ± 1.1(± standard error), NH_4^+ 52.3 % ± 1.1, PO_4^{3-} 49.6 % ± 2.2. The analysis concludes that bioengineered methanotrophic photogranules can be grown in a PBR and used for tertiary UASB effluent post-treatment.
- It was found using XRD analysis that the granule core consisted of calcite and apatite, 59 % and 41 %, respectively.

7 Future research

Proposal for future research were as following:

- Seeding OPGs formed under hydraulic shear to a continuous reactor system might result in a working system. This is because they are acclimatised to the mixing and produce more active phototrophic communities trapped in a more solid EPS matrix. Therefore, testing OPGs formed under hydraulic shear in a continuous is a suggestion for future research. The same effect can be tested by switching to a continuous system after cultivating the OPGs in an SBR system. Therefore, testing OPGs formed under hydraulic shear in a continuous is a suggestion for future research.
- A proposal for future research is to cultivate the OPGs using the UASB effluent in a system closed from the atmosphere. The effluent will then have more methane and CO_2 in the influent of the PBR which in theory will have more carbon and nitrogen available for growth.
- To better understand why inoculation in a continuous reactor did not work, but inoculation in an SBR worked an experiment testing both systems and comparing them is suggested for future research. For this experiment it is suggested to use a wastewater that has not been treated by an anaerobic process, this generates more biomass according to the literature.
- Possibilities for nutrient harvesting of the OPG biomass and biosolids should be examined. Results from experiments in this thesis suggest that there is a lot of nutrients available in the biomass. Results also show that the composition of the granular core contains nutrient rich biosolids which can be used as fertilizer. Scanning electron microscopy could be used to enhance the samples and see the crystals in the minerals to further investigate the chemical content of the core.
- A model of the system to see what happens to the nitrate would also be of use to better examine the nutrient cycling in the biomass. Nitrate can be used by nitrate-oxidising bacteria to remove N_2, it can be used as a N-source for the phototrophic community, and it can be used as a electron acceptor for the anaerobic methanotrophic archaea in the anoxic phase of the OPGs or during light attenuation.

8 References

Abouhend, A. S., McNair, A., Kuo-Dahab, W. C., Watt, C., Butler, C. S., Milferstedt, K., Hamelin, J., Seo, J., Gikonyo, G. J., El-Moselhy, K. M., & Park, C. (2018). The Oxygenic Photogranule Process for Aeration-Free Wastewater Treatment. *Environmental Science & Technology*, *52*(6), 3503-3511. https://doi.org/10.1021/acs.est.8b00403

Abouhend, A. S., Milferstedt, K., Hamelin, J., Ansari, A. A., Butler, C., Carbajal-González, B. I., & Park, C. (2020). Growth Progression of Oxygenic Photogranules and Its Impact on Bioactivity for Aeration-Free Wastewater Treatment. *Environmental Science & Technology*, *54*(1), 486-496. https://doi.org/10.1021/acs.est.9b04745

Ansari, A. A., Abouhend, A. S., & Park, C. (2019). Effects of seeding density on photogranulation and the start-up of the oxygenic photogranule process for aeration-free wastewater treatment. *Algal Research*, *40*, 101495. https://doi.org/https://doi.org/10.1016/j.algal.2019.101495

Aqeel, H., Weissbrodt, D. G., Cerruti, M., Wolfaardt, G. M., Wilén, B.-M., & Liss, S. N. (2019). Drivers of bioaggregation from flocs to biofilms and granular sludge [10.1039/C9EW00450E]. *Environmental Science: Water Research & Technology*, *5*(12), 2072-2089. https://doi.org/10.1039/C9EW00450E

Bellier, N., Chazarenc, F., & Comeau, Y. (2006). Phosphorus removal from wastewater by mineral apatite. *Water Research*, *40*(15), 2965-2971. https://doi.org/https://doi.org/10.1016/j.watres.2006.05.016

Boedeker, C., & Immers, A. (2009). No more lake balls (Aegagropila linnaei Kützing, Cladophorophyceae, Chlorophyta) in The Netherlands? *Aquatic Ecology*, *43*(4), 891-902. https://doi.org/10.1007/s10452-009-9231-1

Brehm, U., Palinska, K., & Krumbein, W. (2004). Laboratory cultures of calcifying biomicrospheres generate ooids - A contribution to the origin of oolites. *Carnets de Géologie*, *3*.

Bunce, J. T., Ndam, E., Ofiteru, I. D., Moore, A., & Graham, D. W. (2018). A Review of Phosphorus Removal Technologies and Their Applicability to Small-Scale Domestic Wastewater Treatment Systems [Review]. *Frontiers in Environmental Science*, *6*. https://doi.org/10.3389/fenvs.2018.00008

Cai, Y., Zheng, Y., Bodelier, P. L. E., Conrad, R., & Jia, Z. (2016). Conventional methanotrophs are responsible for atmospheric methane oxidation in paddy soils. *Nature Communications*, *7*(1), 11728. https://doi.org/10.1038/ncomms11728

Carter, S., & Lumen-Learning. (2017). Light-Dependent Reactions. In. lumenlearning.com: Lumen Learning.

Case, D. H., Akira, I., Yuki, M., Patricia, T., J., O. V., & Fumio, I. (2017). Aerobic and Anaerobic Methanotrophic Communities Associated with Methane Hydrates Exposed on the Seafloor: A High-Pressure Sampling and Stable Isotope-Incubation Experiment [Original Research]. *Frontiers in Microbiology*, *8*. https://doi.org/10.3389/fmicb.2017.02569

Chisti, Y. (2018). Chapter 2 - Society and Microalgae: Understanding the Past and Present. In I. A. Levine & J. Fleurence (Eds.), *Microalgae in Health and Disease Prevention* (pp.

11-21). Academic Press. https://doi.org/https://doi.org/10.1016/B978-0-12-811405-6.00002-5

Crittenden, J. C., Trussell, R. R., Hand, D. W., Howe, K. J., & Tchobanoglous, G. (2012). Coagulation and Flocculation. In *MWH's Water Treatment: Principles and Design, Third Edition* (pp. 541-639). https://doi.org/https://doi.org/10.1002/9781118131473.ch9

D'Acunto, B., Frunzo, L., Luongo, V., & Mattei, M. R. (2019). Mathematical Modeling of Biofilms. In *Introduction to Biofilm Engineering* (Vol. 1323, pp. 245-273). American Chemical Society. https://doi.org/doi:10.1021/bk-2019-1323.ch012

10.1021/bk-2019-1323.ch012

da Costa, N. P. A. V., Libardi, N., Schambeck, C. M., Filho, P. B., & da Costa, R. H. R. (2020). Impact of additive application on the establishment of fast and stable aerobic granulation. *Applied microbiology and biotechnology*, *104*(13), 5697-5709. https://doi.org/10.1007/s00253-020-10657-1

Desmidt, E., Ghyselbrecht, K., Zhang, Y., Pinoy, L., Van der Bruggen, B., Verstraete, W., Rabaey, K., & Meesschaert, B. (2015). Global Phosphorus Scarcity and Full-Scale P-Recovery Techniques: A Review. *Critical Reviews in Environmental Science and Technology*, *45*. https://doi.org/10.1080/10643389.2013.866531

Deutz, P. (2020). Circular Economy. In A. Kobayashi (Ed.), *International Encyclopedia of Human Geography (Second Edition)* (pp. 193-201). Elsevier. https://doi.org/https://doi.org/10.1016/B978-0-08-102295-5.10630-4

Dmitriy, S., Pishchalnikov, R. Y., Eichacker, L. A., & Govindjee. (2013). Oxygenic Photosynthesis in Cyanobacteria. In A. K. Srivastava, A. N. Rai, & B. A. Neilan (Eds.), *Stress Biology of Cyanobacteria* (pp. 369). CRC Press Taylor & Francis group.

Garcia-Pichel, F., & Castenholz, R. W. (2001). Chapter 14 Photomovement of microorganisms in benthic and soil microenvironments. In D.-P. Häder & A. M. Breure (Eds.), *Comprehensive Series in Photosciences* (Vol. 1, pp. 403-420). Elsevier. https://doi.org/https://doi.org/10.1016/S1568-461X(01)80018-1

Hanson, R. S., & Hanson, T. E. (1996). Methanotrophic bacteria. *Microbiological reviews*, *60*(2), 439-471. https://doi.org/10.1128/mr.60.2.439-471.1996

Harper, D. (1992). Eutrophication of Freshwaters. In *Eutrophication of Freshwaters* (Vol. 1, pp. 327). Springer Netherlands. https://doi.org/10.1007/978-94-011-3082-0

Heffernan, B., Blanc, J., & Spanjers, H. (2012). Evaluation of greenhouse gas emissions from municipal UASB sewage treatment plants. *Journal of Integrative Environmental Sciences*, *9*(sup1), 127-137. https://doi.org/10.1080/1943815X.2012.696546

Heidorn, T., Camsund, D., Huang, H.-H., Lindberg, P., Oliveira, P., Stensjø, K., & Lindblad, P. (2011). Synthetic biology. In C. Voigt (Ed.), *Methods in Enzymology* (Vol. 497-498, pp. 540-572). Academic Press. https://www-vlebooks-com.ezproxy.uis.no/Vleweb/Product/Index/410117?page=0

Henze, M., Dupont, R., Grau, P., & de la Sota, A. (1993). Rising sludge in secondary settlers due to denitrification. *Water Research*, *27*(2), 231-236. https://doi.org/https://doi.org/10.1016/0043-1354(93)90080-2

Henze, M., Gujer, W., Mino, T., & van Loosdrecht, M. C. M. (2000). *Activated sludge models ASM1, ASM2, ASM2d and ASM3*. IWA Publishing.

Iguchi, H., Sato, I., Yurimoto, H., & Sakai, Y. (2013). Stress resistance and C1 metabolism involved in plant colonization of a methanotroph Methylosinus sp. B4S. *Archives of microbiology*, *195*(10-11), 717-726. https://doi.org/http://dx.doi.org/10.1007/s00203-013-0922-6

Joosten, E. D., Hamelin, J., & Milferstedt, K. (2020). Simple Time-lapse Imaging for Quantifying the Hydrostatic Production of Oxygenic Photogranules. *Bio-protocol*, *10*(19), e3784. https://doi.org/10.21769/BioProtoc.3784

Knief, C. (2015). Diversity and Habitat Preferences of Cultivated and Uncultivated Aerobic Methanotrophic Bacteria Evaluated Based on pmoA as Molecular Marker [Review]. *Frontiers in Microbiology*, *6*. https://doi.org/10.3389/fmicb.2015.01346

Kuo-Dahab, W. C., Stauch-White, K., Butler, C. S., Gikonyo, G. J., Carbajal-González, B., Ivanova, A., Dolan, S., & Park, C. (2018). Investigation of the Fate and Dynamics of Extracellular Polymeric Substances (EPS) during Sludge-Based Photogranulation under Hydrostatic Conditions. *Environmental Science & Technology*, *52*(18), 10462-10471. https://doi.org/10.1021/acs.est.8b03033

Laspidou, C. S., & Rittmann, B. E. (2002). A unified theory for extracellular polymeric substances, soluble microbial products, and active and inert biomass. *Water Research*, *36*(11), 2711-2720. https://doi.org/https://doi.org/10.1016/S0043-1354(01)00413-4

Lettinga, G., van Velsen, A. F. M., Hobma, S. W., de Zeeuw, W., & Klapwijk, A. (1980). Use of the upflow sludge blanket (USB) reactor concept for biological wastewater treatment, especially for anaerobic treatment. *Biotechnology and Bioengineering*, *22*(4), 699-734. https://doi.org/https://doi.org/10.1002/bit.260220402

Li, Q., Peng, C., Zhang, J., Li, Y., & Song, X. (2021). Nitrogen addition decreases methane uptake caused by methanotroph and methanogen imbalances in a Moso bamboo forest. *Scientific Reports (Nature Publisher Group)*, *11*(1). https://doi.org/http://dx.doi.org/10.1038/s41598-021-84422-3

Li, X., Lu, Y., Li, N., Wang, Y., Yu, R., Zhu, G., & Zeng, R. J. (2022). Mixotrophic Cultivation of Microalgae Using Biogas as the Substrate. *Environmental Science & Technology*, *56*(6), 3669-3677. https://doi.org/10.1021/acs.est.1c06831

Lobato, L. C. S., Chernicharo, C. A. L., & Souza, C. L. (2012). Estimates of methane loss and energy recovery potential in anaerobic reactors treating domestic wastewater. *Water Science and Technology*, *66*(12), 2745-2753. https://doi.org/10.2166/wst.2012.514

Madigan, M. T., Bender, K. S., Buckley, D. H., Sattley, W. M., & Stahl, D. A. (2019a). *Brock Biology of Microorganisms* (Vol. 15). Pearson Education Limited.

Madigan, M. T., Bender, K. S., Buckley, D. H., Sattley, W. M., & Stahl, D. A. (2019b). Functional Diversity of Microorganisms. In S. Beauparlant (Ed.), *Brock Biology of Microorganisms* (Vol. 15, pp. 487-530). Pearson Education Limited.

Madigan, M. T., Bender, K. S., Buckley, D. H., Sattley, W. M., & Stahl, D. A. (2019c). Metabolic Diversity in Microorganisms. In S. Beauparlant (Ed.), *Brock Biology of Microorganisms* (Vol. 15, pp. 428-487). Pearson Education Limited.

Madigan, M. T., Bender, K. S., Buckley, D. H., Sattley, W. M., & Stahl, D. A. (2019d). Microbial Growth and Its Control. In S. Beauparlant (Ed.), *Brock Biology of Microorganisms* (Vol. 15, pp. 173-209). Pearson Education Limited.

Madigan, M. T., Bender, K. S., Buckley, D. H., Sattley, W. M., & Stahl, D. A. (2019e). Microbial metabolism. In S. Beauparlant (Ed.), *Brock Biology of Microorganisms* (Vol. 15, pp. 109-138). Pearson Education Limited.

Madigan, M. T., Bender, K. S., Buckley, D. H., Sattley, W. M., & Stahl, D. A. (2019f). Molecular Biology of Microbial Growth. In S. Beauparlant (Ed.), *Brock Biology of Microorganisms* (Vol. 15, pp. 238-251). Pearson Education Limited.

Malin, G., & Pearson, H. W. (1988). Aerobic Nitrogen Fixation in Aggregate-forming Cultures of the Nonheterocystous Cyanobacterium Microcoleus chthonoplastes. *Microbiology*, *134*(7), 1755-1763. https://doi.org/10.1099/00221287-134-7-1755

Mazel, D., & Marlière, P. (1989). Adaptive eradication of methionine and cysteine from cyanobacterial light-harvesting proteins. *Nature*, *341*(6239), 245-248. https://doi.org/10.1038/341245a0

Mikesková, H., Novotný, Č., & Svobodová, K. (2012). Interspecific interactions in mixed microbial cultures in a biodegradation perspective. *Applied microbiology and biotechnology*, *95*(4), 861-870. https://doi.org/10.1007/s00253-012-4234-6

Milferstedt, K., Hamelin, J., Park, C., Jung, J., Hwang, Y., Cho, S.-K., Jung, K.-W., & Kim, D.-H. (2017a). Biogranules applied in environmental engineering. *International Journal of Hydrogen Energy*, *42*(45), 27801-27811. https://doi.org/10.1016/j.ijhydene.2017.07.176

Milferstedt, K., Kuo-Dahab, W. C., Butler, C. S., Hamelin, J., Abouhend, A. S., Stauch-White, K., McNair, A., Watt, C., Carbajal-González, B. I., Dolan, S., & Park, C. (2017b). The importance of filamentous cyanobacteria in the development of oxygenic photogranules. *Scientific Reports*, *7*(1). https://doi.org/10.1038/s41598-017-16614-9

Milucka, J., Kirf, M., Lu, L., Krupke, A., Lam, P., Littmann, S., Kuypers, M. M., & Schubert, C. J. (2015). Methane oxidation coupled to oxygenic photosynthesis in anoxic waters. *The ISME Journal*, *9*(9), 1991-2002. https://doi.org/10.1038/ismej.2015.12

Miyaji, A. (2011). Chapter fourteen - Particulate Methane Monooxygenase from Methylosinus trichosporium OB3b. In A. C. Rosenzweig & S. W. Ragsdale (Eds.), *Methods in Enzymology* (Vol. 495, pp. 211-225). Academic Press. https://doi.org/https://doi.org/10.1016/B978-0-12-386905-0.00014-0

Nouha, K., Kumar, R. S., Balasubramanian, S., & Tyagi, R. D. (2018). Critical review of EPS production, synthesis and composition for sludge flocculation. *Journal of Environmental Sciences*, *66*, 225-245. https://doi.org/https://doi.org/10.1016/j.jes.2017.05.020

Nultsch, W., & Häder, D.-P. (1979). PHOTOMOVEMENT OF MOTILE MICROORGANISMS. *Photochemistry and Photobiology*, *29*(2), 423-437. https://doi.org/https://doi.org/10.1111/j.1751-1097.1979.tb07072.x

Oswald, K., Milucka, J., Brand, A., Hach, P., Littmann, S., Wehrli, B., Kuypers, M. M. M., & Schubert, C. J. (2016). Aerobic gammaproteobacterial methanotrophs mitigate methane emissions from oxic and anoxic lake waters. *Limnology and Oceanography*, *61*(S1), S101-S118. https://doi.org/10.1002/lno.10312

Ouazaite, H. (2021). *Exploration of micriobial activities that cause oxygen microenvironments within oxygenic photogranules for wastewater treatment* [Doctor, Université de Montpellier]. Université de Montpellier.

Ouazaite, H., Milferstedt, K., Hamelin, J., & Desmond-Le Quéméner, E. (2021). Mapping the biological activities of filamentous oxygenic photogranules. *Biotechnology and Bioengineering*, *118*(2), 601-611. https://doi.org/10.1002/bit.27585

Park, C., & Dolan, S. (2015). *Algal-Sludge Granule for Wastewater Treatment and Bioenergy Feedstock Generation* (USA Patent No. U. o. Massachusetts. https://patentimages.storage.googleapis.com/26/5c/47/3155f044e83f9d/WO2015112654A2.pdf

Park, S., Brown, K. W., & Thomas, J. C. (2002). The effect of various environmental and design parameters on methane oxidation in a model biofilter. *Waste Management & Research: The Journal for a Sustainable Circular Economy*, *20*(5), 434-444. https://doi.org/10.1177/0734242x0202000507

Rahalkar, M. C., Pandit, P. S., Dhakephalkar, P. K., Pore, S., Arora, P., & Kapse, N. (2016). Genome Characteristics of a Novel Type I Methanotroph (Sn10-6) Isolated from a Flooded Indian Rice Field. *Microbial ecology*, *71*(3), 519-523. https://doi.org/http://dx.doi.org/10.1007/s00248-015-0699-z

Rahman, M. M., Salleh, M. A. M., Rashid, U., Ahsan, A., Hossain, M. M., & Ra, C. S. (2014). Production of slow release crystal fertilizer from wastewaters through struvite crystallization – A review. *Arabian Journal of Chemistry*, *7*(1), 139-155. https://doi.org/https://doi.org/10.1016/j.arabjc.2013.10.007

Redfield, A. C. (1934). On the proportions of Organic Derivatives in Sea Water and Their Relation to the Composition of Plankton. *James Johnstone Memorial Volume, University Press of London*, 176-192.

Rice, E. W., Baird, R. B., Eaton, A. D., & Clesceri, L. S. (2012). Standard methods for the examination of water and wastewater, American Public Health Association. *American Water Works Association, Water Environment Federation*.

Safitri, A. S. (2016). *Biogas potential of high strength municipal wastewater treatment in laboratory scale up-flow anaerobic slugde blanket (UASB) reactors* (Publication Number Masteroppgave/UIS-TN-IMN/2016) University of Stavanger, Norway]. University of Stavanger, Norway. https://uis.brage.unit.no/uis-xmlui/bitstream/handle/11250/2410784/Safitri_AnissaSukma.pdf?sequence=1&isAllowed=y

Safitri, A. S., Hamelin, J., Kommedal, R., & Milferstedt, K. (2021). Engineered methanotrophic syntrophy in photogranule communities removes dissolved methane. *Water Research X*, *12*, 100106. https://doi.org/https://doi.org/10.1016/j.wroa.2021.100106

Sanz-Luque, E., Chamizo-Ampudia, A., Llamas, A., Galvan, A., & Fernandez, E. (2015). Understanding nitrate assimilation and its regulation in microalgae. *Frontiers in plant science*, *6*, 899-899. https://doi.org/10.3389/fpls.2015.00899

Schneider, J., & Campion-Alsumard, T. L. (1999). Construction and destruction of carbonates by marine and freshwater cyanobacteria. *European Journal of Phycology*, *34*(4), 417-426. https://doi.org/10.1080/09670269910001736472

Sengar, A., Basheer, F., Aziz, A., & Farooqi, I. H. (2018). Aerobic granulation technology: Laboratory studies to full scale practices. *Journal of Cleaner Production*, *197*, 616-632. https://doi.org/https://doi.org/10.1016/j.jclepro.2018.06.167

Sgarbossa, A., Checcucci, G., & Lenci, F. (2002). Photoreception and photomovements of microorganisms. *Photochemical & photobiological sciences : Official journal of the European Photochemistry Association and the European Society for Photobiology*, *1*, 459-467. https://doi.org/10.1039/B110629E

Shively, J. M., Cannon, G. C., Heinhorst, S., Fuerst, J. A., Bryant, D. A., Gantt, E., Maupin-Furlow, J. A., Schüler, D., Pfeifer, F., Docampo, R., Dahl, C., Preiss, J., Steinbüchel, A., & Federici, B. A. (2009). Intracellular Structures of Prokaryotes: Inclusions, Compartments and Assemblages. In M. Schaechter (Ed.), *Encyclopedia of Microbiology (Third Edition)* (pp. 404-424). Academic Press. https://doi.org/https://doi.org/10.1016/B978-012373944-5.00048-1

Siddharth, T., Sridhar, P., Vinila, V., & Tyagi, R. D. (2021). Environmental applications of microbial extracellular polymeric substance (EPS): A review. *Journal of Environmental Management*, *287*, 112307. https://doi.org/https://doi.org/10.1016/j.jenvman.2021.112307

Singh, J. S., & Singh, D. P. (2017). Methanotrophs: An Emerging Bioremediation Tool with Unique Broad Spectrum Methane Monooxygenase (MMO) Enzyme. In J. S. Singh & G. Seneviratne (Eds.), *Agro-Environmental Sustainability: Volume 2: Managing Environmental Pollution* (pp. 1-18). Springer International Publishing. https://doi.org/10.1007/978-3-319-49727-3_1

Singh, N., Sonani, R., Rastogi, R., & Madamvar, D. (2015). The phycobilisomes: An early requisite for efficient photosynthesis in cyanobacteria. *EXCLI Journal*, *14*, 268-289. https://doi.org/10.17179/excli2014-723

Solano, C., Echeverz, M., & Lasa, I. (2014). Biofilm dispersion and quorum sensing. *Current Opinion in Microbiology*, *18*, 96-104. https://doi.org/https://doi.org/10.1016/j.mib.2014.02.008

Stal, L. J. (1995). Physiological ecology of cyanobacteria in microbial mats and other communities. *New Phytologist*, *131*(1), 1-32. https://doi.org/https://doi.org/10.1111/j.1469-8137.1995.tb03051.x

Stanbridge, H. H. (1976). *History of Sewage Treatment in Britain*. Institute of Water Pollution Control. https://books.google.no/books?id=w6tvSwAACAAJ

Stasinakis, A. (2015). Wastewater treatment process impact on energy savings and greenhouse gas emissions. *Water Science & Technology*, *71*, 2015. https://doi.org/10.2166/wst.2014.521

Stocker, T. F., Qin, D., Plattner, G.-K., Tignor, M., Allen, S. K., Boschung, J., Nauels, A., Xia, Y., Bex, V., & Midgley, P. M. (2013). *Climate Change 2013: The Physical Science Basis. Contribution of*

Working Group I to the Fifth Assessment Report of the Intergovernmental Panel on Climate Change (IPCC, 2013: Summary for Policymakers, Issue.

Sukačová, K., Trtílek, M., & Rataj, T. (2015). Phosphorus removal using a microalgal biofilm in a new biofilm photobioreactor for tertiary wastewater treatment. *Water Research*, *71*, 55-63. https://doi.org/https://doi.org/10.1016/j.watres.2014.12.049

Takeuchi, N., Kohshima, S., & Seko, K. (2001). Structure, Formation, and Darkening Process of Albedo-reducing Material (Cryoconite) on a Himalayan Glacier: A Granular Algal Mat Growing on the Glacier. *Arctic, Antarctic, and Alpine Research*, *33*(2), 115-122. https://doi.org/10.1080/15230430.2001.12003413

Tandeau de Marsac, N., & Houmard, J. (1993). Adaptation of cyanobacteria to environmental stimuli: new steps towards molecular mechanisms. *FEMS Microbiology Reviews*, *10*(1-2), 119-189. https://doi.org/10.1111/j.1574-6968.1993.tb05866.x

Tavormina, P. L., Kellermann, M. Y., Antony, C. P., Tocheva, E. I., Dalleska, N. F., Jensen, A. J., Valentine, D. L., Hinrichs, K. U., Jensen, G. J., Dubilier, N., & Orphan, V. J. (2017). Starvation and recovery in the deep-sea methanotroph M ethyloprofundus sedimenti. *Molecular Microbiology*, *103*(2), 242-252. https://doi.org/10.1111/mmi.13553

Tchobanoglous, G., Stensel, H. D., Tsuchihashi, R., Burton, F., Abu-Orf, M., Bowden, G., pfrang, W., & Eddy, M. (2014a). Anaerobic suspended and attached growth biological treatment processes. In *Wastewater Engineering: treatment and resource recovery* (Fifth Edition ed., Vol. 2, pp. 1059-1109). McGraw-Hill Education.

Tchobanoglous, G., Stensel, H. D., Tsuchihashi, R., Burton, F., Abu-Orf, M., Bowden, G., pfrang, W., & Eddy, M. (2014b). Biosolids processing, resource recovery and beneficial use. In *Wastewater Engineering: treatment and resource recovery* (Fifth Edition ed., Vol. 2, pp. 1561-1651). McGraw-Hill Education.

Tchobanoglous, G., Stensel, H. D., Tsuchihashi, R., Burton, F., Abu-Orf, M., Bowden, G., pfrang, W., & Eddy, M. (2014c). Fundamentals of Biological Treatment. In *Wastewater Engineering: treatment and resource recovery* (Fifth Edition ed., Vol. 1, pp. 551-684). McGraw-Hill Education.

Tchobanoglous, G., Stensel, H. D., Tsuchihashi, R., Burton, F., Abu-Orf, M., Bowden, G., pfrang, W., & Eddy, M. (2014d). Physical Unit Processes. In *Wastewater Engineering: treatment and resource recovery* (Fifth Edition ed., Vol. 1, pp. 419-448). McGraw-Hill Education.

Tenore, A., Mattei, M. R., & Frunzo, L. (2021). Multiscale modelling of oxygenic photogranules. *arXiv pre-print server*. https://doi.org/None

arxiv:2104.12273v1

Tibocha-Bonilla, J. D., Zuñiga, C., Godoy-Silva, R. D., & Zengler, K. (2018). Advances in metabolic modeling of oleaginous microalgae. *Biotechnology for biofuels*, *11*, 241. https://doi.org/http://dx.doi.org/10.1186/s13068-018-1244-3

Tiron, O., Bumbac, C., Manea, E., Stefanescu, M., & Nita Lazar, M. (2017). Overcoming Microalgae Harvesting Barrier by Activated Algae Granules. *Scientific Reports*, *7*(1). https://doi.org/10.1038/s41598-017-05027-3

Trebuch, L. M., Oyserman, B. O., Janssen, M., Wijffels, R. H., Vet, L. E. M., & Fernandes, T. V. (2020). Impact of hydraulic retention time on community assembly and function of photogranules for wastewater treatment. *Water Research*, *173*, 115506. https://doi.org/https://doi.org/10.1016/j.watres.2020.115506

Trego, A. C. M., S.; Collins, G. (2019). Granular Biofilms: Formation, Function, Application, and New Trends as Model Microbial Communities. *Preprints*, 1-51. https://doi.org/10.20944/preprints201906.0053.v1

Tyrrell, T. (2001). Redfield Ratio. In J. H. Steele (Ed.), *Encyclopedia of Ocean Sciences* (pp. 2377-2387). Academic Press. https://doi.org/https://doi.org/10.1006/rwos.2001.0271

van der Ha, D., Bundervoet, B., Verstraete, W., & Boon, N. (2011). A sustainable, carbon neutral methane oxidation by a partnership of methane oxidizing communities and

microalgae. *Water Research*, *45*(9), 2845-2854. https://doi.org/https://doi.org/10.1016/j.watres.2011.03.005

van der Ha, D., Nachtergaele, L., Kerckhof, F.-M., Rameiyanti, D., Bossier, P., Verstraete, W., & Boon, N. (2012). Conversion of Biogas to Bioproducts by Algae and Methane Oxidizing Bacteria. *Environmental Science & Technology*, *46*(24), 13425-13431. https://doi.org/10.1021/es303929s

Vézina, S., & Vincent, W. F. (1997). Arctic cyanobacteria and limnological properties of their environment: Bylot Island, Northwest Territories, Canada (73°N, 80°W). *Polar Biology*, *17*(6), 523-534. https://doi.org/10.1007/s003000050151

Walter, M. R., Bauld, J., & Brock, T. D. (1976). Chapter 6.2 Microbiology and Morphogenesis of Columnar Stromatolites (Conophyton, Vacerrilla) from Hot Springs in Yellowstone National Park. In M. R. Walter (Ed.), *Developments in Sedimentology* (Vol. 20, pp. 273-310). Elsevier. https://doi.org/https://doi.org/10.1016/S0070-4571(08)71140-3

Wang, D., & Li, A. (2022). Effect of zero-valent iron and granular activated carbon on nutrient removal and community assembly of photogranules treating low-strength wastewater. *Science of The Total Environment*, *806*, 151311. https://doi.org/https://doi.org/10.1016/j.scitotenv.2021.151311

Whittenbury, R., Phillips, K. C., & Wilkinson, J. F. (1970). Enrichment, Isolation and Some Properties of Methane-utilizing Bacteria. *Journal of General Microbiology*, *61*(2), 205-218. https://doi.org/10.1099/00221287-61-2-205

Wingender, J., Neu, T. R., & Flemming, H.-C. (1999). What are Bacterial Extracellular Polymeric Substances? In J. Wingender, T. R. Neu, & H.-C. Flemming (Eds.), *Microbial Extracellular Polymeric Substances: Characterization, Structure and Function* (pp. 1-19). Springer Berlin Heidelberg. https://doi.org/10.1007/978-3-642-60147-7_1

Wood, A. M. (1979). CHLOROPHYLL a:b RATIOS IN MARINE PLANKTONIC ALGAE1. *Journal of Phycology*, *15*(3), 330-332. https://doi.org/10.1111/j.0022-3646.1979.00330.x

Wu, X., Kong, L., Pan, J., Feng, Y., & Liu, S. (2022). Metagenomic Approaches to Explore the Quorum Sensing-Mediated Interactions Between Algae and Bacteria in Sequence Membrane Photo-Bioreactors [Original Research]. *Frontiers in Bioengineering and Biotechnology*, *10*. https://doi.org/10.3389/fbioe.2022.851376

Yuan, S., Gao, M., Zhu, F., Afzal, M. Z., Wang, Y.-K., Xu, H., Wang, M., Wang, S.-G., & Wang, X.-H. (2017). Disintegration of aerobic granules during prolonged operation [10.1039/C7EW00072C]. *Environmental Science: Water Research & Technology*, *3*(4), 757-766. https://doi.org/10.1039/C7EW00072C

Yun, J., Zhang, H., Deng, Y., & Wang, Y. (2015). Aerobic methanotroph diversity in Sanjiang wetland, Northeast China. *Microbial ecology*, *69*(3), 567-576. https://doi.org/http://dx.doi.org/10.1007/s00248-014-0506-2

Zhu, J., Lei, X., Quan, J., & Yue, X. (2019). Algae Growth Distribution and Key Prevention and Control Positions for the Middle Route of the South-to-North Water Diversion Project. *Water*, *11*(9), 1851. https://www.mdpi.com/2073-4441/11/9/1851

Appendix

Table 5 shows the result from the chemical analysis of the feed media (UASB effluent) for the experimental period. Note that after 21.03.2022 feed media was stored in bulk. All results are in mgL^{-1}. Ammonium was measured as NH_4^+-N, phosphate was measured as PO_4^{3-}-P.

Table 5: Results from chemical analysis of feed media for the experimental period

Date	CODs In	TSS	VSS	TN In	TP In	NH_4^+ In	NO_3^- In	PO_4^{3-} In	Ph In	T In	TVFA In	ALK In
17.02.2022	237,3	0,0	0,0	57,0	25,6	55,0	0,1	22,5	8,2	21,0	123,0	465,6
18.02.2022	307,5	0,0	0,0	54,6	24,9	53,0	0,2	23,7	8,1	21,0	152,0	690,5
21.02.2022	346,3	0,0	0,0	50,2	30,3	44,0	0,8	29,5	7,8	21,0	102,0	960,5
22.02.2022	375,1	0,0	0,0	61,3	28,5	59,0	0,3	26,3	7,9	21,0	79,6	456,2
23.02.2022	232,8	0,0	0,0	54,5	26,9	51,0	0,6	22,2	7,8	21,0	84,0	465,2
24.02.2022	349,3	0,0	0,0	47,0	25,6	45,0	0,3	24,5	7,9	19,0	56,3	356,2
25.02.2022	362,7	0,0	0,0	49,2	23,1	48,0	0,4	22,6	8,1	21,0	45,0	269,0
01.03.2022	243,6	0,0	0,0	46,7	40,0	45,7	0,1	39,5	8,2	20,0	145,4	1023,0
02.03.2022	352,2	0,0	0,0	46,7	37,0	45,7	0,2	36,5	8,0	21,0	79,0	463,0
03.03.2022	679,1	0,0	0,0	46,7	37,0	45,7	0,3	36,5	8,2	21,0	120,4	468,5
04.03.2022	569,6	0,0	0,0	42,1	38,9	40,3	0,1	37,1	8,1	20,0	89,9	541,3
07.03.2022	450,7	0,0	0,0	42,1	38,9	40,3	0,1	37,1	7,5	20,0	77,0	365,5
08.03.2022	544,8	0,0	0,0	43,5	38,9	41,7	0,3	36,5	7,6	20,0	89,4	169,5
09.03.2022	319,4	0,0	0,0	43,5	38,9	42,0	0,3	36,5	7,9	19,0	102,4	89,4
10.03.2022	413,7	0,0	0,0	43,5	38,9	42,0	0,2	36,5	7,9	21,0	101,2	102,2
11.03.2022	320,0	0,0	0,0	48,0	32,9	47,0	0,2	32,2	8,0	21,0	46,7	98,6
14.03.2022	477,6	0,0	0,0	48,0	32,9	47,0	0,3	32,2	8,4	21,0	44,3	73,0
15.03.2022	664,9	0,0	0,0	52,1	31,6	51,6	0,3	30,3	8,1	21,0	46,6	123,0
16.03.2022	626,9	0,0	0,0	52,1	31,6	51,6	0,3	30,3	8,1	21,0	36,2	76,5
17.03.2022	514,0	0,0	0,0	52,1	31,6	51,6	0,3	30,3	8,0	21,0	36,2	159,5
18.03.2022	486,6	0,0	0,0	52,9	32,2	52,0	0,1	31,0	8,1	21,0	36,2	99,5
21.03.2022	365,6	0,0	0,0	53,6	34,6	52,4	0,2	32,5	8,0	21,0	76,6	102,3

22.03.2022	365,6	0,0	0,0	53,6	34,6	52,4	0,2	32,5	8,0	21,0	76,6	102,3
23.03.2022	365,6	0,0	0,0	53,6	34,6	52,4	0,2	32,5	8,0	21,0	76,6	102,3
24.03.2022	456,6	0,0	0,0	69,4	35,0	63,7	0,2	32,7	8,2	21,0	120,4	56,6
25.03.2022	456,6	0,0	0,0	69,4	35,0	63,7	0,2	32,7	8,2	21,0	120,4	56,6
28.03.2022	456,6	0,0	0,0	69,4	35,0	63,7	0,2	32,7	8,2	21,0	120,4	56,6
29.03.2022	456,6	0,0	0,0	69,4	35,0	63,7	0,2	32,7	8,2	21,0	120,4	56,6
30.03.2022	426,0	0,0	0,0	79,5	29,8	79,0	0,3	28,4	7,8	21,0	145,9	130,6
31.03.2022	426,0	0,0	0,0	79,5	29,8	79,0	0,3	28,4	7,8	21,0	145,9	130,6
01.04.2022	426,0	0,0	0,0	79,5	29,8	79,0	0,3	28,4	7,8	21,0	145,9	130,6
04.04.2022	426,0	0,0	0,0	79,5	29,8	79,0	0,3	28,4	7,8	21,0	145,9	130,6
05.04.2022	521,2	0,0	0,0	123,6	30,5	122,5	0,2	29,5	7,7	21,0	115,6	79,2
06.04.2022	521,2	0,0	0,0	123,6	30,5	122,5	0,2	29,5	7,7	21,0	115,6	79,2
07.04.2022	521,2	0,0	0,0	123,6	30,5	122,5	0,2	29,5	7,7	21,0	115,6	79,2
08.04.2022	521,2	0,0	0,0	123,6	30,5	122,5	0,2	29,5	7,7	21,0	115,6	79,2
11.04.2022	426,9	0,0	0,0	65,6	32,2	64,9	0,3	30,2	8,0	21,0	89,6	69,4
13.04.2022	426,9	0,0	0,0	65,6	32,2	64,9	0,3	30,2	8,0	21,0	89,6	69,4
15.04.2022	426,9	0,0	0,0	65,6	32,2	64,9	0,3	30,2	8,0	21,0	89,6	69,4
18.04.2022	426,9	0,0	0,0	65,6	32,2	64,9	0,3	30,2	8,0	21,0	89,6	69,4
19.04.2022	396,9	0,0	0,0	68,5	33,5	68,2	0,3	33,0	7,5	21,0	78,4	156,6
20.04.2022	396,9	0,0	0,0	68,5	33,5	68,2	0,3	33,0	7,5	21,0	78,4	156,6
21.04.2022	396,9	0,0	0,0	68,5	33,5	68,2	0,3	33,0	7,5	21,0	78,4	156,6
22.04.2022	444,7	0,0	0,0	59,9	29,0	58,7	0,2	27,5	7,8	20,0	107,5	109,5
25.04.2022	444,7	0,0	0,0	59,9	29,0	58,7	0,2	27,5	7,8	20,0	107,5	109,5
26.04.2022	444,7	0,0	0,0	59,9	29,0	58,7	0,2	27,5	7,8	20,0	107,5	109,5
27.04.2022	421,8	0,0	0,0	70,2	31,5	68,9	0,2	31,2	7,6	21,0	145,9	125,6
28.04.2022	421,8	0,0	0,0	70,2	31,5	68,9	0,2	31,2	7,6	21,0	145,9	125,6
29.04.2022	502,3	0,0	0,0	80,6	34,5	75,6	0,1	32,7	7,7	21,0	203,5	250,3
02.05.2022	502,3	0,0	0,0	80,6	34,5	75,6	0,1	32,7	7,6	21,0	203,5	250,3
03.05.2022	502,3	0,0	0,0	80,6	34,5	75,6	0,1	32,7	7,8	21,0	203,5	250,3
04.05.2022	502,3	0,0	0,0	80,6	34,5	75,6	0,1	32,7	7,5	21,0	203,5	250,3
05.05.2022	502,3	0,0	0,0	80,6	34,5	75,6	0,1	32,7	7,0	21,0	203,5	250,3

06.05.2022	610,2	0,0	0,0	110,4	35,9	107,5	0,3	34,6	7,4	21,0	150,6	150,6
09.05.2022	610,2	0,0	0,0	110,4	35,9	107,5	0,3	34,6	7,2	21,0	150,6	150,6
10.05.2022	610,2	0,0	0,0	110,4	35,9	107,5	0,3	34,6	7,6	21,0	150,6	150,6
11.05.2022	610,2	0,0	0,0	110,4	35,9	107,5	0,3	34,6	7,8	21,0	150,6	150,6
12.05.2022	610,2	0,0	0,0	110,4	35,9	107,5	0,3	34,6	7,4	21,0	150,6	150,6
13.05.2022	610,2	0,0	0,0	110,4	35,9	107,5	0,3	34,6	7,6	21,0	150,6	150,6

Table 6 shows the result from the chemical analysis of the PBR effluent for the experimental period. Note that VSS was measured periodically after 02.03.2022. All results are in mgL^{-1}. Ammonium was measured as NH_4^+-N, phosphate was measured as PO_4^{3-}-P. Results for total nitrogen is missing 03.03.2022 because concentration was higher than the test kit range ($150 mgN \cdot L^{-1}$). Results for NH_4^+ is missing 03.03.2022 and 04.03.2022 because concentration was higher than the test kit range ($16\ mgNH_4^+\text{-}N \cdot L^{-1}$). Results for NH_4^+ is missing 15.03.2022 due to analytical errors. Some days PO_4^{3-} was higher than TP, which should not happen. The reason PO_4^{3-} is higher some days might be from two things. One being that the samples often were diluted and results from the spectrometer only gave one decimal reading which might lead to a calculation error (put example her). Another reason might be human error when sampling.

Table 6: Results from chemical analysis of PBR effluent for the experimental period

Date	CODs Eff	TSS Eff	VSS Eff	TN Eff	TP Eff	NH_4^+ Eff	NO_3^- Eff	PO_4^{3-} Eff	Ph Eff	T Eff	TVFA Eff	ALK Eff
17.02.2022	159,0	239,5	230,3	50,3	15,3	42,0	0,5	15,1	8,2	20,0	54,0	120,0
18.02.2022	206,0	265,3	263,3	44,0	14,2	43,0	0,5	13,6	8,3	19,0	51,0	465,0
21.02.2022	232,0	215,9	213,3	70,2	21,6	26,3	0,7	14,5	8,0	22,0	23,0	632,0
22.02.2022	251,3	260,3	251,6	43,0	13,6	39,0	1,2	13,2	8,1	21,0	0,0	102,0
23.02.2022	156,0	263,0	259,5	63,9	19,5	40,0	0,5	11,9	7,8	20,0	0,0	59,9
24.02.2022	234,0	298,3	284,2	47,0	10,6	34,2	0,3	9,7	8,2	20,0	50,0	230,0
25.02.2022	243,0	186,3	178,5	28,0	23,3	28,0	0,4	8,7	8,1	21,0	40,0	120,4
01.03.2022	163,2	285,5	271,5	18,5	17,9	7,8	0,3	26,3	9,1	19,0	135,4	832,1
02.03.2022	236,0	202,3	196,3	49,0	23,2	19,5	0,2	17,8	7,9	21,0	46,3	165,9

03.03.2022	455,0	272,1			22,2		0,3	21,9	8,0	21,0	79,0	376,7
04.03.2022	381,6	341,3		151,5	25,5		0,4	25,7	8,9	21,0	29,9	598,1
07.03.2022	302,0	263,3	259,3	75,6	20,0	31,6	0,3	17,6	7,8	20,0	36,9	269,5
08.03.2022	365,0	258,2	250,1	69,6	19,5	25,9	0,3	18,6	8,6	19,0	40,6	126,3
09.03.2022	214,0	163,0	154,0	59,8	15,9	26,6	0,4	15,7	8,2	19,0	76,4	16,0
10.03.2022	277,2	207,9	198,6	63,5	14,4	23,2	0,5	6,6	9,0	21,0	0,0	23,2
11.03.2022	214,4	296,0		61,0	16,8	21,8	0,6	4,7	9,0	21,0	0,0	3,3
14.03.2022	320,0	196,6	186,6	79,0	21,2	26,8	0,4	19,8	8,4	20,0	23,2	50,6
15.03.2022	445,5	246,8	233,3	75,2	24,1		0,2	25,6	7,8	21,0	25,7	98,4
16.03.2022	420,0	163,4	158,4	69,5	20,1	19,8	0,4	19,5	7,6	20,0	0,0	26,6
17.03.2022	344,4	230,6		114,0	23,3	43,2	0,4	15,4	7,0	21,0	0,0	86,2
18.03.2022	326,0	222,8	217,4	76,5	22,5	14,5	0,3	17,0	7,5	20,0	19,6	70,5
21.03.2022	132,6	351,8	334,5	53,5	14,5	28,6	0,3	7,8	9,0	21,0	0,0	42,9
22.03.2022	156,3	286,4		76,6	16,5	32,3	0,2	8,9	8,1	21,0	0,0	79,5
23.03.2022	231,7	173,9		80,0	17,8	32,6	0,5	18,1	7,5	21,0	0,0	90,9
24.03.2022	198,6	203,2	189,6	76,3	26,6	33,7	0,4	21,6	7,8	21,0	0,0	128,6
25.03.2022	203,3	130,2	126,3	56,3	23,3	25,6	0,5	20,3	7,9	21,0	0,0	203,1
28.03.2022	215,2	153,2		49,6	19,5	19,5	0,2	18,9	8,1	21,0	0,0	240,6
29.03.2022	258,7	119,8	114,9	84,5	17,3	66,7	0,5	18,7	8,4	21,0	0,0	234,8
30.03.2022	239,5	227,9		73,5	16,6	67,9	0,5	21,5	8,7	21,0	0,0	171,0
31.03.2022	125,4	169,8	159,5	78,2	18,6	32,6	0,4	18,6	8,2	20,0	0,0	176,3
01.04.2022	187,6	265,6		66,9	19,6	31,6	0,2	19,1	8,1	19,0	0,0	183,6
04.04.2022	189,0	663,5	605,0	88,0	18,9	53,0	0,8	18,4	8,8	21,0	0,0	191,3
05.04.2022	254,3	236,3		104,0	23,6	81,7	0,6	28,0	8,4	21,0	0,0	335,7
06.04.2022	164,7	173,9	166,3	77,5	18,0	54,9	0,4	17,9	7,7	21,0	0,0	278,7
07.04.2022	256,3	268,3		101,3	22,3	59,6	0,4	21,3	8,1	20,0	0,0	168,5
08.04.2022	111,2	106,1		66,5	15,3	50,8	0,5	14,5	8,4	21,0	0,0	235,9
11.04.2022	201,6	189,6	187,6	56,6	24,3	25,6	0,6	21,3	8,2	21,0	0,0	201,4
13.04.2022	145,2	258,5		46,6	21,0	20,1	0,7	19,6	8,0	21,0	0,0	156,3
15.04.2022	102,3	246,3	239,6	89,3	19,6	42,3	0,5	18,9	8,1	21,0	0,0	186,2
18.04.2022	157,3	281,0		63,0	15,3	34,7	0,7	13,5	9,1	19,0	0,0	210,4

19.04.2022	145,2	222,3		76,3	21,3	39,5	0,0	20,3	8,0	20,0	0,0	223,7
20.04.2022	144,3	148,3	147,6	101,6	20,4	34,5	0,3	19,6	8,1	21,0	0,0	176,2
21.04.2022	130,7	123,5		71,0	15,1	60,3	0,0	18,1	8,2	21,0	0,0	185,0
22.04.2022	107,1	85,5		45,5	12,2	36,4	0,0	12,1	7,9	21,0	0,0	203,7
25.04.2022	123,3	128,5		68,0	15,6	32,5	0,0	14,9	8,2	20,0	0,0	250,6
26.04.2022	112,8	140,6	126,9	56,0	14,5	28,6	0,2	14,2	8,0	21,0	0,0	225,4
27.04.2022	169,1	202,6	194,1	135,5	25,4	110,7	0,4	29,2	8,0	21,0	0,0	392,4
28.04.2022	105,6	156,5		58,4	17,8	24,6	0,2	16,9	7,8	21,0	0,0	198,6
29.04.2022	141,6	267,0		88,0	17,9	71,9	0,0	17,5	7,9	21,0	0,0	293,6
02.05.2022	135,0	265,1	235,5	62,3	23,3	52,3	0,3	22,9	8,2	21,0	0,0	150,6
03.05.2022	132,7	307,2		54,5	13,4	22,8	0,3	11,9	8,7	21,0	0,0	32,4
04.05.2022	146,4	250,0		46,6	21,2	36,5	0,1	20,9	8,1	21,0	0,0	63,5
05.05.2022	146,7	268,6	260,0	99,0	20,0	69,4	0,0	16,7	8,6	21,0	0,0	223,1
06.05.2022	138,5	201,4		66,5	13,8	46,9	0,0	11,6	8,4	21,0	0,0	182,7
09.05.2022	151,3	397,0	384,6	69,0	17,7	34,3	0,2	12,7	9,0	21,0	0,0	46,7
10.05.2022	299,3	320,0		115,0	23,1	164,3	0,0	20,7	8,2	21,0	0,0	333,2
11.05.2022	230,5	163,6		70,5	22,0	49,5	0,0	21,2	7,9	20,0	0,0	210,3
12.05.2022	217,8	132,2		87,5	16,4	65,5	0,0	14,2	7,9	21,0	0,0	281,0
13.05.2022	231,0	162,2	136,5	63,3	19,5	50,3	0,1	17,6	8,1	21,0	0,0	90,5

Calculations

Removal efficiency:

$$\%\, removal\ efficiency = \frac{Influent\ mgL^{-1} - effluent\ mgL^{-1}}{influent\ mgL^{-1}}$$ Equation (6)

Organic loading rate:

$$OLR = Cin.QinV$$ Equation (7)

Hydraulic retention time:

$$HRT = VQin$$ Equation (8)

Nitrogen loading rate:

$$NLR = \frac{CNin.Qin}{V}$$ Equation (9)

Phosphorous loading rate:

$$PLR = \frac{CPin.Qin}{V}$$ Equation (10)

Settling time:

$$S = \frac{1}{2}(V + V_0)t$$ Equation (11)

Red field ratio:

For Carbon:

COD concentration	454,8	mgCOD/l
Specific COD for biomass	1,42	mgVSS/mgCOD
Carbon as VSS	320,28	mgVSS/l

Carbon compound in COD	NaHCO3	C6H12O6	NH4CH3COO	CaCO3	CO2	
Fraction of biomass	28,80 %	64,00 %	3,60 %	6 %	4 %	
Molecular weight	84	180	77	100	44	g/mol
Mole per litre	3,81	1,78	4,16	3,20	7,28	mmol/litre
Including fraction	1,10	1,14	0,15	0,19	0,29	mmol/litre
Sum of carbon in moles	2,87	mmol/l				

For nitrogen and phosphorous average for TN and TP was used for conversion to mole/l.